School of Pharmacy

Laboratory of Biophysics and Surface Analysis

Extrusion Based 3D Printing as a Novel Technique for Fabrication of Oral Solid Dosage Forms

Shaban Khaled

BSc in Pharmacy & Pharmaceutical Sciences, MSc in Nanoscience

Thesis Submitted To the University of Nottingham

For The Degree of Doctor of Philosophy

31st May 2016

Acknowledgements

I would like to express my deep gratefulness to my academic supervisors; Dr. Jonathan Burley, Prof. Clive Roberts and Prof. Morgan Alexander for their inspiring guidance and constant encouragement throughout the course of my research work. I also thank my internal supervisor Prof. Martyn Davies for his helpful of academic suggestions. I would like to thank people at CBS building, School of Pharmacy, especially Prof. Kevin Shakesheff and Dr. Jing Yang for giving me access to the 3D printers, Dr Omer Qutashi for his good support and discussion, Teresa Marshel for her training and lab Inductions, and my colleagues for their cooperation and support.

I also thank people from Boots Science Building, School of pharmacy especially Colin Wells, Mike, Mrs Judith Greenfield Mrs. Gail Atkinson, Mrs. Julia Crouch, Paul Cooling, and Tom Boot for their help in administrative paper work and training, everyone in LBSA division, Burley's group, and my colleagues for providing such a nice atmosphere for working. I thank as well people in School of Chemistry especially Dr. William Lewis for the training and support on XRPD instrument. Lastly, I acknowledge the financial support which I received from the Libyan government.

This thesis is dedicated to my family members and my wife who have always been there for me and especially throughout my studying in the UK. To my father, Abdussalam, who had been my prime inspiration, to my mother, Salma, who has been supporting me till the day of submission, to my wife who has been supporting and looking after me throughout my studying, and to my brothers and my sisters for their unconditional love, affection and support.

List of Publications

S.A. Khaled, J.C. Burley, M.R. Alexander, C.J. Roberts, Desktop 3D printing of controlled release pharmaceutical bilayer tablets, Int. J. Pharm., 461 (2014) 105-111.

S.A. Khaled, J.C. Burley, M.R. Alexander, J. Yang, C.J. Roberts, 3D printing of tablets containing multiple drugs with defined release profiles, Int. J. Pharm., 494 (2015) 643-650.

S.A. Khaled, J.C. Burley, M.R. Alexander, J. Yang, C.J. Roberts, 3D printing of five-in-one dose combination polypill with defined immediate and sustained release profiles, J. Control. Release, 217 (2015) 308-314.

List of Abbreviations

ATR-FTIR	Attenuated Total Reflectance Fourier Transform Infrared Spectroscopy
APIs	Active Pharmaceutical Ingredients
ABS	Acrylonitrile Butadiene Styrene
ASA	Acetylsalicylic Acid
B/MDDSs	Bio/mucoadhesive drug delivery systems
BSE	Backscattered Electrons
BMI	Body Mass Index
BMS	Bristol-Myers Squibb
CCS	Croscarmellose Sodium
CPOPTs	Controlled Porosity Osmotic Pump Tablets
CT	Compressed Tablet
CSD	Cambridge Structural Database
CA	Cellulose Acetate
CADD	Computer Aided Designed Data
CAD	Computer Aided Device
DSC	Differential Scanning Calorimetry
DDS	Drug Delivery Systems
DOD	Drop On Demand
DMSO	Dimethyl Sulfoxide
EOPTs	Elementary Osmotic Pump Tablets
ER	Extended Release
EMC	Enhanced Machine Controller
FDM	Fused Deposition Melting

List of abbreviations

GI	Gastro-Intestinal
GIT	Gastro-Intestinal-Tract
GBTs	Guaifenesin Bi-layer Tablets
HPMC	Hydroxypropyl Methyl Cellulose
HIV	Human Immunodeficiency Virus
HCl	Hydrochloric Acid
HPC	Hydroxypropyl Cellulose
HMI	Human Machine Interface
HMG-CoA	Hydroxy-3-Methylglutaryl–Coenzyme A
HCT	Hydrochlorothiazide
IJ	InkJet
IV	Intravenous
IUD	intrauterine device
MCC	Microcrystalline Cellulose
MC	Methyl Cellulose
MDSC	Modulated Differential Scanning Calorimetry
MCTs	Multiple Compressed Tablets
NTI	Narrow Therapeutic Index
ODDTs	Osmotic Drug Delivery Systems
ODDSs	Osmotic Drug Delivery Systems
OTC	Over The Counter
PAA	Polyacrylic Acid
PLA	Poly Lactic Acid
PEG-DA	Poly-(Ethylene Glycol) Diacrylate

List of abbreviations

PLGA	Poly Lactic-co-Glycolic Acid
PBS	Phosphate Buffer Saline
PVA	Poly Vinyl Alcohol
PEA	poly-Ester Amide
PAA	Poly Acrylic Acid
PPM	Part Per Million
PEG	Poly Ethylene Glycol
PPOPTs	Push Pull Osmotic Pump Tablets
PVP	Poly Vinyl Pyrrolidone
PSI	Pound-force per Square Inch
RP-HPLC	Reverse Phase High Performance Liquid Chromatography
RP	Rapid Prototyping
SOPTs	Sandwiched Osmotic Pump Tablets
SSG	Sodium Starch Glycolate
SLS	Selective Laser Sintering
SFFF	Solid Free Form Fabrication
SEM	Scanning Electron Microscopy
SR	Sustained Release
SLA	Stereolithography
SE	Secondary Electrons
SEI	Secondary Electron Images
3D	Three Dimensional
2D	Two Dimensional
TA	Thermo-Analytical

List of abbreviations

T_g	Glass transitions
TPMT	Thiopurine S-methyltransferase
TSP.12 H_2O	Tri Sodium Phosphate dodecahydrate
TEM	Transmission Electron Microscopy
UV	Ultra-Violet
USP	United States Pharmacopoeia
UV-Vis	UltraViolet-Visible Spectrophotometry
XRPD	X-Ray Powder Diffraction
XML	Extensible Mark-up Language File
ZnSe	Zinc Selenide

Abstract

Extrusion based three dimensional (3D) printing is defined as a process used to make a 3D object layer by layer directly from a computer aided device (CAD). The application of extrusion based 3D printing process to manufacture functional oral solid tablets with relatively complex geometries is demonstrated in this thesis.

In Chapter 3 the viability of using a basic desktop 3D printer (Fab@Home) to print functional guaifenesin bilayer tablets (GBTs) is demonstrated. Guaifenesin is an over the counter (OTC) water soluble medicine used as expectorant for reduction of chest congestion caused by common cold and infections in respiratory system. The bilayer tablets were printed using the standard pharmaceutical excipients; hydroxypropyl methyl cellulose (HPMC) 2208, 2910, sodium starch glycolate (SSG), microcrystalline cellulose (MCC) and polyacrylic acid (PAA) in order mimic the commercial model formulation (Mucinex®) guaifenesin extended-release bilayer tablets. The 3D printed guaifenesin bilayer tablets (GBTs) were evaluated for mechanical properties as a comparison to the commercial GBTs and were found to be within acceptable range as defined by the international standards stated in the USP. Drug releases from the 3D printed GBTs were decreased as the amount of HPMC 2208 increased due to the increased wettability, swelling properties and gel barrier formation of the HPMC. The 3D printed GBTs also showed, as required, two release profiles: immediate release (IR) from the top layer containing disintegrants; SSG and MCC and sustained release (SR) profile from the lower layer containing HPMC 2208. The kinetic drug release data from the 3D printed and commercial GBTs were best modelled using the Korsmeyer–Peppas model with *n* values between 0.27 and 0.44. This suggests Fickian diffusion drug release through a hydrated HPMC gel layer. Other physical characterisations: X-Ray Powder Diffraction (XRPD), Attenuated Total Reflectance Fourier Transform Infrared Spectroscopy (ATR-FTIR), and

Abstract

Differential Scanning Calorimetry (DSC) showed that there was no detectable interaction between guaifenesin and the used excipients in both 3D printed and commercial GBTs.

A more complex printer (RegenHu 3D bioprinter) was subsequently used to print complex multi-active tablets containing captopril, nifedipine, and glipizide as a model therapeutic combination. These drugs are frequently used to treat hypertension and diabetes mellitus. The 3D printed tablets were evaluated for drug release and showed that captopril was released by osmosis through permeable cellulose acetate (CA) film and both glipizide and nifedipine were released by diffusion through the hydrophilic HPMC 2208 matrix. According to XRPD and ATR-FTIR results, there was no detectable interaction between the actives and the used excipients.

In the final experimental chapter, a combined treatment regimen: atenolol, ramipril, hydrochlorothiazide (anti-hypertensive medications), pravastatin (cholesterol lowering agent), and aspirin (anti-platelets) were printed into more complex geometry (polypill) using the RegenHu 3D bioprinter. This combined drug regimen is manufactured by Cadila Pharmaceuticals Limited as a capsule formulation under the trade name of Polycap™ and is currently the only polypill formulation commercially available and is used to treat and prevent cardiovascular diseases. The printed polypills were characterized for drug release using USP dissolution testing and showed the intended immediate and sustained release profiles based upon the active/excipient ratio used. Aspirin and hydrochlorothiazide were immediately released after the polypill contacted the dissolution medium, and atenolol, ramipril, and pravastatin were released over a period of 12 hrs. XRPD and ATR-FTIR showed that there was no detectable interaction between the actives and the used excipients.

In this work, extrusion based 3D printing technique was used to print oral solid dosage forms with complex and well-defined geometries and function. The technology of 3D printing could

offer the opportunity to print oral tablets with high and precise drug dosing and controlled drug release profiles tailored for sub-populations or individuals. If the manufacturing and regulatory issues associated with 3DP can be resolved such personalised medicine delivered by 3D printing could improve patient compliance and provide more effective treatment regimes.

Table of Contents

Abstract VIII

List of Figures XVIII

List of Tables XXV

Chapter 1 Introduction 1

1.1. Oral solid dosage forms 1

1.2. Tablets manufacturing process 1

1.2.1. Ingredients used in tablets formulation 1

1.2.2. Granulation and direct compression processes 2

1.2.2.1. Dry and wet granulation 2

1.2.2.2. Direct compression 3

1.2.3. Granule lubrication 4

1.2.4. Powder compaction 5

1.2.5. Compression methods 5

1.2.5.1. Single-punch tablet machine 6

1.2.5.2. Rotary tablet machine 7

1.2.6. Molded Tablets 7

1.2.7. Coating processes 8

1.3. Types of oral solid dosage forms (tablets) 9

1.3.1. Compressed Tablet (CT) 9

1.3.2. Multiple Compressed Tablets (MCTs) 9

1.3.2.1. Layered tablets 9

1.3.2.2. Press-coated tablets 10

1.3.3. Oral osmotic drug delivery systems (tablets).....11

1.3.3.1. Controlled Porosity Osmotic Pump Tablets (CPOPTs).....11

1.3.3.2. Elementary Osmotic Pump Tablets (EOPTs).....12

1.3.3.3. Push Pull Osmotic Pump Tablets (PPOPTs).....12

1.3.3.4. Sandwiched Osmotic Pump Tablets (SOPTs).....13

1.4. Drug release mechanisms from polymeric matrix devices 15

1.4.1. Drug release by swelling.....15

1.4.2. Drug release by erosion 16

1.4.3. Drug release by osmosis 16

1.5. Stability in drug formulations 17

1.6. Challenging in fabrication of complex oral tablets with a desired release profile....19

1.7. Three Dimensional (3D) Printing.....21

1.7.1. Introduction.....21

1.7.2. The current technologies in 3D printing 21

1.7.2.1. Stereolithography (SLA).....22

1.7.2.2. Fused deposition melting (FDM) 23

1.7.2.3. Selective laser sintering (SLS) 24

1.7.2.4. Inkjet (IJ) printing 25

1.7.2.5. Extrusion base 3D printing technique 26

1.7.3. Applications of 3D printing techniques 27

1.7.3.1. Applications of 3D printers in drug formulation.....27

1.7.3.2. Applications of 3D printing technology in life science.....29

1.7.3.3. Critiques of different types of 3D printers (why extrusion based 3D printing)

31

1.7.4. Advantages and drawbacks of pharmaceutical 3D printing technology.....32

1.8. Aims and objectives.....33

Chapter 2 Preparation methods, 3D printing and screening techniques.....35

2.1. Preparation methods.....35

2.1.1. Preparation of hydroxypropyl methylcellulose gel (binder).....35

2.1.2. Extrusion based 3D printing process.....36

2.1.2.1. Design of 3D oral solid tablets.....36

2.1.2.2. Preparation of medicated paste.....37

2.1.2.3. Cartridge/barrel tool filling process.....38

2.1.2.4. Execution of printing job.....39

2.2. 3D printing techniques.....39

2.2.1. Fab@Home 3D printer.....39

2.2.2. 3D Discovery® instrument.....40

2.3. Characterisation techniques.....41

2.3.1. Differential scanning calorimeter (DSC).....41

2.3.2. Scanning Electron Microscopy (SEM).....43

2.3.3. Attenuated Total Reflection-Fourier Transform InfraRed (ATR-FTIR).....46

2.3.4. X-Ray Powder Diffractometer (XRPD).....47

2.3.5. Reverse Phase High Performance Liquid Chromatography (RP-HPLC).....48

2.3.6. Tablet friability tester.....49

2.3.7. Tablet hardness tester.....50

Chapter 3 Desktop 3D printing of Controlled Release Pharmaceutical Bilayer Tablets.....52

3.1. Abstract.....52

3.2. Introduction 53

3.3. Aims and objectives 55

3.4. Active ingredient 55

3.4.1. Guaifenesin 55

3.5. Materials and methods 56

3.5.1. Materials 56

3.5.2. Methods 57

3.5.2.1. Design of the 3D printed GBT 57

3.5.2.2. Preparation of hydroxypropyl methylcellulose (HPMC) aqueous gel 58

3.5.2.3. Extrusion based 3D printing process of GBTs 58

3.5.2.4. In vitro drug release 60

3.5.2.5. ATR-FTIR 61

3.5.2.6. XRPD 61

3.5.2.7. DSC 62

3.5.2.8. Physical properties of the 3D printed and commercial GBTs (USP tests) 62

3.5.2.9. Statistical analysis 63

3.6. Results and discussion 63

3.6.1. Dissolution profiles 63

3.6.2. ATR-FTIR 68

3.6.3. XRPD 68

3.6.4. DSC 70

3.6.5. Physical properties 71

3.6.6. Drug release kinetics 75

3.7. Conclusions 78

Table of Contents

Chapter 4 Desktop 3D Printing of Tablets Containing Multiple Drugs with Defined Release Profiles 79

4.1. Abstract 79

4.2. Introduction 80

4.3. Aims and objectives 81

4.4. Materials and methods 81

4.4.1. Materials 81

4.4.2. Methods 82

4.4.2.1. Design of multi-active tablets 82

4.4.2.2. Preparation of HPMC 2280 hydro-alcoholic gel 84

4.4.2.3. 3D printing process of multi-active tablets 85

4.4.2.4. Printing parameters and ink filling 88

4.4.2.5. Drug concentration measurement for dissolution studies 89

4.4.2.6. In vitro drug release 90

4.4.2.7. SEM 91

4.4.2.8. XRPD 91

4.4.2.9. ATR-FTIR 91

4.4.2.10. Content uniformity and weight variation 91

4.5. Results and discussion 92

4.5.1. In vitro drug dissolution 92

4.5.2. SEM 93

4.5.3. Drug release kinetics 93

4.5.4. XRPD 97

4.5.5. ATR-FTIR 99

4.5.6. Content uniformity and weight variation 100

4.6. Conclusions 100

Chapter 5 Desktop 3D Printing of Five-In-One Dose Combination Polypill with Defined Immediate and Sustained Release Profiles 102

5.1. Abstract 102

5.2. Introduction 103

5.3. Aims and objectives 105

5.4. Material and methods 105

5.4.1. Materials 105

5.4.2. Methods 106

5.4.2.1. Design of polypill 106

5.4.2.2. Extrusion based 3D printing process of polypill 107

5.4.2.3. Dissolution studies 111

5.4.2.4. XRPD 112

5.4.2.5. ATR-FTIR 113

5.5. Results and discussion 113

5.5.1. In vitro drug dissolution 113

5.5.2. XRPD 114

5.5.3. ATR-FTIR 117

5.6. Release Kinetics 118

5.7. Pharmaceutical considerations 120

5.8. Conclusions 121

Table of Contents

Chapter 6 General Conclusion and Future Work.....123

Biography.....131

LIST OF FIGURES

Figure 1.1: Schematic diagram of granulation methods by different techniques [13] 4

Figure 1.2: Powder compaction stages [1] 5

Figure 1.3: Schematic diagram summarizes the associated steps with single-punch 6

Figure 1.4: Schematic diagram of rotary tablet press cycle 7

Figure 1.5: Tablet triturate moulds. 8

Figure 1.6: Schematic diagram of controlled porosity osmotic pump tablet before and during dissolution process. 12

Figure 1.7: Schematic diagram of elementary osmotic pump tablet before and during dissolution process. 12

Figure 1.8: Schematic diagram of push pull osmotic pump tablet before and during dissolution process. 13

Figure 1.9: Schematic diagram of sandwiched osmotic pump tablet before and during dissolution process. 14

Figure 1.10: Schematic illustration of surface and bulk erosion [44] 16

Figure 1.11: Schematic diagram showing delayed flow of the drug solution because of osmotic potential gradient through a microporous membrane [55] 17

Figure 1.12: Schematic diagram of a typical stereolithography (3D printer) [87] 22

Figure 1.13: Schematic diagram of fused deposition modelling [90] 23

Figure 1.14: Schematic illustration of selective laser sintering (SLS) process [94] 24

Figure 1.15: Schematic diagram of continuous inkjet technology Schematic diagram of demand inkjet technology (left) and 3D inkjet printer (right) [95, 96] 25

Figure 1.16: Images of 3D printed drug loaded tablets, (A) paracetamol and (B) 4-ASA. PGGDA/PEG300 loading in the 3D printed tablets; 35%/65%, 65%/35% and 27

90%/10% from left to right [78]

Figure 1.17: Schematic representation of the printed PVA–Dex21P on the PLGA drop cast film (structure A): (a) top view, (b) side view and (c) scroll configuration [114] 28

Figure 1.18: In situ repair: femoral extrusion printing substrate (left) with induced chondral and osteochondral defects (right) [117] 30

Figure 1.19: Replica Porcine Aortic Valves; 3D digital configuration made by Fab@home software (top) and extruded valves in different angles (bottom) [118] 30

Figure 2.1: Schematic diagrams of preparation of HPMC 2910 gel (1% w/v) and hydro-alcoholic gel [108] 36

Figure 2.2: Schematic diagram of design and extrusion based 3D printing processes of 3D oral solid tablets. 37

Figure 2.3: Schematic diagram of extrusion based 3D printing process. 38

Figure 2.4: Schematic diagram of cartridge/barrel tool filling process. 38

Figure 2.5: Photograph image (right) and schematic diagram (left) of Fab@Home 3D printer. 40

Figure 2.6: Photograph image of RegenHU 3D bio-printer. 41

Figure 2.7: Photographic images of DSC Q2000 and schematic diagram of DSC cell. 42

Figure 2.8: Digital images of SEM (left) and vacuum sputter coater (right). 44

Figure 2.9: Schematic diagram of SEM. 45

Figure 2.10: SEM photograph of a pellet formulation before (left), and after (right) dissolution test [143] 45

Figure 2.11: Photograph image of ATR-FTIR (Agilent Cary 360 FTIR), and schematic diagram of sample platform 46

List of Figures

Figure 2.12: Photograph image and schematic diagram of XRPD (X'Pert PRO, PANalytical, Almelo, Netherlands) 47

Figure 2.13: Schematic diagram of HPLC. 48

Figure 2.14: Photograph images of HPLC 1100. 49

Figure 2.15: Photographic images of Erweka dual drum semiautomatic tablet friability tester. 50

Figure 2.16: Photographic images of tablet hardness tester. 51

Figure 3.1: Photographic image of guaifenesin extended-release bi-layer tablets. 57

Figure 3.2: Chemical structures of (a) guaifenesin, (b) HPMC, (c) MCC, (d) carbopol 974NP polymer, (e) SSG. 57

Figure 3.3: Schematic structural diagram of GBT. 58

Figure 3.4: Schematic diagram of extrusion based 3D printing process of GBTs. 59

Figure 3.5: Schematic diagram of the Fab@Home printer model 2 (right). Images at different scales of 3D printer produced guaifenesin bilayer tablets (L/W/H = 15.5 × 6.3 × 7 mm) and commercial GBT (L/W/H = 16.4 × 9.6 × 5.91 mm). (ii) Top view and (iii) underside view of commercial GBT. (iv) & (v) Gel barrier surrounding commercial GBT and 3D printed bilayer tablet after 2 hrs dissolution test, respectively. (vi) Top view (vii) side view & (viii) underside view of individual 3D printed bilayer tablets (left). The scale bar (ii-viii) is 10 mm. 59

Figure 3.6: Dissolution profile of guaifenesin tablets; GBT-HPMC (6 % w/w), GBT-HPMC (8 % w/w), GBT-HPMC (10 % w/w), GBT-HPMC (14 % w/w) and commercial GBT. The error bars are the standard error in the mean where n = 6. 64

Figure 3.7: Calibration curve of guaifenesin in phosphate buffer media pH 6.8 (left) and acidic media (right) at 274 nm. 64

Figure 3.8: 600 mg guaifenesin bilayer tablet (GBT) (GBT-HPMC 6 % (w/w), 66

GBT-HPMC 8 % (w/w), GBT-HPMC 10 % (w/w) and commercial GBT) subjected to dissolution testing at various times. Scale bar at the bottom of the photograph is in centimetres.

Figure 3.9: Mechanism of drug release from HPMC matrix bilayer tablet. 67

Figure 3.10: FTIR spectroscopy image of pure guaifenesin, GBT-HPMC (6 % w/w), GBT-HPMC (8 % w/w) GBT-HPMC (10 % w/w) GBT-HPMC (14 % w/w), and SR layer of commercial GBTs (left), and pure guaifenesin, IR layer of the 3D printed GBTs and IR layer of the commercial GBTs (right). 68

Figure 3.11: XRPD patterns of calculated and pure (as received) guaifenesin. 69

Figure 3.12: XRPD patterns of pure guaifenesin, GBT-HPMC (6 % w/w), GBT-HPMC (8 % w/w), GBT-HPMC (10 % w/w), GBT-HPMC (14 % w/w), and SR layer of the commercial GBTs (left) and pure guaifenesin, IR layer of the 3D printed GBTs and IR layer of the commercial GBTs (right). 70

Figure 3.13: DSC scans of pure guaifenesin, GBT-HPMC (6 % w/w), GBT-HPMC (8 % w/w), GBT-HPMC (10 % w/w), GBT-HPMC (14 % w/w), GBT-HPMC (16 % w/w), and SR layer of the commercial GBTs (left) and pure guaifenesin, IR layer of the 3D printed GBTs and IR layer of the commercial GBTs (right). 70

Figure 3.14: Box plot summery of weight variation (mg) (i), thickness (mm) (ii), hardness (kg cm-2) (iii) and friability (%) (iv) for GBT-HPMC (6 % w/w), GBT-HPMC (8 % w/w), GBT-HPMC (10 % w/w), GBT-HPMC (14 % w/w) and commercial GBT. 73

Figure 3.15: Representative release plots by fitting experimental release data, from the in vitro release of of 600 mg sustained release guaifenesin bilayer tablets; GBT-HPMC 6 % (w/w), GBT-HPMC 8 % (w/w), GBT-HPMC 10 % (w/w), GBT-HPMC 14 % (w/w) and commercial GBT to (a) Zero-order, (b) First-order, (c) Higuchi and 77

(d) Korsmeyer-Peppas kinetic equations.

Figure 4.1: Image of chemical structures of the active ingredients in the 3 D printed multi-active tablets; (a) nifedipine, (b) captopril, (c) glipizide. 82

Figure 4.2: Schematic structural diagram of captopril osmotic pump and nifedipine and glipizide SR tablet. 83

Figure 4.3: Schematic diagram of 3D printing process of multi-active tablets. 85

Figure 4.4: Photograph of regenHU 3D printer (left) [206], and image of multi-active tablet (right) composed of captopril osmotic pump compartment (bottom), and nifedipine (hole I) and glipizide (hole II) SR compartments (top) and joining layer (middle). 89

Figure 4.5: Representative chromatogram of the 3D printed tablets. 90

Figure 4.6: Cumulative % release from the three drug-loaded compartments of the 3D multi-active tablets. 92

Figure 4.7: SEM micrograph of a captopril osmotic pump tablet before (top) and after (bottom) dissolution test. 93

Figure 4.8: Representative release plots by fitting experimental release data, from the in vitro release of captopril osmotic pump compartments; HPMC (0 %, w/w), HPMC (3.5 %, w/w), and HPMC (7.5 %, w/w) to (a) Zero-order, (b) First-order, (c) Higuchi and (d) Korsmeyer–Peppas kinetic equations. 95

Figure 4.9: Representative release plots by fitting experimental dissolution data, from the in vitro release of nifedipine SR compartments; HPMC (3.5 %, w/w), HPMC (7.1 %, w/w), and HPMC (10.7 %, w/w) to (a) Zero-order, (b) First-order, (c) Higuchi and (d) Korsmeyer–Peppas kinetic equations. 96

Figure 4.10: Representative release plots by fitting experimental dissolution data, 97

from the in vitro release of glipizide SR compartments; HPMC (7.1 %, w/w), HPMC (10.7 %, w/w), and HPMC (14.2 %, w/w) to (a) Zero-order, (b) First-order, (c) Higuchi and (d) Korsmeyer–Peppas kinetic equations.

Figure 4.11: XRPD patterns of pure nifedipine, Nif-HPMC (7.1 % w/w), lactose, PEG 6000, and HPMC (left) (from the top to the bottom), pure glipizide, Glip-HPMC (10.7 % w/w), tromethamine, lactose, PEG 6000, and HPMC (middle) (from the top to the bottom), and pure captopril, Cap-HPMC (0 % w/w), lactose, NaCl, and MCC (left) (from the top to the bottom). 98

Figure 4.12: FTIR spectra of pure glipizide, and Glip-HPMC (10.7 % w/w) formulation (left), and pure nifedipine, and Nif-HPMC (7.5 % w/w) formulation (middle), and pure captopril, and Cap-HPMC (0 % w/w) formulation. 99

Figure 5.1: image of chemical structures of the active ingredients in the 3 D printed polypill; (a) Atenolol, (b) ramirpil, (c) aspirin, (d) hydrochlorothiazide, (e) pravastatin. 106

Figure 5.2: Schematic structural diagram of the polypill design, showing the aspirin and hydrochlorothiazide immediate release compartment and atenolol, pravastatin, and ramipril sustained release compartments. 107

Figure 5.3: Schematic diagram of 3D printing process polypill. 108

Figure 5.4: Photograph of regenHU 3D printer (left) [206], and image of multi-active tablet (right) (5.85mm (height) × 6mm (radius) composed of SR compartments, and IR dotted compartment. 111

Figure 5.5: Representative Chromatogram of the 3D printed polypill. 112

Figure 5.6: In vitro cumulative drug release profile of each drug from the five drug-loaded compartments of the polypill. 113

Figure 5.7: XRPD patterns of the calculated and reference (measured) aspirin (top- 115

left), hydrochlorothiazide (top-right), atenolol (bottom-left), and ramipril (bottom-right).

Figure 5.8: XRPD patterns of ASA-HCT-formul., pure aspirin, pure hydrochlorothiazide, (polyvinylpyrrolidine) PVP k30, and sodium starch glycolate (top-left), Pra-formul. (HPMC 15% w/w), pure pravastatin, lactose, and HPMC (top-right), Aten-formul. (HPMC 15% w/w), pure atenolol, lactose, and HPMC (bottom-left), and Ram-formul. (HPMC 15% w/w), pure ramipril, lactose, and HPMC (bottom-right). 116

Figure 5.9: FTIR spectra of pure actives; aspirin (top left), hydrochlorothiazide (top left), pravastatin (top right), atenolol (bottom left), and ramirpil (bottom right) and its formulations (from the top to the bottom). 118

Figure 5.10: Representative release plots by fitting experimental release data, from the in vitro release of ASA_HCT-IR compartment to (a) Zero-order, (b) First-order, (c) Higuchi and (d) Korsmeyer–Peppas kinetic equations. The first four data points (5, 15, 30, and 60 min) only were used due to the drug release being complete. 119

Figure 5.11: Representative release plots by fitting experimental release data, from the in vitro release of pravastatin sustained release compartment; PRA-HPMC (15 %, w/w), ATEN-HPMC (15 %, w/w), and RAM-HPMC (15 %, w/w) to (a) Zero-order, (b) First-order, (c) Higuchi and (d) Korsmeyer–Peppas kinetic equations. 120

Figure 6.1: Schematic diagram represents how application of 3D printer in manufacturing distribution could change the drug manufacturing process. 128

Figure 6.2: Schematic diagram continuous process of 3D printer of oral solid dosage forms. 129

LIST OF TABLES

Table 1.1: Examples of common excipients and their main roles in drug formulation [7] 2

Table 1.2: Different types of tablets dosage forms; tablets ingested orally, used in oral cavity and other tablets used by other routes [19, 20] 14

Table 3.1: The percentage composition of various ingredients in guaifenesin IR feed stock (dried formulae). 60

Table 3.2: The percentage composition of various ingredients in guaifenesin SR feed stock (dried formulae). 60

Table 3.3: Percentage of weight variation of 3D printed formulation and commercial bilayer tablets. 72

Table 3.4: Fitting experimental release data, from the in vitro release of GBT-HPMC (6 % w/w), GBT-HPMC (8 % w/w), GBT-HPMC (10 % w/w), GBT-HPMC (14 % w/w) and commercial GBT to (a) Zero-order, (b) First-order, (c) Higuchi and (d) Korsmeyer-Peppas kinetic equations at different dissolution mediums; 12 hrs (acidic medium (2 hrs)-buffer medium (10 hrs)). 76

Table 4.1: The composition of various ingredients in captopril formulation at different HPMC 2280 concentration (% w/w) feed stock (dried formulae). 85

Table 4.2: The percentage composition of the coating for captopril formulation in feed stock (dried formulae). 86

Table 4.3: The percentage composition of various ingredients in the joining layer feed stock (dried formula). 87

Table 4.4: The percentage composition of various ingredients in nifedipine and glipizide formulation feed stock. 88

List of Tables

Table 5.1: The weight percentage composition of various ingredients in cellulose acetate shell for SR formulation in feed stock (dried formulae). 108

Table 5.2: The weight percentage composition of various ingredients in atenolol, pravastatin, and ramipril formulation feed stock for the sustained release compartments of the polypill. 109

Table 5.3: The weight percentage composition of various ingredients in aspirin and hydrochlorothiazide IR formulation feed stock for the IR compartment of the polypill. 110

Table 6.1: Outlining the key properties of different types of the 3D printers used in the this thesis 126

Chapter 1 Introduction

1.1. Oral solid dosage forms

Capsules and tablets are the most frequently administered oral solid medicaments [1]. These solid dosage forms contain a uniform quantity of medicine with or without diluents. They are administered as a single unit and are referred to as solid unit dosage forms [2]. Tablets are defined as oral solid pharmaceutical dosage forms prepared by either single or multiple compressions of drug and/or excipient particles (and in certain cases with molding). They can contain one or more active pharmaceutical ingredient (APIs) blended with number of excipients such as disintegrants, binders, and filler or diluents [3, 4]. Tablets differ in their shape, size, and weight according to amount of drug in each single unit dose and method of administration [5]. The oral route remains the most used for drug administration among pharmaceutical dosage forms [3]. This is basically because of ease of mass manufacture, safe and convenient way of drug administration, ease of swallowing (for most patients), accurate dosing, low price and more physically and chemically stability compared with liquid dosage forms. However, oral tablets have number of challenges such as they are not generally suitable for poorly water-soluble drugs (low bio-availability), some medicines resist compression into dense compacts, bitter testing drugs, stomach irritation, and difficulty of swallowing in some patient groups (e.g. children and unconscious patients) [3, 4]

1.2. Tablets manufacturing process

In the tablet manufacturing process, it is important that every tablet contains an accurate quantity of active ingredient and has good physical and mechanical properties to pass the quality control regulations and deliver safe products into patients. Furthermore, improper or insufficient mixing of powder blend and particles segregation due to different powder densities and poor particle size distribution may lead to unacceptable content uniformity and batch fail. Flow properties, formulation stability, and physico-chemical properties of active ingredients are also should be addressed during the tablet manufacturing process. Materials with poor flow properties should be granulated to ensure good particle size distribution and homogenous mixture before compressed into tablets. Two different granulation techniques are frequently used in pharmaceutical industries: dry and wet granulation. Materials with good flow and compression properties can be directly compressed [6].

1.2.1. Ingredients used in tablets formulation

During the normal manufacturing process of pharmaceutical tablets, different excipients are added in addition to the active ingredient, to improve for example drug flowability, tablet compressibility, and physical properties of the final product. Excipients should be pharmaceutically inactive and not decrease the active ingredient stability (Table 1.1) [7].

Table 1.1: Examples of common excipients and their main roles in drug formulation [7].

Name of excipient	**Main function in drug formulation**
Lactose, mannitol, sorbitol, and MCC*	Diluent, filler, and bulking agent
PVP, sorbitol, sodium alginate, glucose, gelatin, and cellulose derivatives	Binder and adhesive
MCC*, cross-linked PVP**, SSG***, alginate, and crosscarmellose	Disintegrants to facilitate tablets breaking up when in contact with water
Stearic acid, magnesium stearate, talc, and colloidal silica	Lubricants and glidant to prevent tablets adhering to the surface of dies and punches
Mannitol, lactose, aspartame and saccharin	Flavoring agents, used to give a more pleasant taste or to mask an unpleasant one

MCC* = microcrystalline cellulose, PVP** = polyvinylpyrrolidone, and SSG*** = sodium starch glycolate.

1.2.2. Granulation and direct compression processes

Tablets are formed of compressed powder, and can be manufactured via different processes including granulation (dry and wet) and direct compression.

1.2.2.1. Dry and wet granulation

Granulation is used to bring powder particles together, increase powder flowability, density, and compressibility. In wet granulation, an accurate amount of a binder solution is added to the powder mixture causing agglomeration of powder particles. A large volume of binder causes over-wetting of powder particles and produces hard granules, whereas a low volume of binder causes under-wetting of powder particles and produces weak and fragile granules. Hydroxypropyl methyl cellulose (HPMC), polyvinylpyrrolidone (PVP), and polyethylene glycol (PEG) are very common binders. In dry granulation, the powder mixture is

compressed at low pressure to form a compact tablet and then broken up into free flowing uniform granules (Fig. 1.1) [8-11].

1.2.2.2. Direct compression

In direct compression processes, there is no mechanical treatment and physical modification for the powder mixture after mixing process (Fig. 1.1). Formally, the powders or crystalline materials have all the required physical characteristics to give good compressed tablets [8-11]. It is clear that the direct compression process is more preferred than granulation technique because of its simplicity and low run cost. However, direct compression is not always applicable for all materials, because some compounds do not have the specific properties required to be successfully compressed [12]. Furthermore, each one of the above mentioned methods can introduce difficulties in the manufacture of medicine (e.g., drug degradation and form change), leading to possible batch failures and difficulties in optimisation of formulations [8-11].

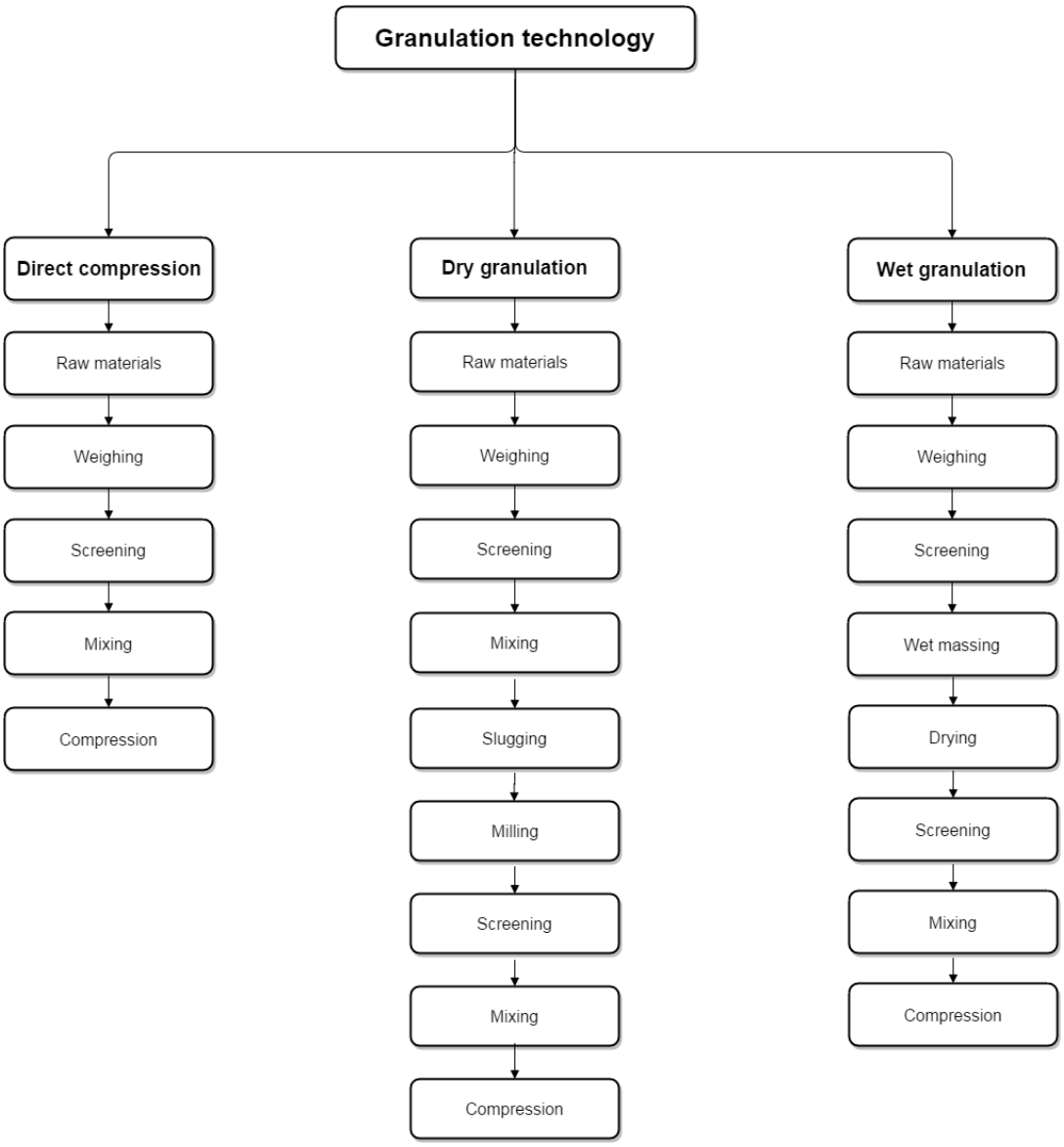

Figure 1.1: Schematic diagram of granulation methods by different techniques [6].

1.2.3. Granule lubrication

This is an important post-granulation step where powdered lubricants like magnesium stearate or stearic acid are used to cover the granules before introduction into the tablet press to avoid tablets sticking into the die [13].

1.2.4. Powder compaction

During powder compression (a volume reduction), many stages have been identified before the final compressed tablet is produced (Fig. 1.2). The first stage is called the consolation phase where the granules or powder particle are adopted in a more efficient packing. During the second stage (reversible or elastic deformation), any decrease or removal in the applied force the packed granules will return into the consolidation phase (the first phase). In the third stage (irreversible or plastic deformation), the applied force is very critical parameter; if excess or quick force is applied brittle-fracture and fracture-debonding of the compressed tablet can occur, respectively. Generally, if any powders or granules have good plastic properties under compression, they will likely form excellent compact [1].

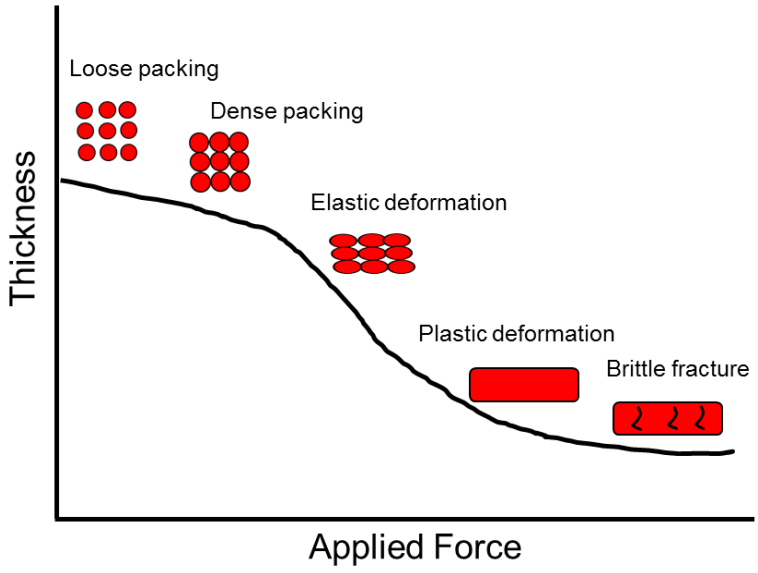

Figure 1.2: Powder compaction stages [1].

1.2.5. Compression methods

After a powder blend is granulated and lubricated, the next step is to produce good pressed tablets with an accurate amount of active drug and good mechanical properties. The number of tablets and speed of the production line are very important when we talk about large scale tablet production. Different tablet presses or tableting machines are used in pharmaceutical

industries ranging from inexpensive low production capacity machines (single-station presses) which can produce thousands of tablets per an hour to expensive, fully computerized, and high production capacity machines (multi-station rotary presses) that can produce hundreds of thousands of tablets per hour. The tablet press equipment should allow the operator to control tablet dimension, shape and the amount of active drug per tablet [14].

1.2.5.1. Single-punch tablet machine

A type of low-volume tableting machine which is commonly used in pharmaceutical industry. It has the capacity to produce thousands of tablets per hour. It can produce one tablet a time. The "punch" in the single-punch tablet machines consisted of two pieces of cast tubular metal (Fig. 1.3). The upper metal piece has a single end which is tapered into a small rod. The lower metal piece has a small hole in the top end of the tube so the upper metal will just fit into the small cavity. Once the powder mixture is filled into the cavity, a press which is fitted into the punches is depressed and released. This means that tablet is pressed and then ejected out of the cavity. Different size and shapes of punches sets are available to allow the production of tablets with different sizes and compression strengths [15].

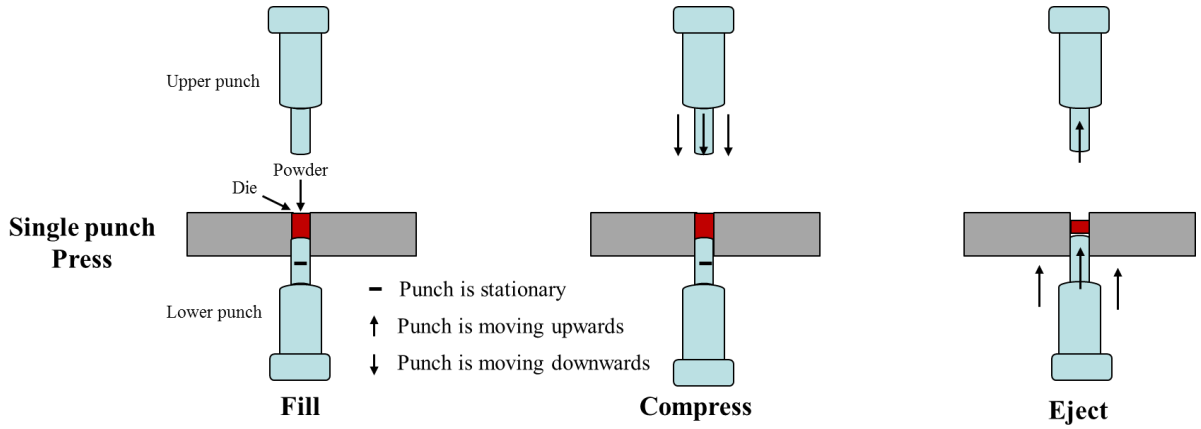

Figure 1.3: Schematic diagram summarizing the main steps when using a single-punch to produce a tablet.

1.2.5.2. Rotary tablet machine

In a rotary tablet machine (multi station presses) the powder/granules are emptied into dies through the feed frame connected to the hopper (Fig. 1.4). The granules are compressed when the upper and lower punches pass between a pair of rollers. The excess powder/granules are wiped off by a blade and moved back into feed frame. The thickness of the tablets is controlled movement of the upper and lower punches which is guided by a fixed cam tracks. After powder is compressed, the upper punch raising cam is used to release the upper punches and raise the lower punches, and the tablets are pushed up above the surface of the dies. The tablet then removed by a sweep off blade and slide down to the tablet collector. At the same time, the lower punch reenters the pull down cam and the cycle is repeated [14].

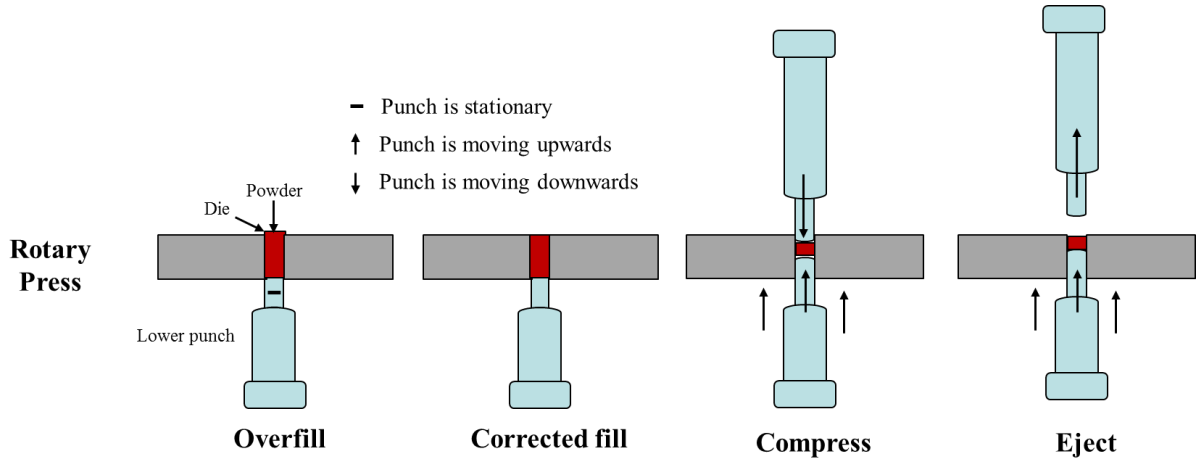

Figure 1.4: Schematic diagram of a rotary tablet press cycle.

1.2.6. Molded Tablets

Molded tablets have number of advantages over other press techniques; they disintegrate quickly in the presence of water and the composition of the dosages can be easily adjusted. Molded tablets are generally prepared by mixing the drugs with sugars such as lactose, dextrose, sucrose, mannitol or other excipients like calcium carbonate or calcium phosphates. Binders like alcohol (typically between 50 – 80 % v/v) and water are frequently used to make molded tablets. After materials weighing and a proper mixing process, the powder mixture is

sieved through an 80-100 mesh sieve. Then the binder is added gradually until paste with good consistency is achieved. The paste is filled into the cavities and pressed into the cavity plate (Fig. 5). A hard rubber spatula instead of metals ones should be used to press the material into the cavities to avoid scratching the metal plate surface. Once the cavity plate is loaded with the medicated soft paste, the plate is then placed on the peg plate where the pegs should be aligned with the holes. The cavity plate is then carefully pressed down onto the peg plate to push the tablets out of the plate cavities. The molded tablets are left on the pegs surface for some time for drying [1].

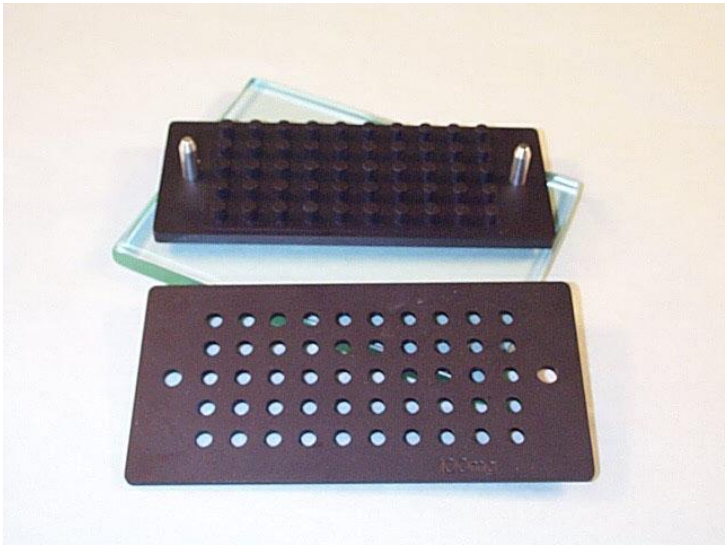

Figure 1.5: Tablet triturate moulds.

1.2.7. Coating processes

Film coating of formed tablets or granules is another common technique used in pharmaceutical industries to control drug release profile, improve drug stability, protect some actives from digestive juice, and mask the unpleasant odour and bitter taste of some medicines. Film coating typically employs a thin polymeric membrane (thickness typically ranging between 20-100 μm) which is used to coat pharmaceutical oral solid tablets [16]. Generally different types of coating can be used to coat oral solid tablets; sugar coating and enteric coating [17, 18]. Common materials used are Eudragit, cellulose derivatives such as

hydroxylpropyl methylcellulose (HPMC), methyl cellulose (MC), hydroxypropyl cellulose (HPC), cellulose acetate (CA), and povidone [7, 17].

1.3. Types of oral solid dosage forms (tablets)

There are different types of tablets available in the market and each type is manufactured to give a certain release profile [19, 20].

1.3.1. Compressed Tablet (CT)

These tablets are manufactured by pressing of powders or granulations with no coating process. It is usually used to deliver drug/s over a short period of time. The materials to be compressed should have good physical properties, such as free flowability, lubrication, and cohesiveness. Most of compressed tablets composed of active ingredient in combination with lubricant, disintegrant, binder, and diluent (filler). In many cases, FDA approved colorants, sweeteners, flavours may be added. Immediate release (IR) tablets are a typical example of the compressed tablets and defined as tablets which release their active ingredients immediately after oral administration [21].

1.3.2. Multiple Compressed Tablets (MCTs)

MCTs are defined as a compressed tablets made by multiple compression cycles. This type of tablet is preferred when there are stability issues between active ingredients and/or one of more excipients or if there is uniformity problem during mixing process of two of more actives. MCTs are also used to achieve repeated or prolonged action [22-25].

1.3.2.1. Layered tablets

Layered tablets are made when additional tablet granules are pressed on a previously compressed tablet. Multi-layered tablets of two, three or more layers can be produced using this technique. Special compression stations are required to produce multi-layered tablets with acceptable physical properties [1]. Multi-layered tablets have some advantages over

conventional ones: they can increase bioavailability; release multiple actives with better execution release profiles; minimise burst release effect; and quick initial drug release rate, reduce drug dosing, higher drug loading, synergetic effect, and ability to separate incompatible actives [26, 27]. UROXATRAL® (alfuzosin HCl extended-release tablets), Mucinex (guaifenesin extended-release bi-layer tablets) are some examples of the currently available multi-layered tablets. However, manufacturing of multi-layered tablets is time consuming, requires a skilled operator, is more complex than conventional tableting, and risks such as separation and capping may occur if compression force is not optimized [26, 27].

1.3.2.2. Press-coated tablets

This is another type of multi-compressed tablets, where a dry coating is used to coat a previously compressed core tablets. Press-coated tablets give advantages over a conventional compressed tablet by the fact that they can used as enteric coated tablets to avoid drug degradation by stomach enzymes, masking the unpleasant taste of bitter compounds, and provide separation of two or more incompatible active ingredients [28].

1.3.3. Oral osmotic drug delivery systems (tablets)

Oral osmotic pump tablets are used to make oral drug administration more accurate, precise in their drug release and hence more convenient for patients than the conventional compressed tablets. The drug release profile from osmotic pump tablets follows zero order kinetics. Osmotic pump tablets are composed of core tablets consisting of active ingredient/s and excipients that swell and/or osmotic properties sealed with a semipermeable or controlled porosity coating membrane/shell. One or more laser drilled orifices of different diameters may be introduced into the semipermeable membrane to allow drug release under the osmotic pressure. Different osmotic pump systems are available: elementary, push pull, and controlled porosity osmotic pump systems [29, 30].

1.3.3.1. Controlled Porosity Osmotic Pump Tablets (CPOPTs)

CPOPTs are osmotic pump tablets in which a core tablet is coated with semi-permeable membrane which contains water soluble leachable pore forming agents (e.g., sorbitol, urea, PEG, KCl, and mannitol) (Fig. 1.6). The membrane is impermeable to solute but permeable to water. The pore forming agent should be well dispersed thought out the membrane wall to achieve controlled drug release over a period of time. Once a CPOPT is exposed to aqueous media in the stomach the pore forming agent starts to leach out leaving pores in the membrane wall (sponge like structure) which then allows drug release as a result of the osmotic pressure changes between inside and outside the tablet. Drug release from the porous membrane depends on membrane thickness, drug solubility, percentage of pore forming agents, and the osmotic pressure across the permeable membrane [31-33].

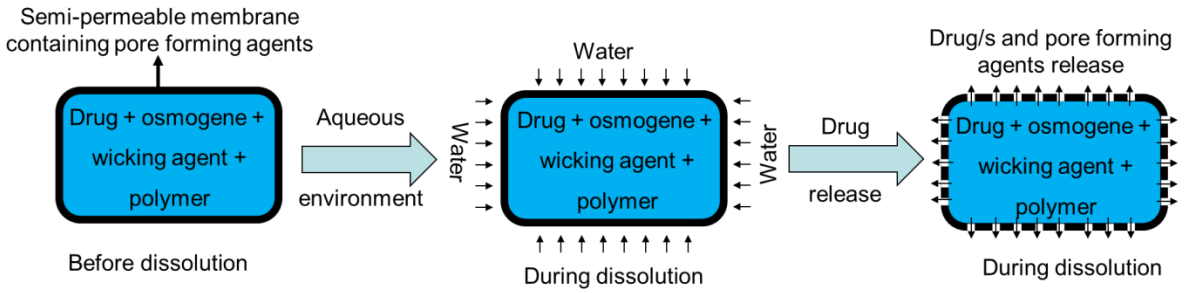

Figure 1.6: Schematic diagram of controlled porosity osmotic pump tablet before and during dissolution process.

1.3.3.2. Elementary Osmotic Pump Tablets (EOPTs)

This type of tablet is formulated by coating a core tablet (composed of active ingredient and osmogene with a suitable osmotic pressure) with a semi-permeable membrane (e.g., cellulose acetate) (Fig. 1.7). The coated tablets are drilled by a laser or mechanical drill to create a small orifice at the top of the tablet. When the tablet is exposed to the aqueous medium in the stomach, the water penetrates the semipermeable membrane and leads to saturate the core and generate hydrostatic pressure which in turn force the drug to be released through the orifice over extended period of time [33].

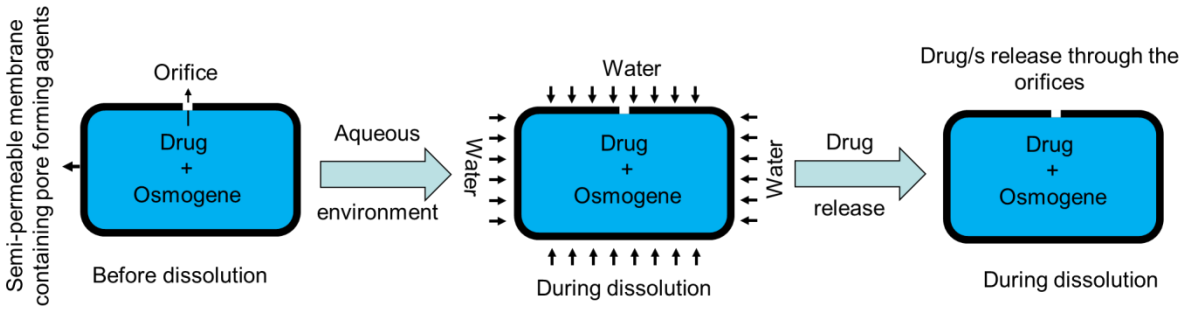

Figure 1.7: Schematic diagram of elementary osmotic pump tablet before and during dissolution process.

1.3.3.3. Push Pull Osmotic Pump Tablets (PPOPTs)

This osmotic system is used to deliver poorly soluble and very soluble drugs at a controlled release rate. It is composed of bilayer core (tablet) coated with a semipermeable membrane.

A small orifice is made by a laser or mechanical drill at the side of drug containing layer (Fig. 1.8). The bilayer tablet is manufactured by a multiple compaction process. The upper layer of the bilayer tablet contains active drug, osmogenes, and other excipients. The lower layer is composed of polymeric osmotic agent (polymeric push compartment). When the push pull osmotic pump tablet is exposed to the aqueous medium, the osmogenes in both layers attract the water molecules into all tablet sides and penetrate the semipermeable membrane causing drug suspension in the upper layer and expansion of the polymeric osmogenes in the lower layer. This process creates osmotic pressure inside the tablet and leads to the drug being 'pushed' out the tablet through the delivery orifice [34].

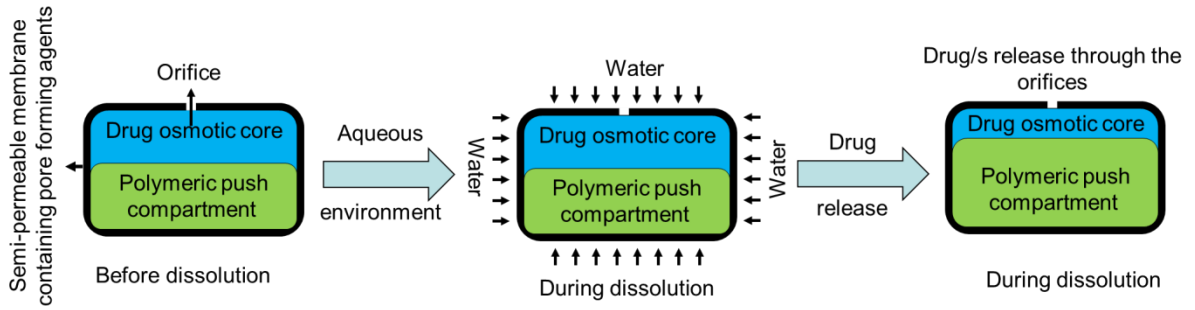

Figure 1.8: Schematic diagram of push pull osmotic pump tablet before and during dissolution process.

1.3.3.4. Sandwiched Osmotic Pump Tablets (SOPTs)

SOPT is another type of osmotic pump delivery system which is manufactured by coating a triple layered tablet (core) with a semipermeable membrane (Fig. 9). The triple layered tablet is produced by a multiple press process, and composed of two drug layers (upper and lower), and a sandwiched push polymeric layer (middle). Two small holes on both tablet faces are drilled by a laser or mechanical drill to create delivery orifices. When the SOPT is exposed to the aqueous medium, the polymeric osmogenes in the middle layer draws the water molecules surrounding the tablet through penetration the semipermeable membrane. This

leads to the polymer expanding and 'pushing' the drug in both upper and lower layers out through the delivery orifices [33].

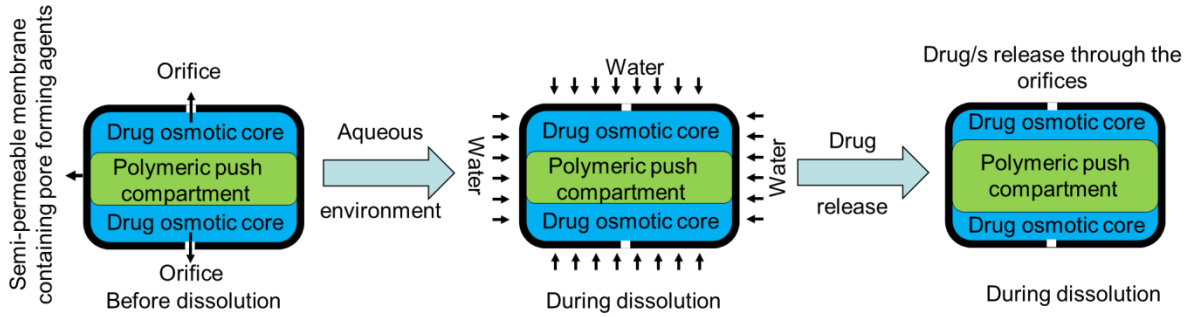

Figure 1.9: Schematic diagram of sandwiched osmotic pump tablet before and during dissolution process.

The below table 1.2 shows examples of different tablets type with a certain release profile (Table 1.2) [19, 20].

Table 1.2: Different types of tablets dosage forms; tablets ingested orally, used in oral cavity and other tablets used by other routes [19, 20].

Type of tablet dosage forms	**Reason/s or advantages**
Repeat action tablets	Release drug/s in intestine
Delayed action and enteric coated tablets	Release drug/s after some time delay, or in intestine
Sugar coated tablets	Elegant, glossy, easy to swallow
Chewable tablets	Used for large tablets
Buccal and sublingual tablets	Quick systemic action (avoiding first-pass effect)
Effervescent tablets	Producing solution within short period of time
Implantable tablets	Prolonged drug release from months to years
Vaginal tablets	Slow dissolution and drug release in vaginal cavity

1.4. Drug release mechanisms from polymeric matrix devices

One of the challenges for conventional dosage forms is producing complex formulations able to control drug release over extended periods of time or to contain a veriable amount of API. Failure to achieve these goals can lead to dosing outside the therapeutic widow [35]. Controlled release formulations offer prolonged drug release from matrix tablets and keep plasma concentrations at the desired therapeutic level with a lower incidence of side effects, decreased dosing frequency, and improved patient compliance [36]. Polymers are frequently used as sustained release matrices to control drug release over long periods of time and to improve drug safety and efficacy [35]. Simple matrix tablets can be prepared by dispersing or dissolving an active ingredient within a suitable polymer until a homogenous physical mixture is ready for extrusion, moulding or compression. The prediction of the drug release process from a drug delivery system is carried out using mathematical models and such models play an important role in drug delivery system design and improvement [37]. Different release mechanisms can be modelled and used to control drug release from polymer matrix devices; swelling [38-40], erosion [41], and osmosis [42, 43].

1.4.1. Drug release by swelling

Bio/mucoadhesive drug delivery systems (B/MDDSs) are common systems for oral controlled release formulations are defined as hydrophilic 3D crosslinked polymeric networks with absorption capacity and a swelling property in aqueous media [44]. B/MDDSs have bioadhesive properties which allow them to stay in the gastro-intestinal-tract (GIT) for a long period of time to provide sustained drug release [35]. Diglycol dimethacrylate and methyl carbitol methacrylate are good polymeric hydrogels examples [39]. When hydrogel based matrix tablets contact an aqueous environment, the hydrogels matrix will start to swell and increase in the thickness followed by dissolution and complete drug release over an extended period of time [38].

1.4.2. Drug release by erosion

Polymeric erosion is another mechanism used for drug release from polymeric matrices. It can be divided into surface and bulk erosion methods (Fig. 1.10) The term of erosion refers to a physical phenomenon which depends on dissolution and diffusion process in which material depletion occurs [45].

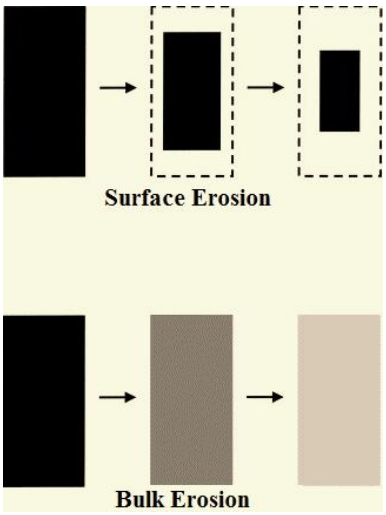

Figure 1.10: Schematic illustration of surface and bulk erosion [41].

Surface erosion takes place when the rate of water molecules permeation in to a polymer bulk is slower than the erosion rate. This type of erosion gives good protection for water labile drugs up to the time of drug release. Drug release by surface erosion follows zero-order kinetics where the external structure of the polymer remains almost unchanged and the drug undergoes limited diffusion. Bulk erosion starts when the water molecules penetrate into the polymeric bulk more rapidly than the erosion rate. Polyanhydrides and polyorthoester are examples on surface erosion, whereas polyesters such as poly lactic acid (PLA) is example of a bulk eroding polymer [35, 41].

1.4.3. Drug release by osmosis

In osmotic drug delivery systems (ODDSs) (see section 1.3.3), drug release follows zero-order kinetics and occurs due to the difference in osmotic pressure between inside and outside

microporous/semipermeable membranes [46]. The mechanism starts when the osmotic tablets contact an aqueous environment and water starts to penetrate the semipermeable membrane (Fig. 1.11) [47, 48]. The osmotic pressure starts as a result of different solute concentration, where a drug diffuses from an area of higher solute concentration to an area of lower solute concentration at a controlled rate [47]. Sapna *et al.* formulated an osmotic device to control the release of pseudoephedrine HCl 60mg through a semipermeable cellulose acetate membrane over period of 12 hours. Pseudoephedrine has short plasma half-life (5-8 hrs), and should be given from three to four times a day to retain the plasma solute concentration at a fixed level [49]. Ditropan XL® (oxybutynin chloride 5, 10 mg), Procardia XL® (Nifedipine), and Sudafed 24® (pseudoephedrine) are examples of ODDSs [43].

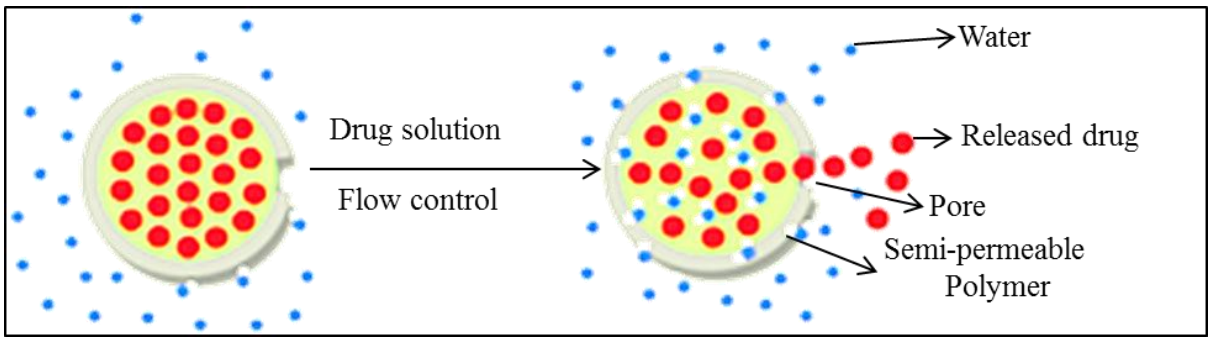

Figure 1.11: Schematic diagram showing delayed flow of the drug solution because of osmotic potential gradient through a microporous membrane [48].

1.5. Stability in drug formulations

The long term stability of drug formulations is one of the major issues in pharmaceutical industries [50]. It is defined as the ability of a particular preparation in a particular package to retain its physical, chemical, microbiological and toxicological conditions within the specified limit determined by the manufacturers over the predetermined time period of storage and use [50]. For example, in 1996, the pharmaceutical company, Abbott, marketed Ritonavir capsules (antiretroviral drug used to treat human immunodeficiency virus-HIV)

[51]. However, two years later, there was a concern in dissolution profile of the drug capsules, due to conformational polymorphism [51]. Moisture, light and oxidation are the main factors which can affect product stability [8-10].

Humidity is another factor which can affect the drug stability within pharmaceutical solid dosage forms [52, 53]. For instance, aspirin tablets are moisture sensitive and slowly degrade to yield acetic acid and an irritating compound, salicylic acid [54]. The latter compound is considered an impurity in aspirin powder which can lead to a decrease in drug purity and initiate abdominal pain due to stomach irritation [29]. Photolysis (decomposition by light) is another factor which can cause significant degradation between photo-sensitive pharmaceutical ingredients [50]. For example, an intravenous (IV) solution of sodium nitroprusside degrades within 4 hours and loses its antihypertensive property if exposed to direct sunlight (ultraviolet irradiation). However, the shelf-life for the same solution can be up to one year if kept away from UV light (e.g., using an amber glass bottle) at room temperature [50]. Finally, oxidation can cause degradation reactions in pharmaceuticals through oxidation processes. For instance, 5-aminosalicylic acid is readily oxidised to quinone-imine, and degrades to a polymeric compound [55].

From all the above-mentioned examples, it is clear that understanding long term stability testing is an essential stage before a drug can come to the market. This provides one of the main drivers to explore techniques capable of point-of-care manufacture (and hence relatively rapid use) such as extrusion based 3D printing. A cheap portable 3D printer has the potential to produce functional solid dosage forms with an accurate tailored dose for relatively quick use by patients.

1.6. Challenging in fabrication of complex oral tablets with a desired release profile

Chronic diseases cause different symptoms and complications which progress by time if left untreated or if an insufficient dose or the wrong medication is prescribed. Drug release time and profile are very important factors to achieve a desired therapeutic effect in different clinical circumstances [45]. For example, constant rate of drug release (zero order) over time is very important to minimize swings in the blood drug concentration. Such changes in drug concentration may cause undesirable side effects or ineffective treatment if overexposure or underexposure, respectively to a drug with narrow therapeutic is occurs [56]. Another important drug release is pulsatile drug delivery systems. In this system, drug release should suit the circadian rhythms of diseases to achieve optimum therapeutic outcome with a minimum adverse effect. For example, in peptic ulcer disease the acid secretion is increased at the night and the afternoon, and therefore high drug concentration is required during these times to produce rapid effect and reduce the consequence of acid secretion followed by gradual release of drug in a small doses during the rest of time to keep acidic secretion from recurring [56]. To achieve a drug release profile suit the nature of disease, complex design of oral tablets is required.

In addition, the attention to the concept of personalized medicine has recently increased as a scheme that foresees the customization of health care to individual patients [45, 57, 58]. It is widely believed that future improvements in disease treatment will be driven by point-of-care and home-based diagnostics linked with genetic testing and emerging technologies such as proteomics and metabolomics analysis [59]. Personalized medicine could also increases the effectiveness of the prescribed treatment regimen and minimizes their adverse effects such as the side effects linked to overdosing of potent medications or drugs with narrow therapeutic index (NTI) [60]. For example, a pharmacogenetic test (thiopurine S-methyltransferase (TPMT) genotype) was used to determine the dose of 6-mercaptopurine [61-63]. In another examples, vitamin K epoxide reductase complex, subunit 1 (VKORC1) and CYP2C9 genotypes were used to define warfarin doses more accurately [60]. The conventional tableting machines are clearly unsuited to personalized medicine and in addition provide stringent restrictions on the complexity achievable in the dosage form (e.g., multiple release profiles and geometries) and require the development of dosage forms with proven long-term stability [58]. However, how are the requisite 'unique' medicines for each patient to be manufactured on a routine basis? Currently no viable method used in manufacturing of solid dosage forms, such as tablets, is suitable. 3D printing technique is proposed as a promising programmed platform to manufacture very complex tablet geometries with customized drug release profiles and tailored drug doses. This would add more advantages in terms of profit, accurate drug doses, and patient compliance to treatment to the pharmaceutical companies, drug prescribers, patients, respectively.

1.7. Three Dimensional (3D) Printing

1.7.1. Introduction

3D printing is not a new technique, it was invented by Charles Hull in 1984, who achieved a patent for the invention two years later (1986). After releasing the technique to the public, it was only used to transfer electronic data onto paper [64]. However, in the last decade, the applications of 3D printing technology have expanded and developed rapidly to include pharmaceutical fabrication and tissue engineering and regenerative medicine, electronics and other applications [65-69]. In 3D printing, physical objects are fabricated by extrusion, UV curing, depositing, or ink jetting material layers one on top of another [70-72]. These successive layers represent cross-sectional or 2D slices of the virtual object being printed [70]. Pharmaceutical 3D printing is an innovative technique which has recently been introduced as a novel tool in pharmaceutical formulation to fabricate complex oral dosage forms required to achieve specific release profiles or for poorly soluble drugs [45, 58, 72, 73]. 3D printing is a significant platform, it can prints a 3D tablets in a programmed, controlled manner and more accurate drug dosing than the conventional existing technologies [73, 74]. However, it may take a long time to be applied for market products as in manufacturing of pharmaceutical products (only one 3D printed drug Spritam (levetiracetam) was approved by FDA in the 31st of July 2015, an anti-epileptic drug produced by a pharmaceutical company called Aprecia) and drug delivery devices [73].

1.7.2. The current technologies in 3D printing

The development of additive techniques or rapid prototyping (RP) has significantly grown to fabricate 3D artefacts with precise features. Printing a 3D object can take from a few minutes to hours, depending on the type of printer used, the condition and the complexity of the item being fabricated. Over the last two decades, RP has been developed and commercialized to

include stereolithgraphy (SLA), fused deposition melting (FDM), selective laser sintering (SLS), inkjet (IJ) printers and extrusion based 3D printing technique [65, 75-79].

1.7.2.1. Stereolithography (SLA)

SLA is still one the most powerful and flexible tools among all other RP techniques. It is used to construct 3D objects with precise geometry in a short time. The technology basically relies on tracing a first layer of a pre-designed object on a photo-curable polymeric resin or liquid using a UV laser beam (Fig. 1.12). The resin is held within a vat, where a movable platform moves up and down to control the thickness of the cured slice of an object. The laser beams hardens the resin and the platform is moved down at programmed distance and allow tracing the second slice. The process is continued until a 3D object is finished and then removed from the tank for further curing. SLA is an accurate, quick process, and fabricates high resolution 3D objects. However, it requires an expensive instrument, need supports, and further curing of objects after the process [80]. Wang, J., et al. were used SLA 3D printer to fabricate paracetamol and 4-aminosalicylic acid (4-ASA) 3D printed extended release tablets [81].

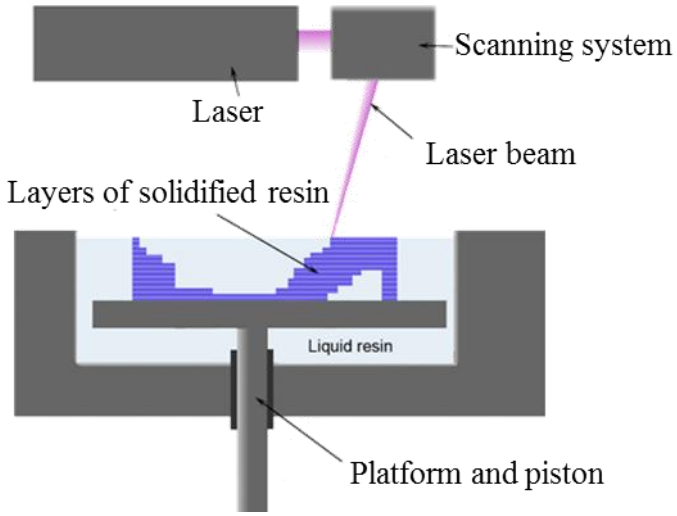

Figure 1.12: Schematic diagram of a typical stereolithography (3D printer) [80].

1.7.2.2. Fused deposition melting (FDM)

FDM is a RP technology developed and patented by Stratasys. In FDM, hot semisolid liquid materials are extruded from an extrusion head which is kept at a controlled temperature just above the melting point of the material being deposited. The materials are extruded through extrusion nozzles side by side on a suitable substrate, until first layer is formed and the process is continued till a 3D object is completely finished (Fig. 1.13). Acrylonitrile butadiene styrene (ABS) and a bioplastic biodegradable material (e.g., polylactic acid (PLA)) are common materials used by FDM. FDM has similar accuracy but, is less expensive than stereolithography. Multi-materials with different properties can be extruded [82, 83]. Skowyra, J., et al., were used FDM 3D printer to fabricate 3D printed prednisolone sustained release tablets [84].

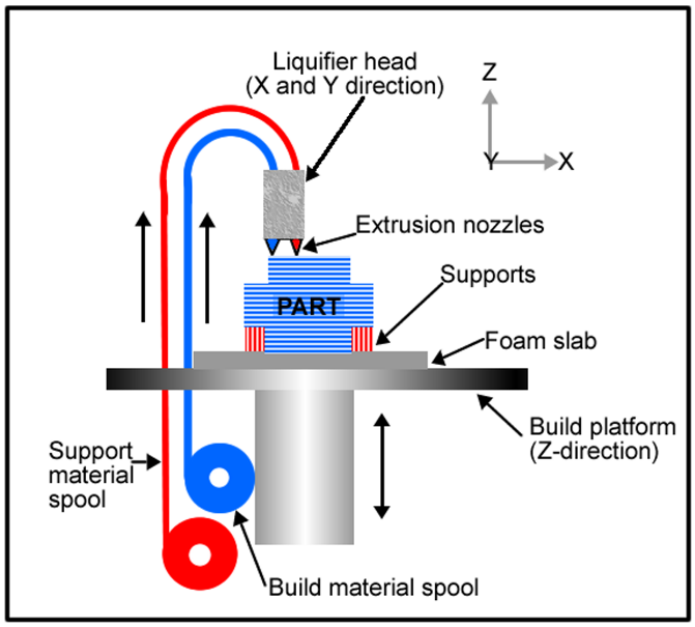

Figure 1.13: Schematic diagram of fused deposition modelling [83].

1.7.2.3. Selective laser sintering (SLS)

SLS is one the most established solid freeform fabrication (SFFF) process in the market. A 3D object is basically fabricated by sintering powder particles deposited on a movable platform using a scanning infrared laser (Fig. 1.14). Like other additive processes, once the first layer is completely fused, another powder layer of a controlled thickness is pushed up by a powder delivery piston and spread on the top of the fused layer using a roller or blade. The process is continued until a 3D model is finished. SLS is an accurate and flexible process. A wide range of materials can be printed with SLS such as, wax, nylon, elastomer, glass, ceramics, and stainless steel materials. Furthermore, the excess powdered materials can be recycled. The main drawbacks of SLS process is that the final 3D model has a relatively rough surface and hence, requires further treatment [80]. Kinstlinger, I.S., et al., were used SLS 3D printer to fabricate a 3D printed polycaprolactone (PCL) lattice for application in bone tissue engineering studies. The findings showed that human mesenchymal stem cells were able to adhere, survive and differentiate on smooth PCL scaffolds [72]. The PCL scaffold perhaps could be used as a good biodegradable implantable devices for controlled drug delivery systems [71].

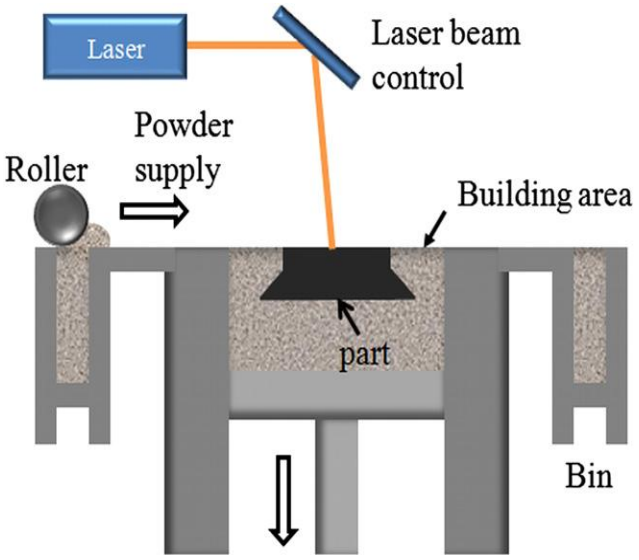

Figure 1.14: Schematic illustration of selective laser sintering (SLS) process [85].

1.7.2.4. Inkjet (IJ) printing

Inkjet printing is operated in continuous or drop on demand (DOD) modes. In continuous inkjet printing, a liquid jet is formed by pressurizing the ink through a nozzle. Imposing a periodic perturbation is used to achieve spaced droplets with uniform size (Fig. 1.15).

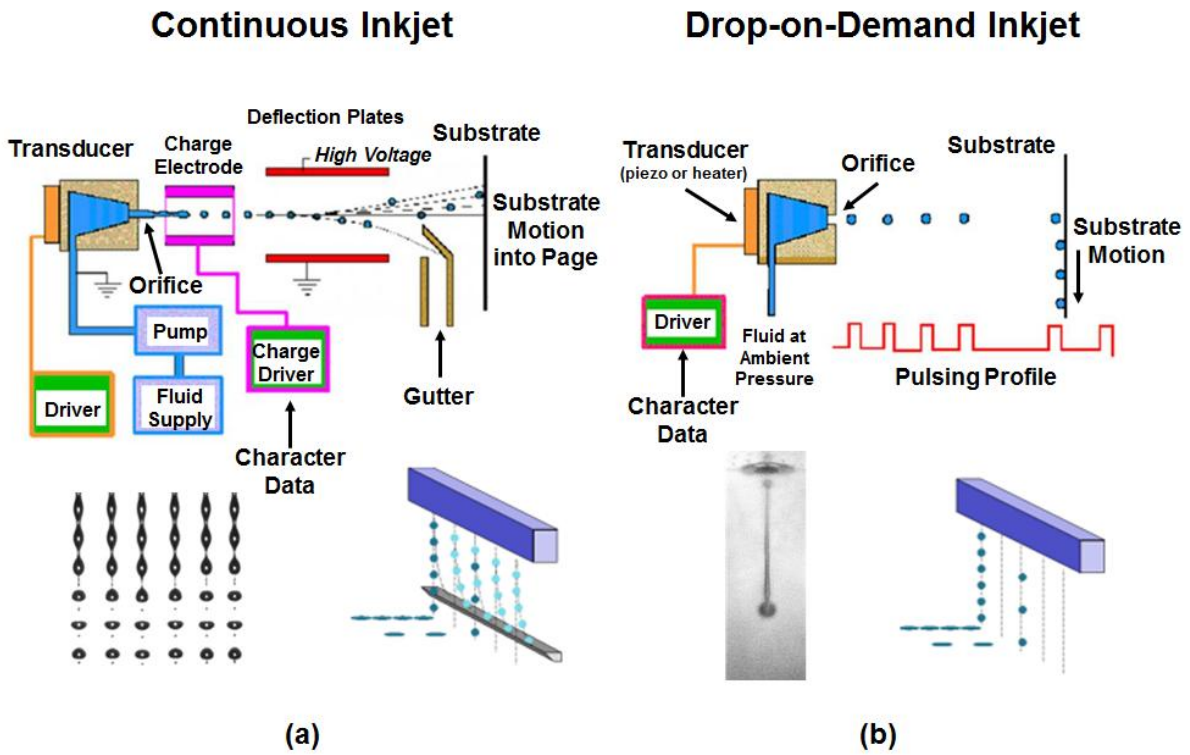

Figure 1.15: Schematic diagram of continuous inkjet technology Schematic diagram of demand inkjet technology (left) and 3D inkjet printer (right) [64, 86].

Currently, this mode is widely used for high speed graphical applications such as, textile printing and labelling. An inkjet based 3D printing system was used to print pharmaceutical formulation [87]. A very thin layer of a powder is delivered on a powder bed surface and sprayed by a selected binding agent through the inkjet head. The binder helps the powder particles to gather and form the shape of the desired product. This process is controlled by means of computer aided design (CAD) [64, 86, 87].

In DOD, excellent control of droplet size and position can be produced (Fig. 1.15) [88]. The ink (the solution to be deposited or printed on a substrate) is dispersed using different mechanisms generating very small droplets [88]. Based on the mechanism or experimental conditions used, DOD can be classified in to four categories; piezoelectric, thermal, acoustic, and electrostatic inkjet [88]. Inkjet based 3D printing technique has high flexibility and potential ability to create objects with defined geometry and surface texture.

An inkjet 3D printer has been used in pharmaceutics to fabricate a new drug delivery system to release paclitaxal (an antitumor drug) at a slow rate with lower toxicity and higher bioavailability than the conventional formulations [89]. Clinically, paclitaxel is only given by intravenous route owing to its poor water solubility and low oral bioavailability [90]. Paclitaxel has high toxicity which could be due to the conventional surfactant (cremophor EL) which added to increase drug solubility [91, 92]. Paclitaxal-loaded monodispersed microspheres were formulated by piezoelectric inkjet printing technology [89, 90]. Solvent evaporation method was used to prepare paclitaxel biodegradable microspheres. The results showed that over (80 %) of the drug were slowly released from the biodegradable microspheres over a period of approximately 50 days [89, 90].

1.7.2.5. Extrusion base 3D printing technique

It is a technique used to construct 3D objects layer by layer. Multiple materials such as polymers, medicated pastes, thermoplastic materials, and hydrogels can be extruded using syringe tools [44, 71, 93, 94]. The most important thing in extrusion based 3D printing is the fact that the materials should be formulated in semi-solid state (pastes). Fab@Home and 3D Discovery® extrusion based 3D printers which were used throughout this thesis are described in more details in Chapter 3, 4 and 5 [66, 94, 95].

1.7.3. Applications of 3D printing techniques

In the last two decades, the printing technology has started to move quickly from the area of newspaper and graphic painting (2D) to act as a novel and promising technique in different research areas, such as life science [96], and drug formulation (3D) [90].

1.7.3.1. Applications of 3D printers in drug formulation

Recently, many studies emphasised the importance of 3D printing technology for the future of drug manufacturing process [45, 65, 71, 81, 84, 97-102]. For example, stereolithography (SLA) was used to fabricate drug-loaded 3D printed tablets with sustained release profiles (Fig. 1.16). In SLA 3D printer, the 3D printed drug loaded tablets were created by focusing a laser beam on a photo-curable resin. In their work, paracetamol (acetaminophen) and 4-aminosalicylic acid (4-ASA) were used as model medications. Diphenyl (2,4,6-trimethylbenzoyl) phosphine oxide and polyethylene glycol diacrylate (PEGDA) were used as a photo-initiator and a monomer, respectively. They successfully printed extended-release paracetamol and 4-ASA tablets containing three different loading (35 %, 65 %, and 90 %) of PEGDA [81].

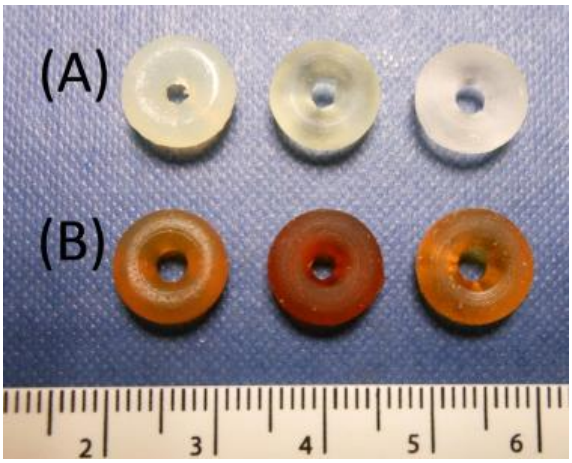

Figure 1.16: Images of 3D printed drug loaded tablets, (A) paracetamol and (B) 4-ASA. PGGDA/PEG300 loading in the 3D printed tablets; 35%/65%, 65%/35% and 90%/10% from left to right [81].

In another example, an extrusion based 3D printing technique was used to fabricate implantable drug delivery assemblies (Fig. 1.17). Different configurations (rolled and layer by layer structures) of PLGA and water-soluble poly (vinyl alcohol) (PVA) were designed using enhanced machine controller (EMC) software. The materials were extruded through a syringe with 100 µm tip diameter and used to encapsulate dexamethason-21-phosphate disodium salt. The drug release from the scaffolds was characterised with dissolution test in a static media of phosphate buffer saline (PBS) solution (10 mM, pH 7.4). The drug release from the structures was successfully controlled over a period of 4-months [100].

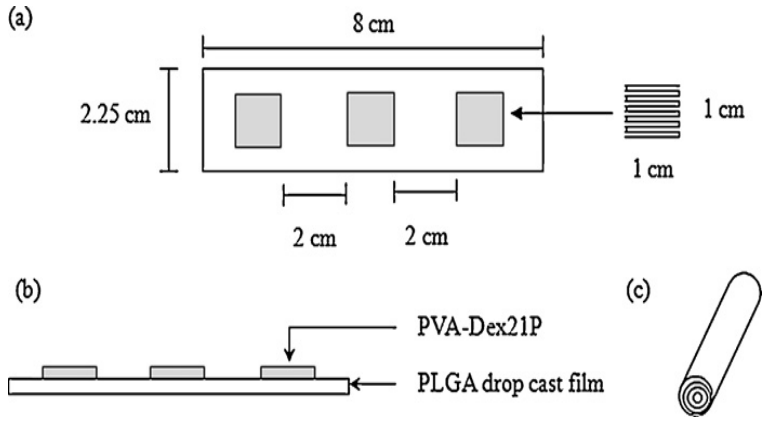

Figure 1.17: Schematic representation of the printed PVA–Dex21P on the PLGA drop cast film (structure A): (a) top view, (b) side view and (c) scroll configuration [100].

In addition, a fused deposition modelling (FDM) 3D printer was used to fabricate drug-loaded 3D printed drug loaded T-shaped implants with controlled release profile over ~ 30 days [71]. In FDM, the long lasting implantable drug-loaded intrauterine device (IUD) was fabricated by extrusion of a hot semisolid of drug loaded PCL from an extrusion head which is kept at a controlled temperature just above the melting point of the drug vehicle (PCL). In their work, indomethacin and polycarbolactone (PCL) were used as a model drug and drug vehicle, respectively. They successfully printed extended-release indomethacin filaments containing three different drug loadings (5 %, 15 %, and 30 %) [71].

More recently, Yajuan S. and Siowling S. have fabricated fully customizable tablets that could deliver drugs with different type of release profile [45]. However, to date no study has showed printing five drugs in a single tablet with a multiple release mechanisms and high drug loadings using extrusion based 3D printing technique [94]. Furthermore, formulation issues such as drug degradation during and after printing processes [65, 84] ink bleeding, migration, and capillary effect due to deposition of binder on powder bed (formulation/binder saturation), poor mechanical properties [101, 102], possible toxicity due to incorporation of photo-initiators, photo-curable polymers or degradants from UV curing could cause obstacles in pharmaceutical industries [45, 81].

1.7.3.2. Applications of 3D printing technology in life science

Based on recent research, 3D bioprinting has a promising future in organ replacement therapy and cardiovascular development ,bone repair [103], and translational medicine [96]. Bioprinting technology has many advantages; it is a novel technology used to print cell pattern and biomaterial scaffold in an accurate way in either 2D or 3D positions [96]. Cohen et al successfully used a Fab@home 3D printer to repair osteochondral defects (Fig. 1.18) [103, 104]. Chondral and osteochondral lesions were *in situ* repaired by deposition of alginate hydrogel and novel matrix made of demineralized bones, respectively. This extrusion process was reproducible and had mean less than (100 µm) of surface extrusion errors. A laser sensor was used to increase the accuracy of the syringe movements in x, y and z directions, scan the workspace pre-and post-printing lesions and achieve quantitative analysis [103].

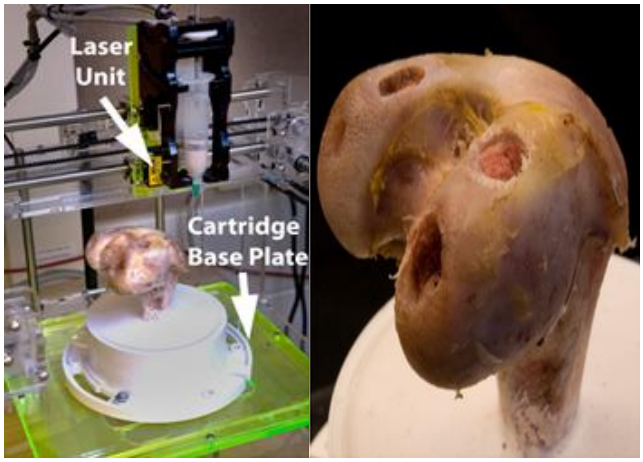

Figure 1.18: In situ repair: femoral extrusion printing substrate (left) with induced chondral and osteochondral defects (right) [103].

At the University of Cornell, Filho et al used modified Fab@home 3D printer to fabricate cardiovascular parts [104]. Different hydrogels; poly-(ester amide) (PEA), alginate, poly-(ethylene glycol) diacrylate (PEG-DA), and commercial photo-initiator were extruded to form replicas porcine aortic valves (Fig. 1.19). The 3D structures had accurate geometry with good mechanical properties [104].

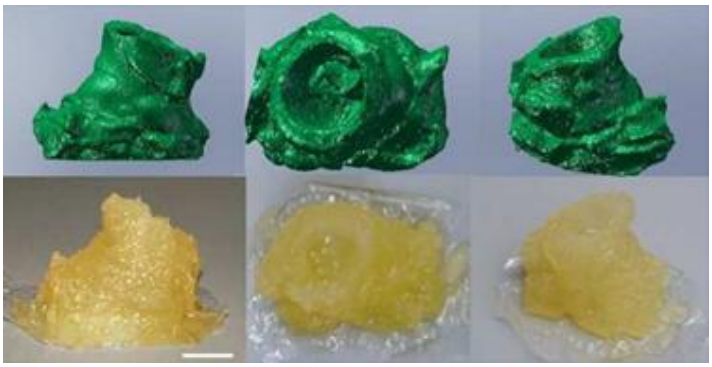

Figure 1.19: Replica porcine aortic valves; 3D digital configuration made by Fab@home software (top) and extruded valves in different angles (bottom) (Bar = 1 cm) [104].

1.7.3.3. Critiques of different types of 3D printers (why extrusion based 3D printing)

In the last few pages, different printed, their mode of action and applications were demonstrated. However, not every 3D printer would be used to print medicine namely pharmaceutical oral solid dosage forms at room temperature. 3D printers like fused deposition melting (FDM), stereolithography (SLA) and inkjet were used to print oral tablets [81, 84]. But, due to drug degradation caused by the heat applied in FDM make it unsuitable for heat sensitive actives [65, 84]. Also, in SLA, and inkjet 3D printers the UV applied, added photo initiator (e.g., irgacure) and monomers (e.g., PEGDA) which are not yet FDA approved for pharmaceutical application via oral rout would lead to possible cell toxicity from free radical produced during curing process and from uncured monomers [105]. Other 3D printer like selective laser sintering (SLS) were used in bone tissue engineering studies, but the 3D printer is clearly not suitable for application in tableting due to the high energetic laser. Extrusion based 3D printing of standard pharmaceutical excipients in a form of paste at room temperature on the other hand would be attractive technique. This would decrease possible drug degradation caused by high temperature and UV radiation. Furthermore, the extrusion technique is well understood process and being used in pharmaceutical industry for long time and the materials used in extrusion process are already having FDA approval for pharmaceutical applications. Other advantages over other 3D printers like less expensive, simplicity, wide range of materials can be printed, rapid process (high production rate at low expense). However, extrusion based 3D printing process has numbers of disadvantages; Coarse resolution compared with inkjet, SLS, and SLA 3D printers, not suitable for humid sensitive materials (degradation), and produces poor physical appearance of the final product caused by tablet shrink (more work required to improve it).

1.7.4. Advantages and drawbacks of pharmaceutical 3D printing technology

Customizing drugs for individual patients using a 3D printer is a promising application which could revolutionalize the pharmaceutical industry. 3D printers could potentially be used to formulate highly tailored medicines, deposition of different active ingredients separated with a compatible polymer, increase patient compliance, and reduce drug side effects and toxicity. Formulation of multi-prescribed medicines into one tablet with a tailored dose and desired drug release profile can be a challenging using a conventional tableting process. Hence, physicians are restricted in achieving an accurate dosing regimen for a specific patient group according to patient's genetic factors, body mass index (BMI) and age [74, 87].

In addition, pharmaceutical 3D printing technologies are expected to facilitate sustained release drugs with corresponding lower toxicity with accurate amount of APIs, and less excipients than the conventional tablets [74, 87, 90-92, 106, 107]. Furthermore, using 3D printers could eliminate a number of steps in tablet pipeline production process, such as powder milling, wet granulation, dry granulation, tablet compression, coating, and long term stability studying tests especially, when there is limited quantity of active ingredients at early drug development stage [74]. 3D printing technologies could also be used to formulate drugs for rapid consumption by individual patients, and therefore, reduce long term stability and transportation issues [106]. For instance, 1,2,3-trinitroxypropane tablets which are used for treatment angina pectoris gradually degrades because of improper long term storage and transportation, and might results in lose drug potency and efficacy [107], if printed locally for immediate use this issue would be addressed.

However, pharmaceutical 3D printing technology has a number of potential drawbacks. The research area is not well-established and needs more development before meeting regulatory considerations or going to mass production. The use of 3D printers for small scale production to supply small batches for pharmacies, hospitals, and clinical studies is perhaps closer.

Furthermore, the current installed software is not designed to control of active ingredients contents, and different parameters should be optimized before printing process [74, 80].

1.8. Aims and objectives

The aim of this thesis room temperature extrusion based 3D printing is introduced as a medicine manufacturing technique for the production of single and multi-active oral solid dosage forms capable of satisfying some regulatory tests and mimicking the release of standard commercial tablets with well-defined and separate controlled release profiles. Also, as an accurate technique for tailoring drug doses for individuals and sub-populations.

In this thesis, the following objective will be explained;

- To print 3D printed tablets started with a simple geometry guaifenesin bilayer tablets to a complex multi-active osmotic pump-controlled release tablets and five-in-one polypill.
- Control the dissolution profile of the actives and also mimic dissolution profile of the commercially available guaifenesin extended release bilayer tablets (Mucinex®).
- Control the drug release profiles based upon the active/excipient ratio used.
- Control the complexity of the tablet geometry by separation the actives and having 5 drug in one tablet.
- Produce 3D tablets with a good physical properties; hardness and friability (acceptable range as defined by the international standards stated in the United States Pharmacopoeia (USP)).
- The printed formulations were evaluated for mechanical and physical properties: hardness, friability, X-Ray Powder Diffraction (XRPD), Attenuated Total Reflectance Fourier Transform Infrared Spectroscopy (ATR-FTIR), and Differential Scanning Calorimetry (DSC) were used to assess drug-excipient interaction.

- The 3D printed tablets were also evaluated for drug release using dissolution testing United States Pharmacopoeia (USP). Scanning Electron Microscopy (SEM) was used to characterise the cellulose acetate (CA) shell before and after dissolution testing.

Chapter 2 Preparation methods, 3D printing and screening techniques

2.1. Preparation methods

2.1.1. Preparation of hydroxypropyl methylcellulose gel (binder)

HPMC gels were prepared using different viscosity grades of HPMC: HPMC 2910 (1%, w/v) for the immediate release (IR) formulations and HPMC 2208 (1%, w/v) for the sustained release (SR) formulations. The following steps were used to prepare HPMC 2910 gel (Fig. 2.1). One gram (1 g) of HPMC 2910 powder was added into 30 ml of hot water (90 $^{\circ}$C) (the water temperature was left stable using a hot plate (90 $^{\circ}$C)) and thoroughly mixed until a good dispersion was formed. Around 70 g of ice was added after the container containing hydrated HPMC was removed from the hot plate and stirred for 30 min to increase the polymer solubility. The formed gel was stored in a refrigerator for 24 h until a smooth homogenous gel with good consistency, free from air bubbles and aggregates was formed [108]. The HPMC 2208 (1 % w/v) gel was prepared using the same method. Hydro-alcoholic gels were prepared by mixing a suitable volume of HPMC 2208 (1 % w/v) or HPMC 2910 (1 % w/v) gel with ethanol at ratio of 25:75 (v/v) and mixing until a homogenous hydro-alcoholic gel was formed. The entrapped air bubbles were removed by centrifugation to produce air bubble free gel. The binder was then stored in a sealed container in a cool and dry place until required

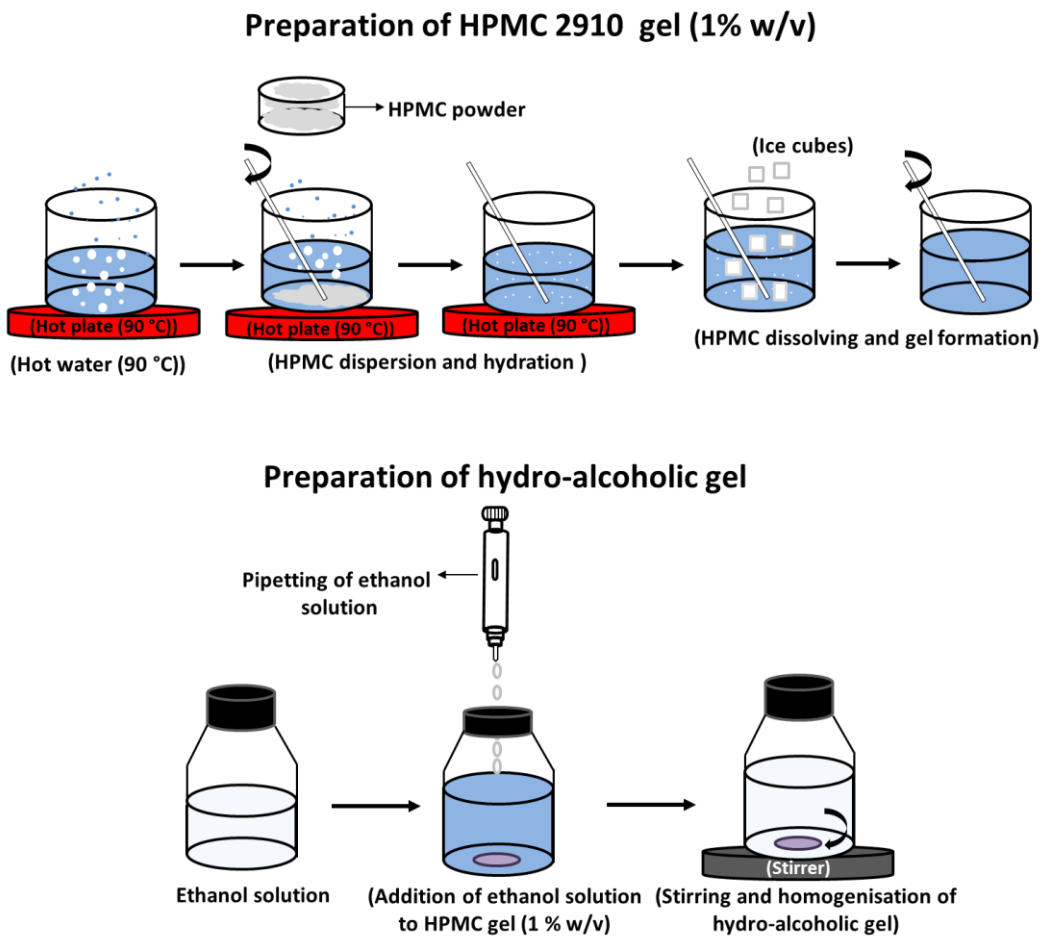

Figure 2.1: Schematic diagrams of preparation of HPMC 2910 gel (1% w/v) and hydro-alcoholic gel [108].

2.1.2. Extrusion based 3D printing process

2.1.2.1. Design of 3D oral solid tablets

A variety of software can be used to design 3D pharmaceutical oral formulations, for example, Fab Studio, BioCAD, Thinkcard. In 3D oral tablet design process used here, the dimensions (x, y, and z) and shape of the tablets were selected based on the size of the traditional oral solid dosage form formulations. The designed file was then saved as (depending on the software used) STereoLithography (STL) which defines the surface geometry of 3D object or BioCad files (frequently used in the RegenHU 3D bio-printer). The

file was then uploaded and the required paste formulation materials for printing filled into syringe tool and the printing process executed (Fig. 2.2).

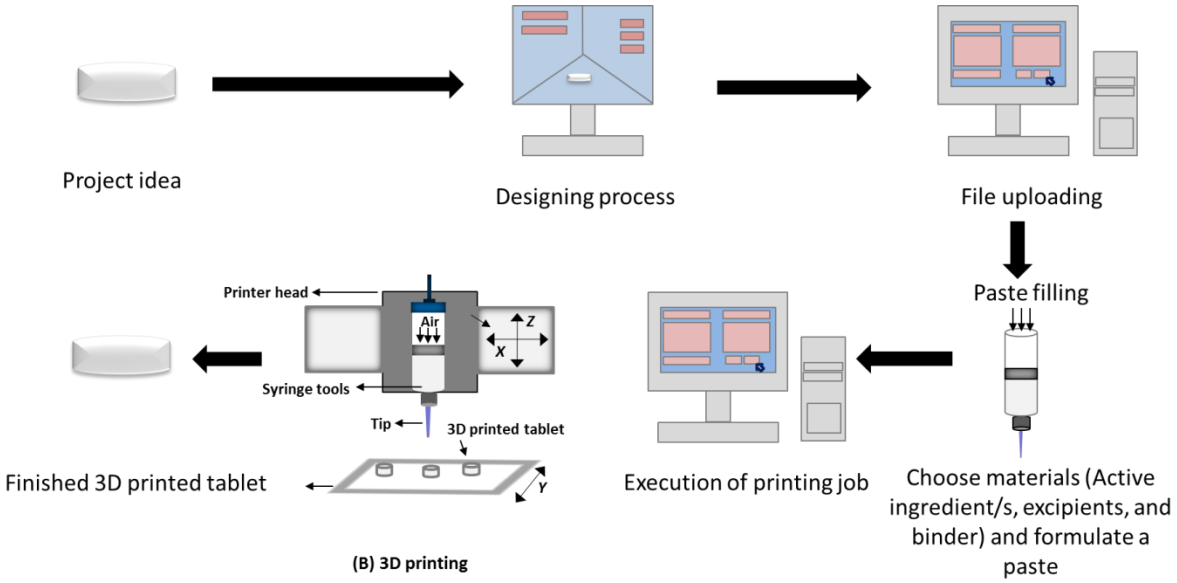

Figure 2.2: Schematic diagram of design and extrusion based 3D printing processes of 3D oral solid tablets.

2.1.2.2. Preparation of medicated paste

Medicated paste is defined as a paste containing active pharmaceutical ingredient/s (APIs). The drug/s and excipient/s were accurately weighed using a Mettler Toledo balance and mixed using a mortar and pestle for 15 min. The required volume of the binder (e.g. HPMC 2910 (1 % w/w) gel or hydro-alcoholic (25:75, v/v) gel) was pipetted and the powder was mixed until a homogenous paste without lumps was formed. Then the medicated paste was filled into the printer cartridges (see the next section 2.1.2.3.) and the printing job was executed (Fig. 2.3).

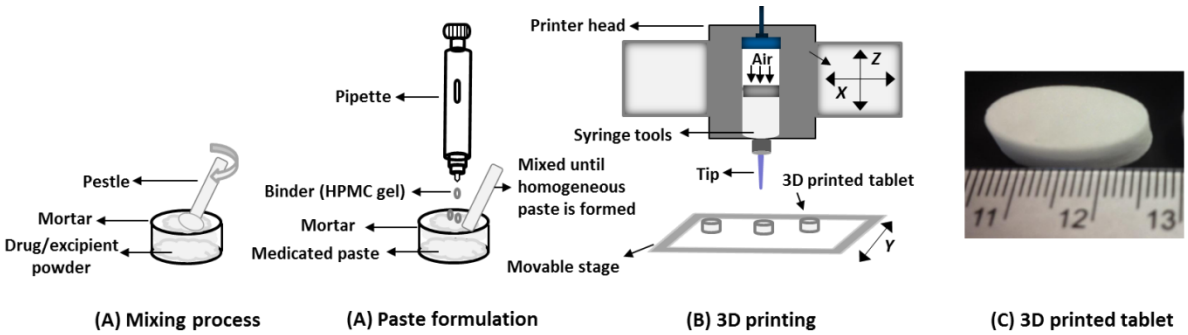

Figure 2.3: Schematic diagram of extrusion based 3D printing process.

2.1.2.3. Cartridge/barrel tool filling process

Depending on the paste viscosity and consistency, either a syringe or a small spatula was used to fill the paste into the barrel/cartridge (a suitable piston should be inserted first in case filling using syringe). A stopper was fixed into Luer-Lock thread after the filling process to avoid unintentional leakage of paste from the cartridge. Once ready for printing, the stopper was removed, and the required nozzle installed. The inserted piston was pushed upwards to remove any trapped air in the barrels and to deliver the paste into the nozzle. The filled cartridge was then installed into the printer head and the printing job executed (Fig. 2.4).

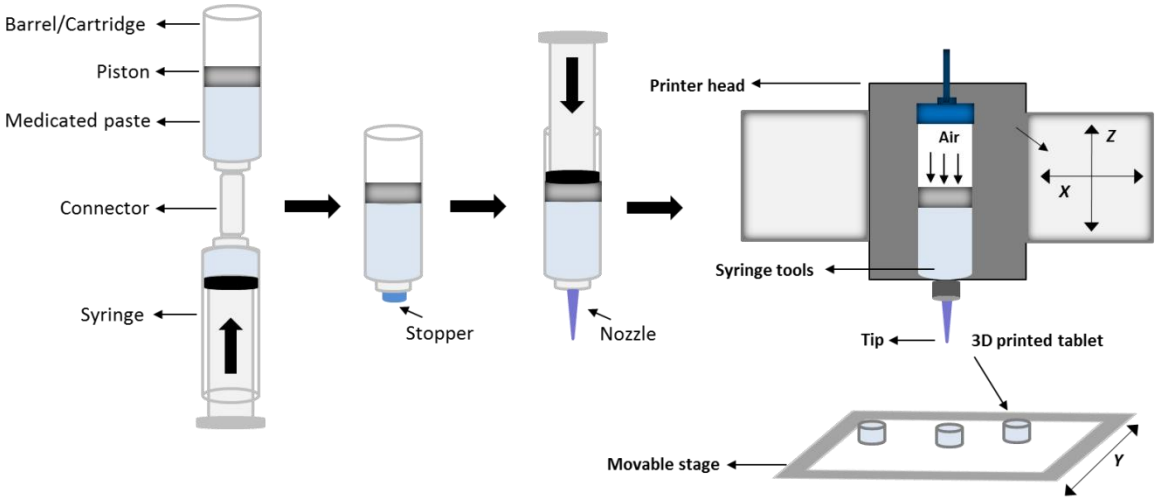

Figure 2.4: Schematic diagram of cartridge/barrel tool filling process.

2.1.2.4. Execution of printing job

From the 3D printing software (Fab Interpreter or 3D Discovery Human Machine Interface (HMI)) a preferred Extensible Mark-up Language file (XML) in the case of the Fab@Home printer, and an ISO file in case of the Bio-printer (3D Discovery® instrument) was uploaded. Such files define the pre-setting values of printing parameters; feed rate, line spacing, and layer thickness, printing head/s, and printing mode (extrusion, jetting, or both). Other parameters such as extrusion pressure distance between nozzle tip and substrate, and printer head position were selected before execution step. The 3D printed tablets were then typically dried in a vacuum dryer at 50°C for 24 hrs and characterised for drug release, physico-chemical properties.

2.2. 3D printing techniques

2.2.1. Fab@Home 3D printer

Fab@Home 3D printer is a freeform fabrication machine used to print static and dynamic 3D entities directly from digital files designed using FabStudio (Fig. 2.5) [77]. The printer was developed by Hod Lipson and Evan Malone in 2006 at Cornell University and retailed for around £700 (as of 2014) [77, 109]. This is a three axis system driven by step motors. Plastic tips with different nozzle sizes can be connected with the syringe and used to extrude a wide range of materials [109]. Unlike the RepRap (another form of free desktop 3D printer used to print 3D objects) printer, Fab@Home extrudes any material compatible with the syringe and uses either in a gel (viscous materials) or paste forms, such as epoxy, silicon, ceramic clay, and silver paste [77, 109, 110]. In addition, water soluble polymers (hydrogels and polyvinyl alcohol (PVA)), biodegradable polymers (Poly Lactic-co-Glycolic Acid (PLGA) and Polylactic acid (PLA)), and APIs (e.g. dexamethasone) have been used in 3D printing scaffolds for drug release and cell growth [44, 77, 93, 109, 110]. Single printed 3D shapes

with multiple materials have been fabricated using Fab@Home model-2 3D printer, such as a zinc-air battery [23] and actuator [109].

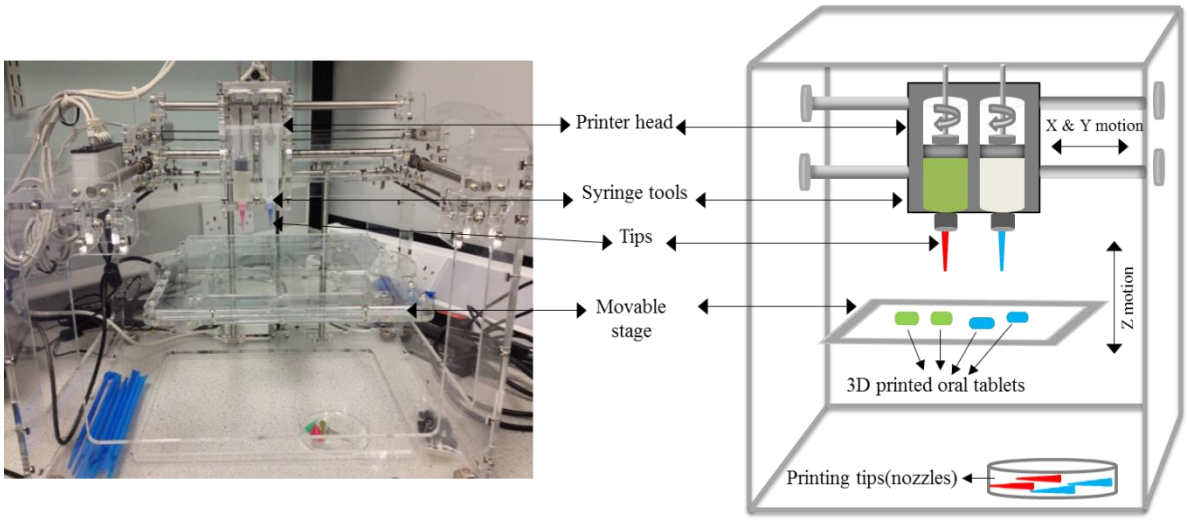

Figure 2.5: Photograph image (right) and schematic diagram (left) of Fab@Home 3D printer.

However, like the RepRap, for good extrusion to be achieved, a number of parameters should be optimised before printing, such as the height between the nozzle and the printer's stage concomitant with slice height, deposition rate, and syringe speed [77]. Furthermore, the printed materials and their viscosities play a crucial role in the resolution of the final shape of a 3D object [77]. Dimensions of the extruded layer and the resolution of the fine structure of a 3D object are highly dependent on the tip internal diameter and the working materials [77, 111]. The Fab@Home 3D printer has a repeatability of ± 100 µm and positioning accuracy of ± 25 µm [77].

2.2.2. 3D Discovery® instrument

The 3D Discovery instrument is a cost-effective 3D bio-printing platform with two print heads and an extruder used to produce a 3D objects. It has been extensively used in tissue engineering and has recently being used in pharmaceutics to print oral solid dosage forms with complex geometries [94, 95]. The 3D Discovery® platform is basically composed of a 3-axis positioning (xyz) system with a tool changer (print heads, extruder, and UV curing unit),

pressure regulator, a building platform with a printing area of 130 x 90 x 60 mm, and console (power switch, emergency stop button, and reset button) (Fig. 2.6). The bio-printing instrument is controlled by 3D Discovery HMI (Human Machine Interface) software whereas the designing process is controlled by BioCAD software, a 3D drawing package developed by RegenHU, used to design 3D scaffolds, patterns, and tissues in which different materials can simply be combined. It has number of advantages over other 3D printers, such as printing at high resolution 80 µm. Also, different printing modes/techniques including contact dispensing/extrusion deposition or time pressure and jetting, and needle dispensing/inkjet can be operated separately or simultaneously during the printing process.

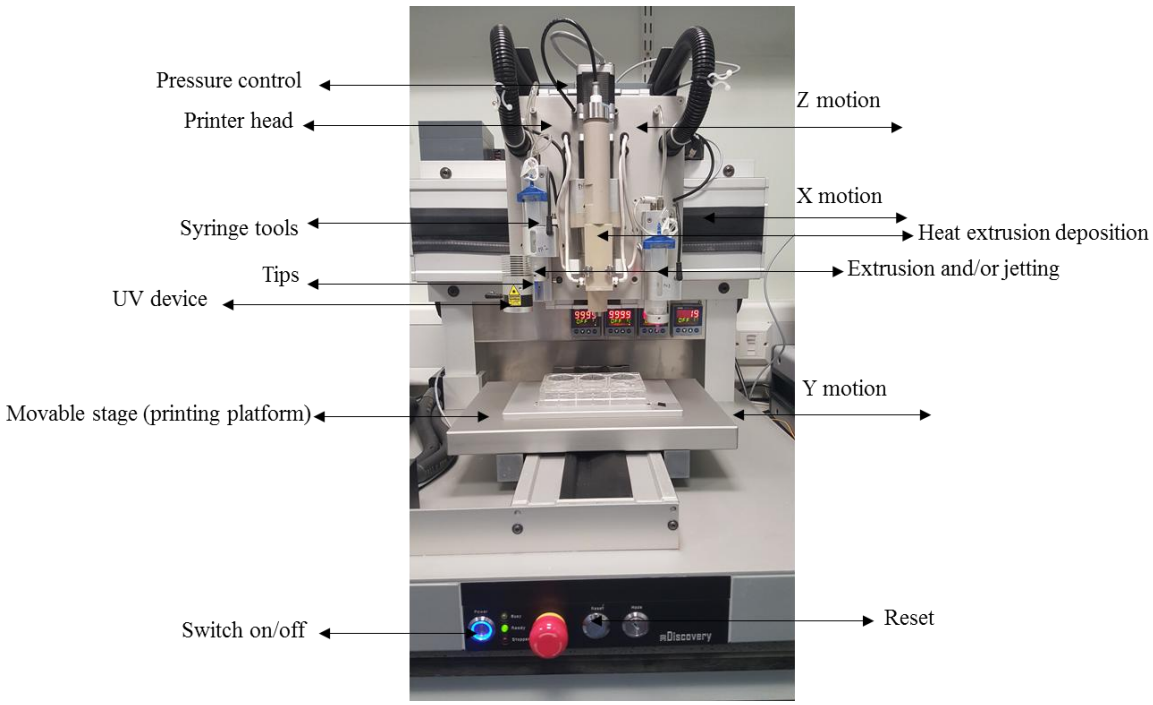

Figure 2.6: Photograph of RegenHU 3D bio-printer.

2.3. Characterisation techniques

2.3.1. Differential scanning calorimeter (DSC)

DSC is a very common technique used in R&D laboratories (Fig. 2.7). It is used to understand the change in the physical and chemical properties of a sample as a function of temperature or time [112]. The first DSC technique was developed by Emmett S. Watson and

Michael J. O'Neill in 1962 [112]. DSC is a Thermo-Analytical (TA) technique used to measure the difference in heat flow between sample and reference as a function of time and temperature [113]. It is often used as a first step in the characterization studies of solid-state forms of active pharmaceutical ingredient [114].

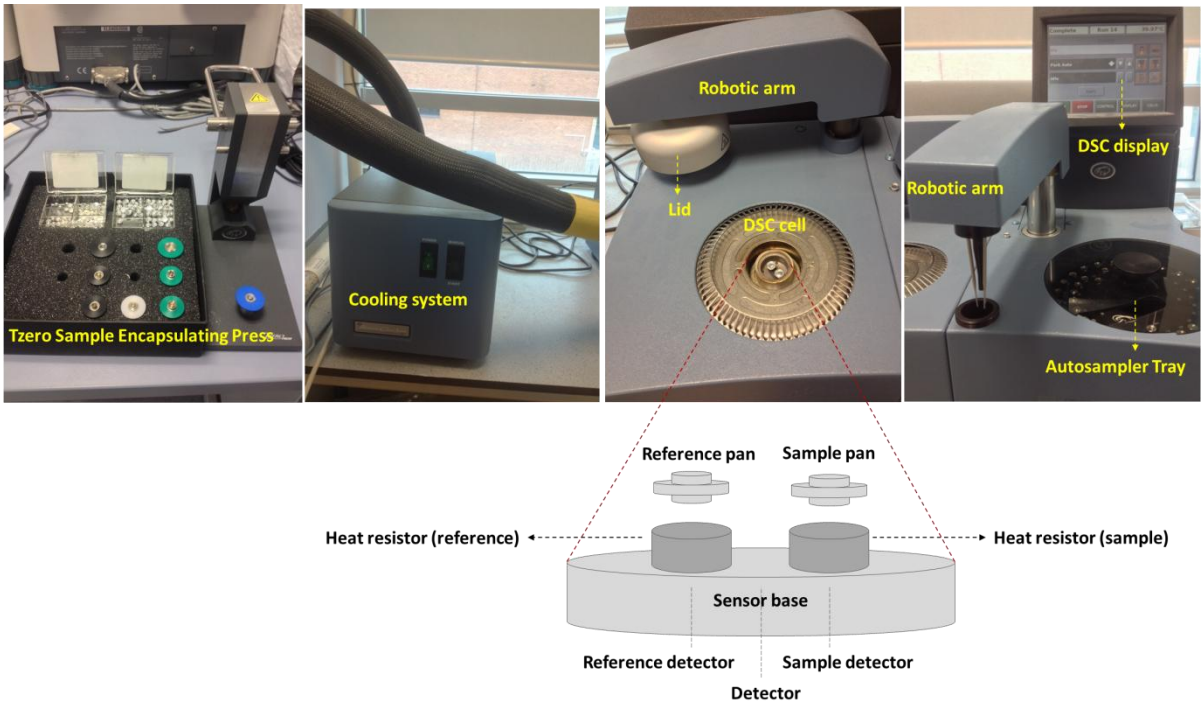

Figure 2.7: Photographic images of DSC Q2000 and schematic diagram of DSC cell.

In DSC, a sample pan contains a known mass of sample and a reference employs an empty pan. When a heating or cooling is applied on a sample with known mass, endothermic (acquire energy) and exothermic (release energy) events like phase changes, glass transitions, melts, and curing are detected [115].

The DSC is commonly used in pharmaceutical industries to characterise single component thermal behaviours such as melting (T_m), crystallization, boiling, sublimation, dehydration, glass transitions (T_g) (a reversible transition takes place in amorphous compounds, and defined as a transition of amorphous compound from brittle or hard state into rubber-like or molten state) [116], polymorphic transitions and to analyse multicomponent mixtures such as

drug-excipient compatibility [117]. An extension of DSC is temperature Modulated Differential Scanning Calorimetry (MDSC); this has higher sensitivity [117].

In addition, DSC is very common technique used together with other techniques; X-Ray Powder Diffraction (XRPD) and Fourier Transform InfraRed (FTIR) in screening of drug-excipient interaction [118, 119]. Drug-excipient compatibility studies are a crucial part of any pre-formulation screening process for new APIs to help decide whether excipients and formulation processes should be avoided at the early stages of a drug development programme [118]. Finally, DSC is frequently used to screen pharmaceutical ingredients for glass transition temperature (T_g) in a single ingredient, such as lyophilized formulations to identify relative physico-chemical stability or in multiple-ingredients mixture to study their miscibility and compatibility [118]. In case of no detected interaction between two amorphous materials, a single T_g peak is detected [120, 121]. Simple equations can be used to predict the T_g of an ideal mixture, such as the Gordon-Taylor or Fox-Flory equations [118, 120, 122].

2.3.2. Scanning Electron Microscopy (SEM)

SEM is a type of electron microscopy used to generate high resolution images by scanning the surface of sample with an electron beam (Fig. 2.8) [123]. In SEM, the focused beam of high energetic electrons interacts with atoms in a sample surface producing various singles of different energy which contain information on the sample's topography and composition. A schematic diagram outlining the main components of SEM is shown in figure 2.9 [123].

Figure 2.8: Digital images of SEM (left) and vacuum sputter coater (right).

Secondary electrons (SE) and backscattered electrons (BSE) are the most commonly signals used for sample imaging [124]. Morphological and topographic information are taken from secondary electron images (SEI), whereas, backscattered electrons images (BSEI) are frequently used for chemical and crystallographic information [124]. Superior resolution (up to around a 1 nm) and wide ranges of magnification (5x-300,000x) made SEM more powerful imaging tool than the traditional optical microscopy in imaging of microstructures. The significant depth of field in SEM is also a great benefit over optical microscopy [123]. Moreover, during sample preparation there is no need to cut thin specimen slices which is required in Transmission Electron Microscopy (TEM) [125]. However, standard SEM has potential drawbacks such as the requirement for ultra-high vacuum conditions and the need for sample coating, and the possibility of artefacts introduction during sample preparation [123].

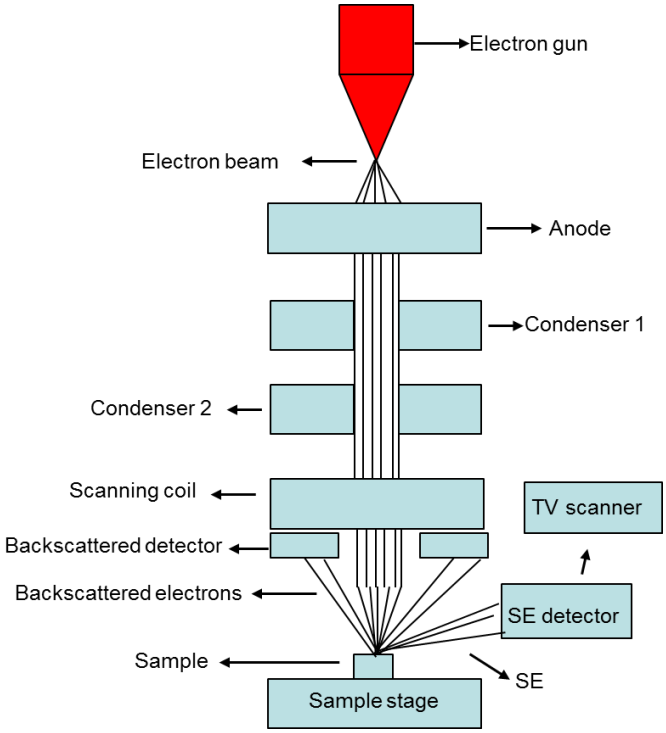

Figure 2.9: Schematic diagram of SEM.

SEM has been used for surface morphology characterisation of drug-excipient formulations such as, biodegradable and non-biodegradable matrix tablets, coated tablets, aerosol and injectable powder, and soft and hard capsules [126]. SEM can be used to ex-situ image drug release during dissolution testing of prolonged release preparation [126, 127]. For example, using SEM Vergote et al. indicated that pore diffusion was the main mechanism of microcrystalline ketprofen release from different wax based pellet formulations (Fig. 2.10) [127].

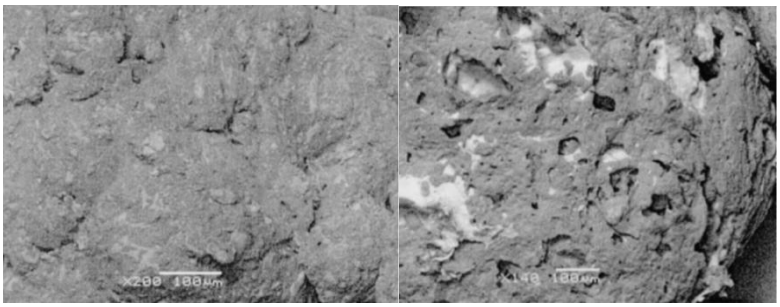

Figure 2.10: SEM photograph of a pellet formulation before (left), and after (right) dissolution test [127].

2.3.3. Attenuated Total Reflection-Fourier Transform InfraRed (ATR-FTIR)

ATR-FTIR is a very common, rapid and non-destructive technique using infrared spectroscopy to analyse samples in solid, semisolid, and liquid states without signifiicant preparation (Fig. 2.11) [93].

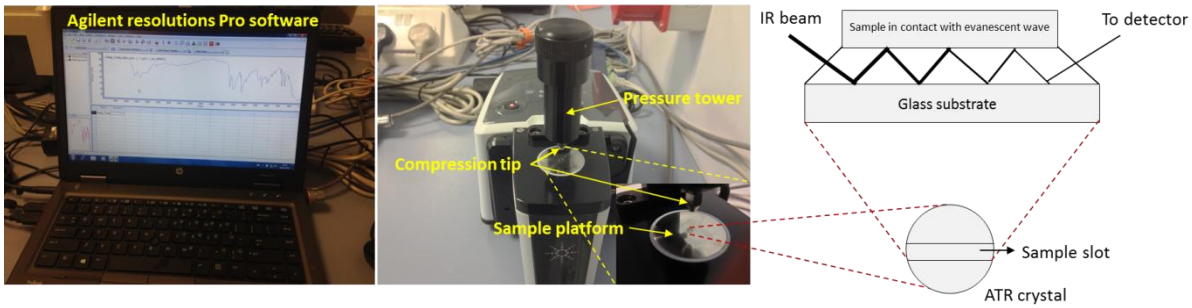

Figure 2.11: Photograph image of ATR-FTIR (Agilent Cary 360 FTIR), and schematic diagram of sample platform.

ATR-FTIR is extensively used for the characterization of drug formulations to interpret kinetic processes in drug delivery [128-130]. Recently, ATR-FTIR has been used in different applications which include studying active drug and excipients distribution and interaction in formulations, drug penetration into membrane, polymorphism, drug release from semisolid preparations, and biological applications such as biofilm formation [93]. The principle of ATR spectroscopy is that an infrared beam is passed onto an optically dense crystal with high refractive index at an angle greater than the critical angle to facilitate total internal reflection. This reflection creates a non-propagating evanescent wave which extends into the sample but penetrates only a few microns (1 μ - 2 μ) [93]. The evanescent wave is then attenuated or altered in the spectral regions where the sample absorbs energy [131]. After a number of reflections in the crystal, the infrared beam exits the crystal and passes to the detector, where the system generates an infrared spectrum [131]. Different materials with high index of refraction are used to make the ATR crystal including, germanium, diamond, and zinc

selenide (ZnSe). Diamond and ZnSe are the most common used materials in ATR analysis [24].

2.3.4. X-Ray Powder Diffractometer (XRPD)

XRPD is a relatively rapid analytical tool used to identify crystalline material phases and define unit-cell dimensions [132]. It is used in pharmaceutics to characterise drug physical state, alone and in solid dispersion mixtures and for the detection of drug-excipient incompatibility [133]. For good quality data, the analysed materials should be ground into homogenous fine powder before scanning. The principle of X-ray diffraction is based on a constructive interference of monochromatic X-rays diffracted from a powder of a crystalline sample [134] that satisfy Bragg's Law ($n\lambda=2d \sin \theta$), where there is a relation between the electromagnetic radiation wavelength (λ), the diffraction angle (θ) and the lattice spacing (d) [134]. In XRPD, the crystalline material is scanned at a range of angles (2θ), and therefore because of the random orientation of the sample particles, all possible diffraction directions of the lattice can be achieved. Then diffracted X-rays signals are recorded and processed through a detector, and the detected signals are converted into count rate (Fig. 2.12).

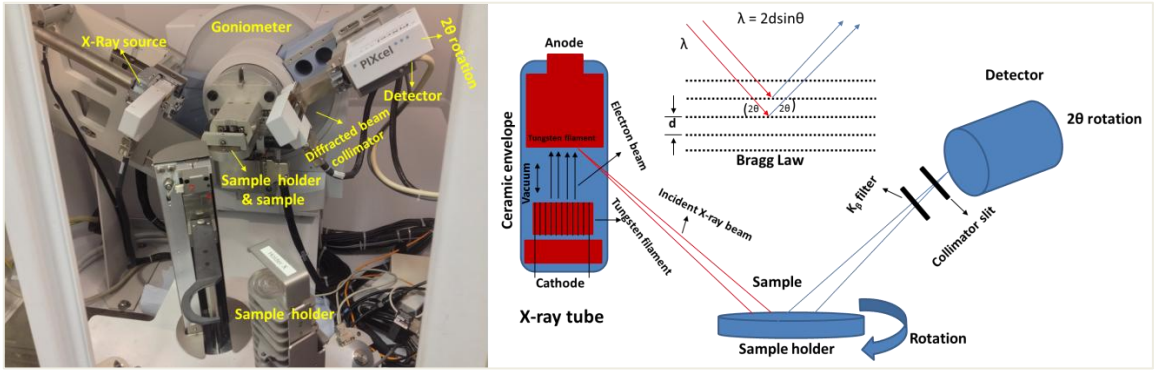

Figure 2.12: Photograph image and schematic diagram of XRPD (X'Pert PRO, PANalytical, Almelo, Netherlands).

2.3.5. Reverse Phase High Performance Liquid Chromatography (RP-HPLC)

Chromatography is an analytical technique used to separate and quantify compounds based on their structural and compositional differences [135]. RP-HPLC is extensively used in pharmaceutics (separation and quantification of active drugs, food (e.g. aspartame, saccharin, and other artificial sweeteners)), and chemistry (separation of similar molecules) [94, 136]. An RP-HPLC instrument is basically composed of a pump with a stable pressure (usually about 200–400 per square inch (psi)), injector, column, UltraViolet-Visible Spectrophotometry (UV-Vis) detector, and display system (a computer) as shown in the schematic diagram (Fig. 2.13) [135].

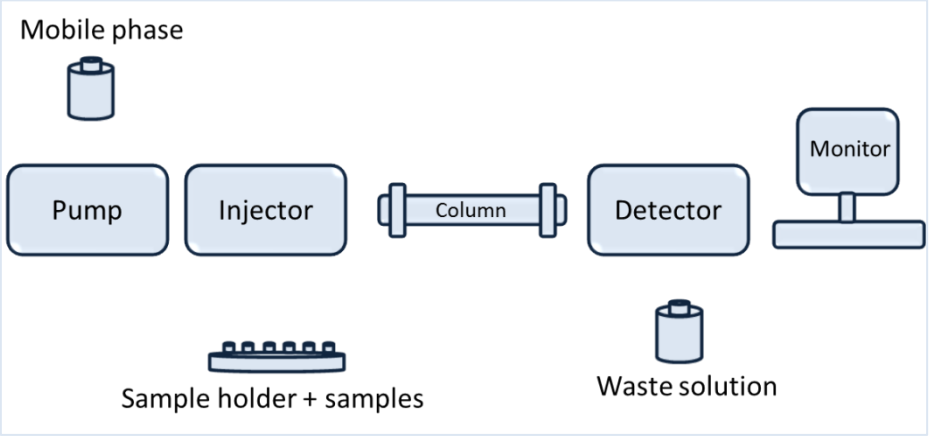

Figure 2.13: Schematic diagram of HPLC.

The instrument is generally based on flowing a sample mixture through an HPLC column which interacts with a stationary phase (octadecyl carbon chain (C18)-bonded to micron-sized porous silica particles) [135]**.** The compounds in the mixture are separated according to the different interactions and affinities with the stationary phase [135]. The sample mixture is transferred through the column by a mobile phase which mainly composed of an aqueous and polar organic solvent [135]. The compounds with strong interactions with the stationary support show slower movement through the column and take longer time to elute than the

compounds with weak interactions with the stationary phase (which move faster through the column and show a short elution time) (Fig. 2.14) [135].

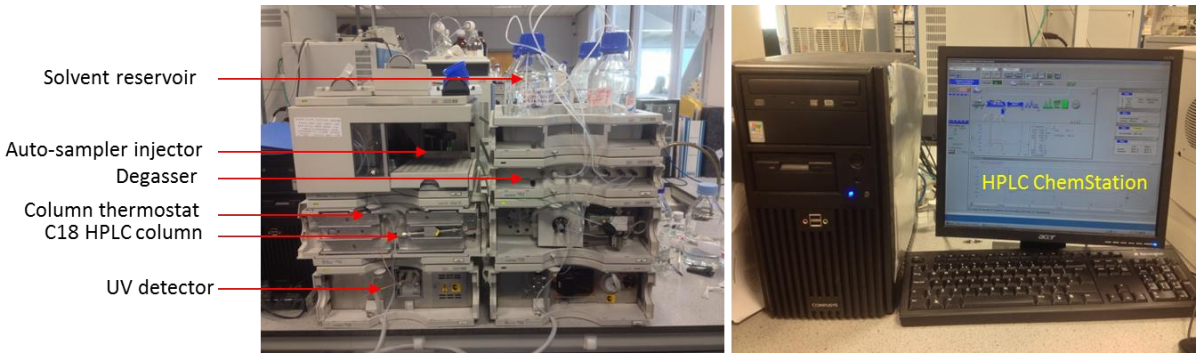

Figure 2.14: Photograph images of HPLC 1100.

The sample mixture separation can be done by one of the following methods; isocratic method where the composition of mobile phase remains constant during the separation process and gradient method where the mobile phase composition is changed during the separation process [135].

2.3.6. Tablet friability tester

This is a relatively simple USP test used to determine a tablets resistance to chipping, capping, and abrasion occurred during manufacturing, packaging, and shipping processes (Fig. 2.15). The standard USP method of the friability test is 25 revolutions per minute for 4 minutes. Ten tablets (for a tablet with unit mass 650 mg or less) corresponding to 6.5 g are dusted and weighed (W1). The tablets are then placed in the friability drum and operated at 25 rpm for 4minutes. The tablets are then carefully removed from the test drum, re-dusted and re-weighed (W2). The weight % loss is calculated from the formula (W-W2)/W1×100 and if the % weight loss is less than 1% then the tablets are accepted and pass the friability test [137].

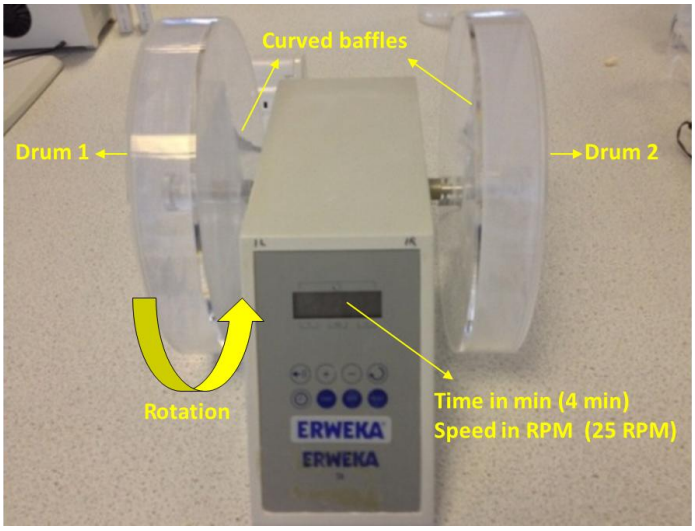

Figure 2.15: Photographic images of Erweka dual drum semiautomatic tablet friability tester.

2.3.7. Tablet hardness tester

Tablet hardness testing is another USP test. It measures the crushing strength and structural integrity of tablets. The test is carried by placing a tablet between two probes, one of which is fixed and the other moveable. The tablet length or diameter (depends on the tablet shape) is measured to calibrate the hardness tester (Fig. 2.16). Then, the motorised probe moves toward the tablet and presses against the fixed probe until the tablet breaks and the force that causes the tablet to break is recorded. Hardness and friability of oral solid dosage forms are both crucial factors in pharmaceutical industries as they determine the dosage form optimum characteristics. Therefore, if the hardness values are high for a certain batch, it means that the tablets may possess low friability, long disintegration time, and low dissolution values and vice versa [137].

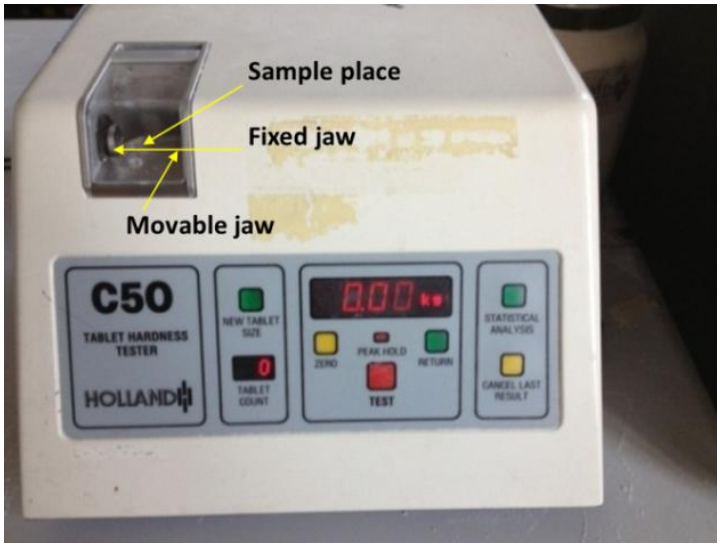

Figure 2.16: Photographic images of tablet hardness tester.

Chapter 3 Desktop 3D printing of Controlled Release Pharmaceutical Bilayer Tablets

3.1. Abstract

A three dimensional (3D) printing extrusion based technique was used for the production of bi-layer tablets capable of satisfying basic physical regulatory tests and mimicking the release of standard commercial tablets. The bi-layer tablets contain one active ingredient (guaifenesin) with immediate and sustained release profiles. Commercial guaifenesin bi-layer tablets (GBTs) were used as a comparator (Mucinex®) for this study. The bi-layer tablet here represents a respiratory treatment for the reduction of chest congestion caused by common cold, infections, or allergies. There was a good comparison of release of the active guaifenesin from the printed hydrophilic matrix compared with the commercially available GBT. The printed formulations were evaluated for physical properties; X-Ray Powder Diffraction (XRPD), Attenuated Total Reflectance Fourier Transform Infrared Spectroscopy (ATR-FTIR), and Differential Scanning Calorimetry (DSC) were used to assess drug-excipient interaction. The 3D printed guaifenesin bi-layer tablets were also evaluated for mechanical properties (friability and hardness) as a comparison to the commercial tablet and were within an acceptable range as defined by the international standards stated in the United States Pharmacopoeia (USP). All formulations (standard tablets and 3D printed tablets) showed Korsmeyer-Peppas type drug release with n values between 0.27 and 0.44 which suggests Fickian diffusion drug release through a hydrated HPMC gel layer.

3.2. Introduction

In this chapter, the first step towards the formulation of guaifenesin bilayer tablets via extrusion based 3D printing technique is demonstrated. It is widely believed that many future improvements in disease treatment will be driven by point-of-care and home-based diagnostics linked with genetic testing and emerging technologies such as proteomics and metabolomics analysis [59]. This has led to the concept of personalized medicine, which foresees the customization of healthcare to an individual patient or patient sub-pupulation [57, 106]. However, how are the requisite 'unique' medicines for each patient to be manufactured on a routine basis? Currently no viable mass manufacturing method used for solid dosage forms, such as tablets, is suitable. Tablets for oral administration are by far the most common dosage form, and are generally prepared by either single or multiple compression processes (and in certain cases with moulding) [3, 4, 138]. This popularity is essentially because of their ease of manufacture, good patient compliance, pain avoidance (compared to injection), and accurate dosing [3, 4]. Powders are prepared for tablet compression via many well-established unit processes such as milling, mixing and granulation (dry and wet) [12, 15]. Each one of these steps can introduce difficulties in the manufacture of a medicine (e.g., drug degradation and form change), leading to possible batch failures and problems in optimization of formulations [8-11]. Tablets are almost universally manufactured at large centralized plants via these processes using tablet presses essentially unchanged in concept for well over a century. This route to manufacture is clearly not well suited to personalized medicine and in addition provides stringent restrictions on the complexity achievable in the dosage form (e.g., multiple release profiles and geometries) and requires the development of dosage forms with proven long-term stability [58].

Two-dimensional (2D) printing of pharmaceutical materials involves the direct printing of a pharmaceutical-based ink on a flat surface [139, 140]. This can, for example, allow the printing of thousands of 2D dots, each potentially containing different polymers, drug loadings, types of drug or release properties [78, 141]. Furthermore, 2D ink-jet printing was used for the production of a formulation in a 2D array of small deposits containing the poorly soluble drug felodipine, an antihypertensive, with polyvinylpyrrolidone (PVP) as an excipient [58]. Such an approach could be used for screening for optimal formulation composition which could then be scaled using three dimensional (3D) printing [78, 142].

Previous research by other workers has also shown that 3D printed formulations are a potential route to personalized medicines [65, 84, 87, 101]. Sandler et al. employed inkjet printing to deposit caffeine, theophylline and paracetamol onto a variety of surfaces (including paper) [87]. However, the amounts of drug deposited were small, with a maximum of 270 μg of drug. For comparison, typical drug loadings in tablets are of the order of 500 mg (e.g., paracetamol, aspirin, and ibuprofen) [87]. In addition, a heat based fused deposition modelling 3D printer (200 °C) has been used to extrude 5-aminosalicylic acid, and 4-aminosalicylic acid and prednisolone loaded poly (vinyl alcohol) (PVA) filaments and produce simple solid tablets [65, 84]. However, this approach would not be suitable generally due to the possibility of heat induced degradation of thermally sensitive drugs. To address the issues of low drug loading in 2D printed formulations and drug degradation, here we investigate using a single step 3D printing process with a low cost (less than £ 695) desktop 3D printer to produce tablets capable of sustained release.

This approach has the potential for producing medicines which would allow patients to be given an accurate and personalized treatment regime, which could include multiple active ingredients, either as a single blend or potentially as layers in a multi-layer printed tablet. For

example, in the future patients suffering from chronic diseases such as cancer and kidney failure could have their treatment and dosage determined using identified genetic markers. Their individual, personalized medicines could potentially then be manufactured for them at, or close to, the point of care [94, 95, 107]. Furthermore, 3D printers would eliminate the previously identified problematic unit processes used in the tablet production process.

3.3. Aims and objectives

This chapter will investigate the 3D printing process of a GBTs using excipients selected based on their potential to mimic the commercially available dosage form in terms of drug release profile, and to characterise the 3D printed GBTs for mechanical and physical properties. Fab@Home 3D printer will be used to print GBTs. United States Pharmacopeia Convention (USP) Type I apparatus and UV-Visible spectrophotometer will be used to study the drugs release from the 3D printed and the commercial GBTs. XRPD will be used to identify the physical form of the actives and match their patterns with the calculated patterns found in Cambridge Structural Database (CSD). Additionally, XRPD, ATR-FTIR and DSC will be used to investigate any changes in physical form of the active within formulations after printing and drying processes. Friability and hardness testers will be used to test the mechanical properties of the 3D printed and the commercial GBTs.

3.4. Active ingredient

3.4.1. Guaifenesin

Guaifenesin is a common over the counter (OTC) drug used as expectorant to increase respiratory tract fluid and loosen pulmonary phlegm [143]. It is water soluble drug, and readily absorbed from small intestine [143]. It is available commercially as a bi-layer tablet (containing 600 mg guaifenesin) under many trade names, e.g., Mucinex®. Because of rapid metabolism and short plasma half-life (one hour), guaifenesin IR formulations offer only

short-term therapeutic effect for patients. Consequently, SR formulations are required to ensure patient compliance and decrease multiple dosing and side effects [143]. The commercial GBTs (Mucinex®) are composed of an immediate release (IR) layer containing100 mg of guaifenesin to provide a rapid alleviation of symptoms via the burst release and a SR layer containing 500 mg of guaifenesin to maintain the therapeutic levels of drug release over an extended time-scale.

3.5. Materials and methods

3.5.1. Materials

Guaifenesin and hydrochloric acid (HCl) 37% Ph. Eur, were purchased from VWR International Ltd. (Leicestershire, UK). Trisodium phosphate dodecahydrate (TSP.12 H2O) and hydroxypropyl methylcellulose (HPMC 2910) (hypromellose®) were supplied by Sigma–Aldrich (Gillingham, UK). Poly (acrylic acid) (PAA) (Carbopol® 974P NF), hydroxypropyl methylcellulose (HPMC 2208) (Methocel™ K100M Premium) were obtained as a gratis from Surfachem Group Ltd. (Leeds, UK), and Colorcon Limited (Dartford Kent, UK), respectively. Microcrystalline cellulose (MCC) (Pharmacel® 102) and sodium starch glycolate (SSG) (Primojel®) were kindly supplied as a gift from DFE Pharma. Guaifenesin Bi-layer Tablets (GBTs) (Mucinex®) were purchased from Reckitt Benckiser Group (Berkshire, UK) (Fig. 3.1).

Figure 3.1: Image box of guaifenesin extended-release bi-layer tablets.

The chemical structures of the active and excipients are presented in figure 3.2.

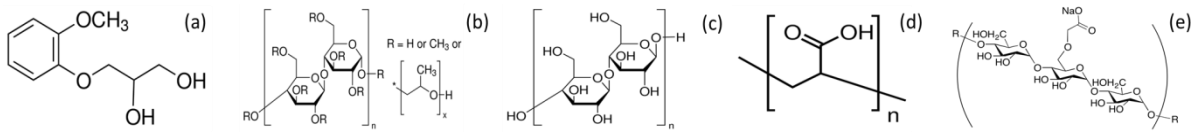

Figure 3.2: Chemical structures of (a) guaifenesin, (b) HPMC, (c) MCC, (d) carbopol 974NP polymer, (e) SSG.

3.5.2. Methods

3.5.2.1. Design of the 3D printed GBT

The active ingredient (guaifenesin) was printed using two different inks (pastes) to achieve the desired burst and controlled release mechanisms (Fig. 3.3). This concept provides flexibility in modifying the dose or drug delivery mechanism through modification of either the drug/excipient loading in the formulation or the excipient composition in the different layer of GBTs. The geometry of the GBTs was designed using a 3D drawing package (FabStudio, Cornell University, USA). FabInterpreter (Cornell University, USA) was used to controls the printer and translate the information in the FAB file to print the GBTs. The designed GBT was scaled for x, y and z dimensions, which represent in our case length (L), width (W), and height (H) of the object, respectively. The dimension (16.4 mm (L) × 9.6 mm

(W) × 6.5 mm (H)) of the 3D printed GBTs was selected according to the drug loading in respect of selected excipients and the dimension of the commercial GBTs. The combined drug and excipients in the GBTs described in the experimental set up were adapted from Mucinex®.

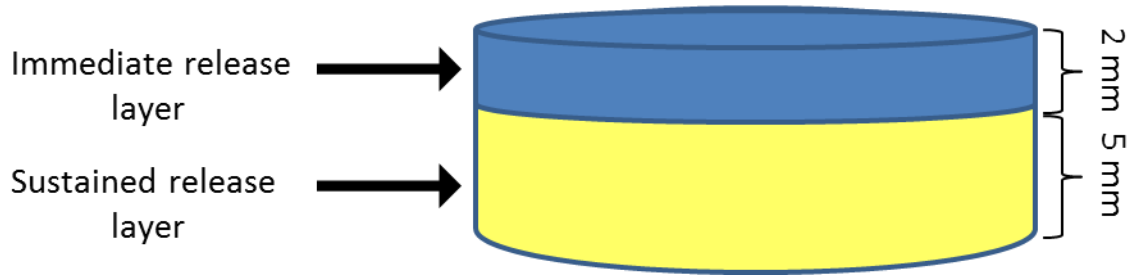

Figure 3.3: Schematic structural diagram of GBT.

3.5.2.2. Preparation of hydroxypropyl methylcellulose (HPMC) aqueous gel

Two HPMC aqueous gels were prepared using different HPMC grades and used as binders; HPMC 2910 (1%, w/v) for the immediate release (IR) formulation and HPMC 2208 (1%, w/v) for the sustained release (SR) formulation (more details found in chapter 2, pages 35 & 36, figure 2.1).

3.5.2.3. Extrusion based 3D printing process of GBTs

The 3D printing process of GBTs is shown in brief in figure 3.4.The guaifenesin powder and required excipients for the IR layer (SSG and MCC) were mixed for 15 min. A pre-adjusted volume of HPMC 2910 (1%, w/v) was added and mixed until a homogenous paste without aggregates and separation was achieved. For the SR layer, different excipients (HPMC 2208 at different percentages and PAA) were mixed with guaifenesin powder. HPMC 2208 (1%, w/v) was used as a binder to hold the ingredients together and form the guaifenesin containing paste.

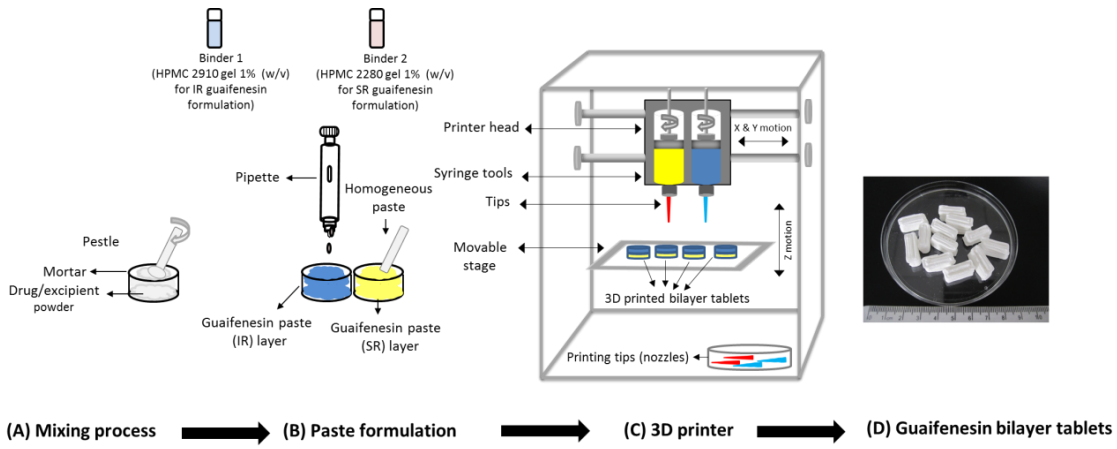

Figure 3.4: Schematic diagram of extrusion based 3D printing process of GBTs.

Each prepared paste was loaded into a separate syringe tool for extrusion from 0.8 mm print tip. The guaifenesin SR layer was first extruded, followed by extrusion of the IR guaifenesin layer (Fig 3.5). The total printing time was 13 min followed by being placed in a drying oven at 40 °C for 24 h for complete drying.

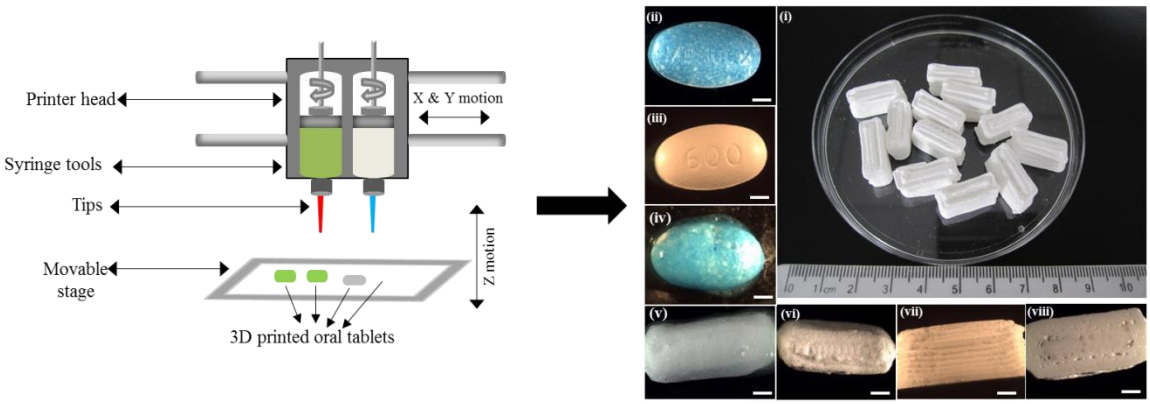

Figure 3.5: Schematic diagram of the Fab@Home printer model 2 (right). Images at different scales of 3D printer produced guaifenesin bilayer tablets (L/W/H = 15.5 × 6.3 × 7 mm) and commercial GBT (L/W/H = 16.4 × 9.6 × 5.91 mm). (ii) Top view and (iii) underside view of commercial GBT. (iv) & (v) Gel barrier surrounding commercial GBT and 3D printed bilayer tablet after 2 hrs dissolution test, respectively. (vi) Top view (vii) side view & (viii) underside view of individual 3D printed bilayer tablets (left). The scale bar (ii-viii) is 10 mm.

The IR functionality was achieved using different disintegrants; MCC and SSG and the SR functionality was achieved using a hydrophilic matrix; HPMC 2208 and PAA, at four different HPMC 2208 percentages; GBT-HPMC (6%, w/w), GBT-HPMC (8%, w/w), GBT-HPMC (10%, w/w) and GBT-HPMC (14%, w/w) according to the formulae shown in Table 3.1 and 3.2.

Table 3.1: The percentage composition of various ingredients in guaifenesin IR feed stock (dried formulae).

Ingredients	**Function/s**	**(% w/w) per IR layer**
Guaifenesin	active ingredient	81
Hydroxypropyl methylcellulose (HPMC) 2910	binder (from the aqueous gel)	2
Sodium starch glycolate (SSG) type A	disintegrant	7
Microcrystalline cellulose (MCC) PH 102	disintegrant	10

Water (removed during drying) is used as a binder and solvent for HPMC 2910.

Table 3.2: The percentage composition of various ingredients in guaifenesin SR feed stock (dried formulae).

Ingredients	**Function/s**	**GBT-HPMC (6 % w/w)**	**GBT-HPMC (8 % w/w)**	**GBT-HPMC (10 % w/w)**	**GBT-HPMC (14 % w/w)**
Guaifenesin	active ingredient	90	88	86	82
HPMC 2208	hydrophilic matrix	6	8	10	14
HPMC 2208	Binder (from the aqueous gel)	2	2	2	2
Polyacrylic acid (PAA)	hydrophilic matrix	2	2	2	2

Water (removed during drying) is used as a binder and solvent for HPMC 2208.

3.5.2.4. In vitro drug release

In vitro drug release studies of commercial GBTs (the IR layer composed of 100 mg guaifenesin, SSG, magnesium stearate and MCC, the SR layer composed of 500 mg guaifenesin, carbomer 934P NF, FD&C blue No. 1 aluminium lake, hypromellose, USP, magnesium stearate NF) and 3D printed GBTs were performed using a United States

Pharmacopeial Convention (USP) Type I apparatus at 50 rpm (Dissolution-Erweka Dt600 Dissolution Tester) in acidic medium for 2 h (representative of the stomach) followed by addition of 0.2 M trisodium phosphate dodecahydrate (TSP.12 H2O) solution to increase the pH to 6.8, for 10 h (representative of the small intestine) to mimic the gastrointestinal fluid pH 6. Tablets from each formulation were placed in acidic dissolution medium 675 ml of 0.1 M hydrochloric acid. 5.0 ml samples were withdrawn at 0.25, 0.5, 1, and 2 h time interval from each vessel. 225 ml of 0.2 M TSP.12H2O was added to each vessel immediately after two hours to raise the solution pH 6.8. The pH was adjusted by adding few drops of 2.0 M HCl. 5.0 ml samples were subsequently removed at 4, 6, 8, 10 and 12 h. The dissolution samples were filtered using standard 20 μm filters (Copley Scientific, UK). 1 ml from each 5 ml sample was diluted by 9 ml of a suitable dissolution medium and analysed with UV–vis spectrophotometer (Cecil UV, Nottingham, UK) at a λ max of 274 nm. The temperature of the dissolution medium was maintained at 37 ± 0.5 °C throughout the test. Two guaifenesin calibration curves were prepared using acidic medium (0.1 M HCl) and a phosphate buffer medium (pH 6.8) and used to identify concentration of unknown samples.

3.5.2.5. ATR-FTIR

The infrared spectra of pure guaifenesin and guaifenesin formulations (IR and SR layers of the commercial and 3D printed GBTs) were obtained using an ATR-FTIR (Agilent Cary 630 FTIR) spectrometer.

3.5.2.6. XRPD

The XRPD patterns of pure guaifenesin and guaifenesin formulations (IR and SR layers of the commercial and 3D printed GBTs) were obtained at room temperature using an X'Pert PRO (PANalytical, Almelo, Netherlands) setup in reflection mode using Cu $K\alpha_1$ (lambda = 1.54 Å) operating in Bragg–Brentano geometry. The generator voltage was set to 40 kV and

the current to 40 mA and the samples were scanned over 2θ range of 5° until 55° in a step size of 0.026°.

3.5.2.7. DSC

DSC was used to determine different melting points and possible interactions between constituents. The DSC measurements were performed on a TA Instruments' DSC Q2000. DSC analysis on drug-excipient multicomponent mixtures was obtained by breaking up tablets and sieving the powders (150 µm). Accurately weighed samples of 3 to 5 mg were sealed in aluminium pans. Scans were performed under nitrogen flow (50 mL/min) at a heating rate of 10 °C/min from 35 °C to 200 °C.

3.5.2.8. Physical properties of the 3D printed and commercial GBTs (USP tests)

3.5.2.8.1. Weight uniformity test

Twenty (20) tablets from each formulation (GBT-HPMC (6%, w/w), GBT-HPMC (8%, w/w), GBT-HPMC (10%, w/w) and GBT-HPMC (14%, w/w) and commercial GBT) were individually weighed and their average (mean) was calculated and compared with percentage of weight variation [144, 145].

3.5.2.8.2. Hardness

Ideal tablets should be hard enough to resist breaking during transportation and storage. However, tablets also should be soft enough to disintegrate and release drug. 6 tablets from each formulation (GBT-HPMC (6%, w/w), GBT-HPMC (8%, w/w), GBT-HPMC (10%, w/w) and GBT-HPMC (14%, w/w) and commercial GBT) were randomly selected and tested for hardness using hardness tester (Hardness tester C50, I Holland Ltd., Holland) [144, 145].

3.5.2.8.3. Friability

Twenty (20) tablets from each formulation (GBT-HPMC (6%, w/w), GBT-HPMC (8%, w/w), GBT-HPMC (10%, w/w) and GBT-HPMC (14%, w/w) and commercial GBT) were

selected randomly and placed on a sieve. The loose dust found over tablets was removed with a soft brush and the tablets were accurately weighed. The tablets were placed in a friability tester and rotated at a constant speed of 25 rpm for a period of 4 min [144-146]. The tablets were cleaned from loose dust and reweighed and the percentage weight loss calculated.

3.5.2.9. Statistical analysis

One-way ANOVA was employed using GraphPad Software to analyse the results (dissolution, weight variation, thickness, hardness, and friability data) and determine whether there are any significant differences between the 3D printed formulations and the commercial GBT. Differences below the calculated probability (p), $p < 0.001$ were considered very significant, between $p = 0.01$ and 0.05 significant and above a probability level, p of 0.05 not significant [147].

3.6. Results and discussion

3.6.1. Dissolution profiles

The dissolution data presented in figure 3.6 shows that all formulations displayed sustained release of guaifenesin over a period of 12 h as required. An initial burst release (>20% in half an hour) of guaifenesin occurred from the IR layer of the formulations. This initial high amount of guaifenesin is attributed to the inclusion of the disintegrants; MCC and SSG. Disintegrants are designed to cause tablets to break up on exposure to water and rapidly release any active ingredients. The weight of the active ingredient in each tablet tested in dissolution tester was calculated form the feed stock dried formulae after identifying individual tablet weight (Table 3.3). Using the standard curves constructed in different pH dissolution medium and the UV measurement of each unknown sample the percentage of drug release was calculated (Fig. 3.7).

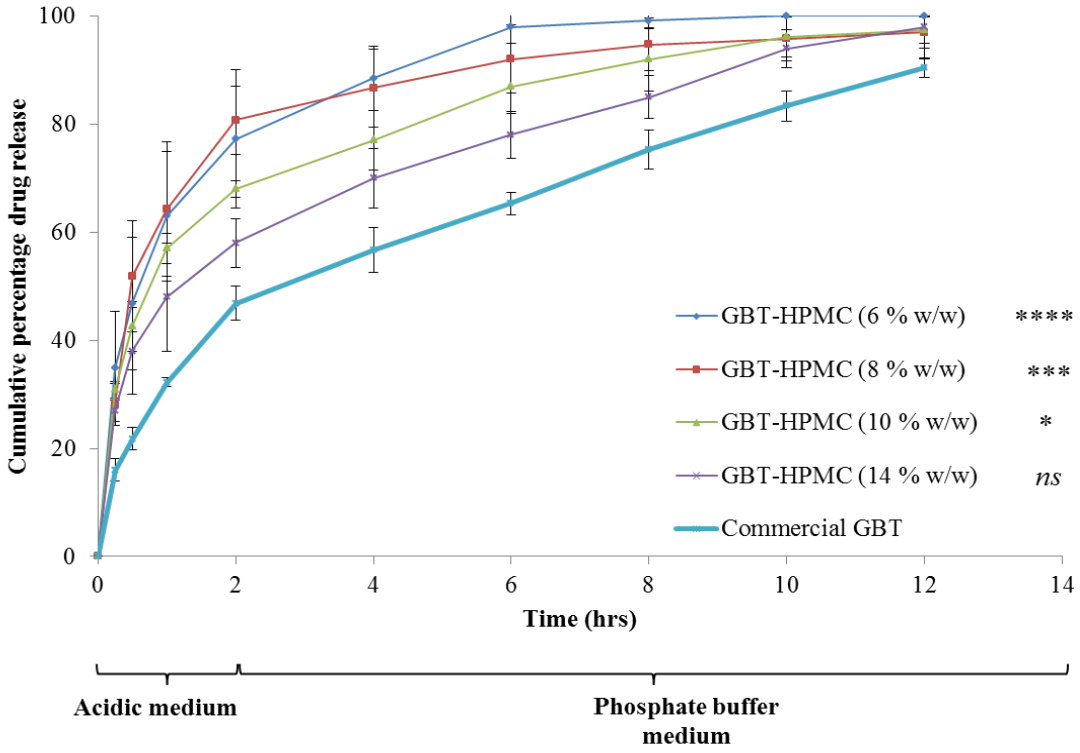

Figure 3.6: Dissolution profile of guaifenesin tablets; GBT-HPMC (6 % w/w), GBT-HPMC (8 % w/w), GBT-HPMC (10 % w/w), GBT-HPMC (14 % w/w) and commercial GBT. The error bars are the standard error in the mean where n = 6.

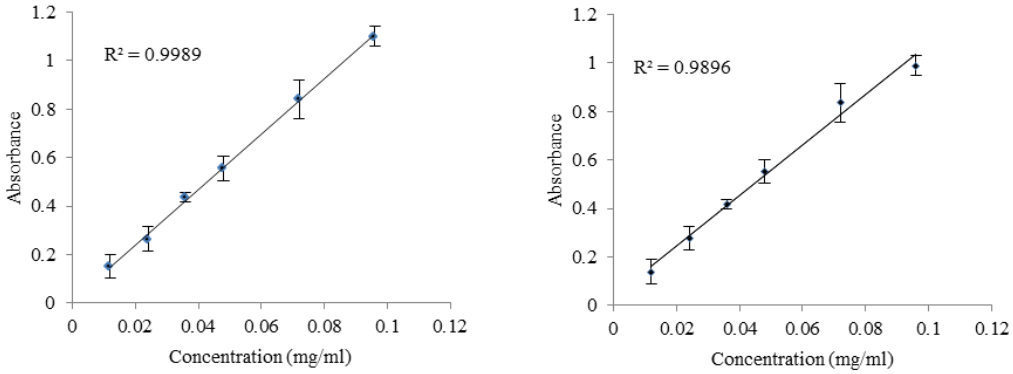

Figure 3.7: Calibration curve of guaifenesin in phosphate buffer media pH 6.8 (left) and acidic media (right) at 274 nm.

The initial release of guaifenesin from the formulations with a low concentration of HPMC 2208 in GBT-HPMC (6%, w/w) and (8% w/w) GBT-HPMC was higher (75% in two hours)

compared to the drug release in the same time period of 65% and 57% from GBT-HPMC (10%, w/w) and GBT-HPMC (14%, w/w), respectively. The initial (the first two hours) guaifenesin release from the commercial GBTs was 47 %, and this is related to release of guaifenesin from the IR layer.

The drug release of guaifenesin from GBT-HPMC (14%, w/w) was noted as the closest to the commercial GBT. One-way ANOVA analysis was used to compare the drug release from 3D formulations with the commercial GBT. The test showed that the difference in drug release was not significant for GBT-HPMC (14%, w/w) ($p > 0.05$), significant for GBT-HPMC (10%, w/w) ($p = 0.01–0.05$), and very significant for GBT-HPMC (6%, w/w) and GBT-HPMC (8%, w/w) ($p < 0.001$). This is consistent with the increased amount of hydrophilic matrix material used (HPMC 2208) (14%, w/w). This increase in concentration of HPMC is expected to lead to improved wettability, enhanced water uptake and greater swelling of the hydrophilic matrix and gel barrier formation which is all consistent with the observed reduction in drug release rate from the formulation with greater amounts of HPMC 2208 (Figure 3.8).

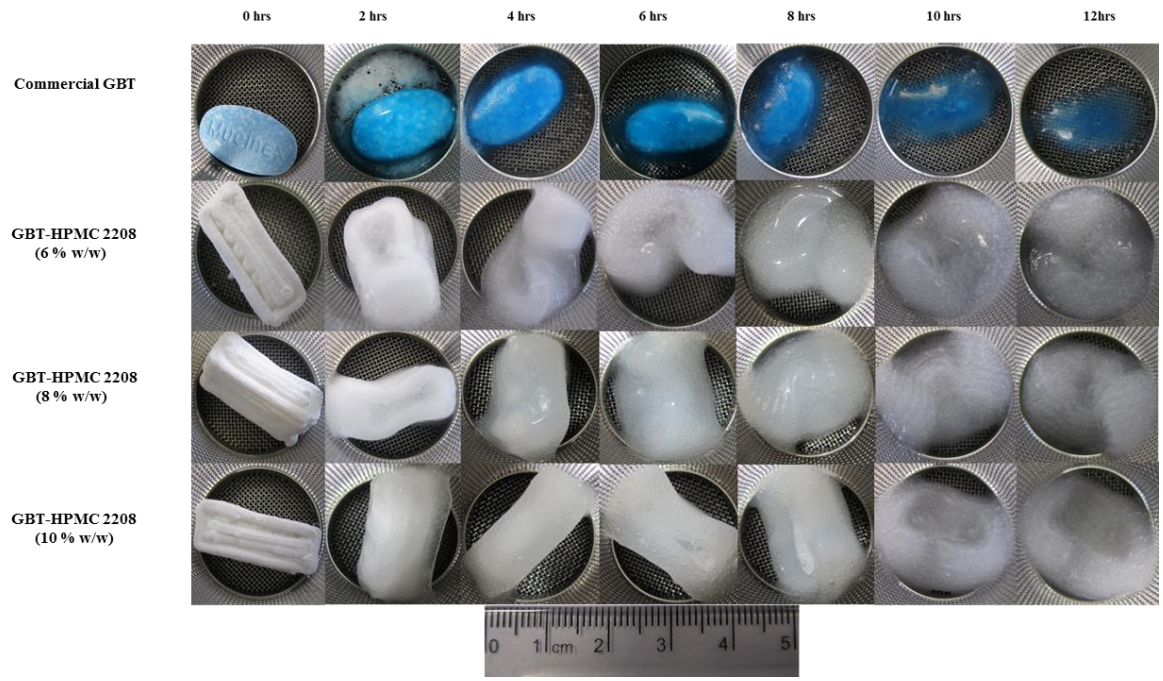

Figure 3.8: 600 mg guaifenesin bilayer tablet (GBT) (GBT-HPMC 6 % (w/w), GBT-HPMC 8 % (w/w), GBT-HPMC 10 % (w/w) and commercial GBT) subjected to dissolution testing at various times. Scale bar at the bottom of the photograph is in centimetres.

However, if the gel layer partially formed or failed, the drug would be released quickly from the tablet surface and cause burst release. This problem was observed in the 3D printed guaifenesin formulation and led to greater burst drug release (>57 %) in the first two hours than the drug released from the commercial bilayer tablets (~ 45 %) in the same period of time (Figure 3.9). The 3D printed formulations are clearly have a different geometry, surface area, and hardness compared to the standard tablets, and hence some difference in drug release as is observed would be expected [148].

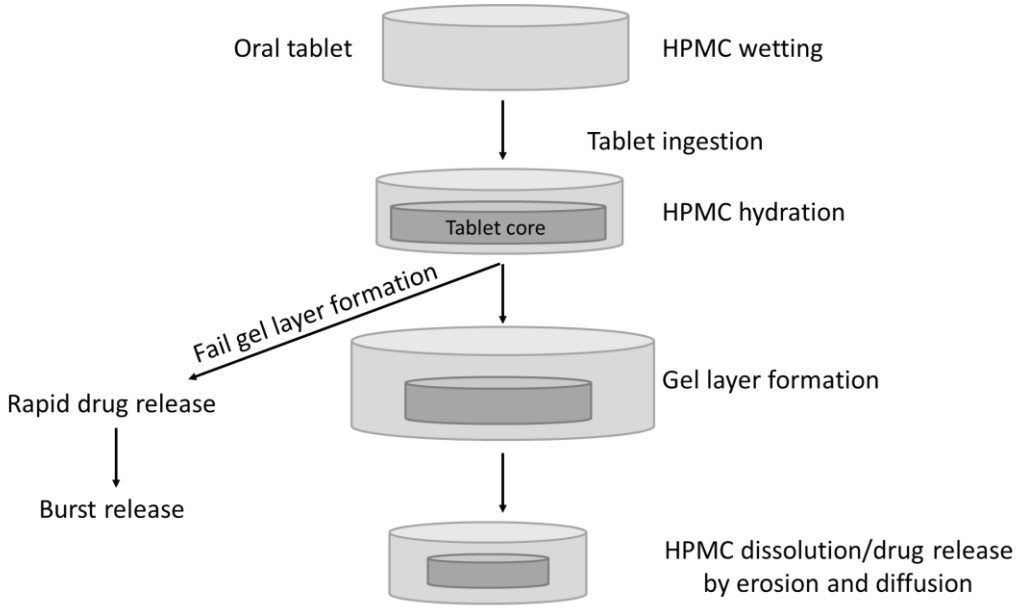

Figure 3.9: Mechanism of drug release from HPMC matrix bilayer tablet.

The type of binder used for paste formation may play an important role in tablet size and post drying tablet shape. Example, when water/low viscosity HPMC (hydrogel) was used as a binder for guaifenesin paste formation, the wet tablet size was greater than the dried size. Also, the 3D printed bilayer tablets were shrunk and led to unpleasant physical appearance. This problem happened due to the hydration, swelling and shrinking effects (polymer just collapse and shrink leaving tablets with irregular surface) of HPMC when the tablet exposed to the water, dried at oven, respectively. However, in the second chapter this problem was decreased by mixing the hydrogel with ethanol at a ratio of 1:3. Hence, a hydro-alcoholic gel was used as it allows better penetration through the HPMC powder particles, retards surface hydration and particle swelling, and provides suitable rheological behaviour of the HPMC for printing [148-150]. The hydro-alcoholic binder also showed faster and better solvent uptake and quick evaporation rate [149].

3.6.2. ATR-FTIR

The finger print region in guaifenesin is the same in both pure drug and the formulations and there was no detectable shift in the wavenumber of relevant peaks in the formulations (Fig. 3.10).

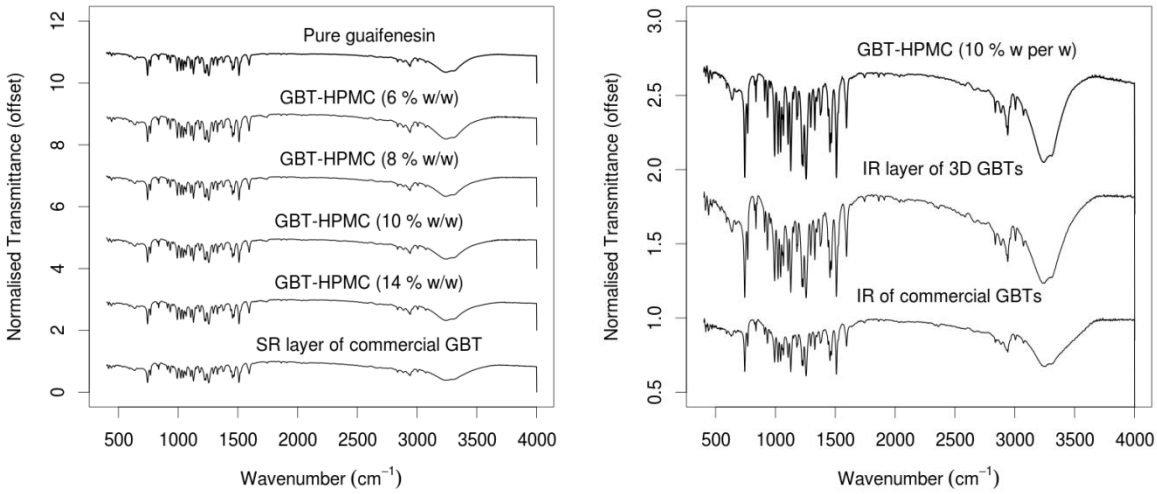

Figure 3.10: FTIR spectroscopy image of pure guaifenesin, GBT-HPMC (6 % w/w), GBT-HPMC (8 % w/w) GBT-HPMC (10 % w/w) GBT-HPMC (14 % w/w), and SR layer of commercial GBTs (left), and pure guaifenesin, IR layer of the 3D printed GBTs and IR layer of the commercial GBTs (right).

3.6.3. XRPD

XRPD data were collected on pure guaifenesin (as received) before printing, and on the mixed formulations containing guaifenesin after printing, in order to study any changes in physical form on printing (Fig. 3.11 and 3.12). The Bragg peaks observed from the pure guaifenesin (as received) had excellent match to the Bragg peaks of guaifenesin (calculated) reported previously in the Cambridge Structural Database (CSD) (Fig. 3.11) [151].

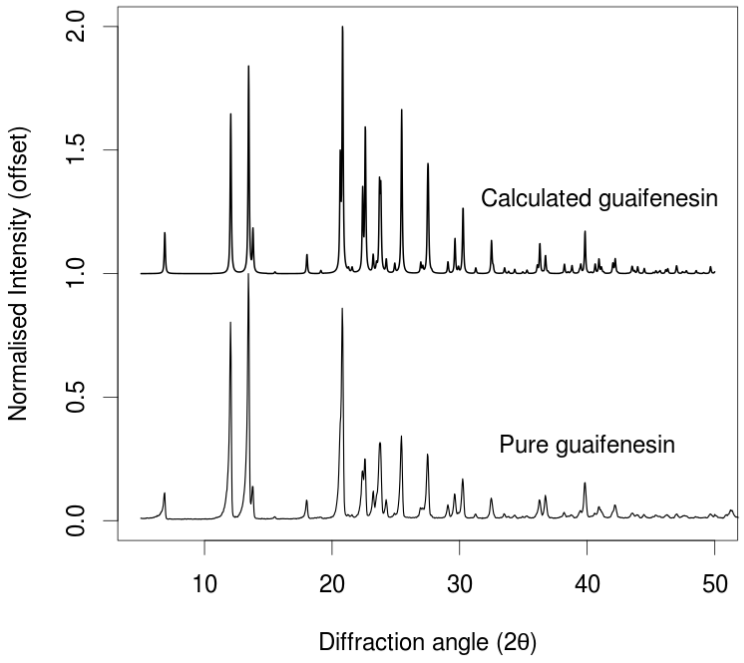

Figure 3.11: XRPD patterns of calculated and pure (as received) guaifenesin.

The results in figure 3.12 shows that the diffraction peaks of guaifenesin remained unaltered in the formulations. XRPD did not evidence incompatibility between guaifenesin and the chosen excipients (PAA, and HPMC K100M (6-14 %)) in the sustained release layer of the 3D printed and commercial GBTs, and (MCC, SSG, and HPMC K4M) in the immediate release layer of the 3D printed and commercial GBTs.

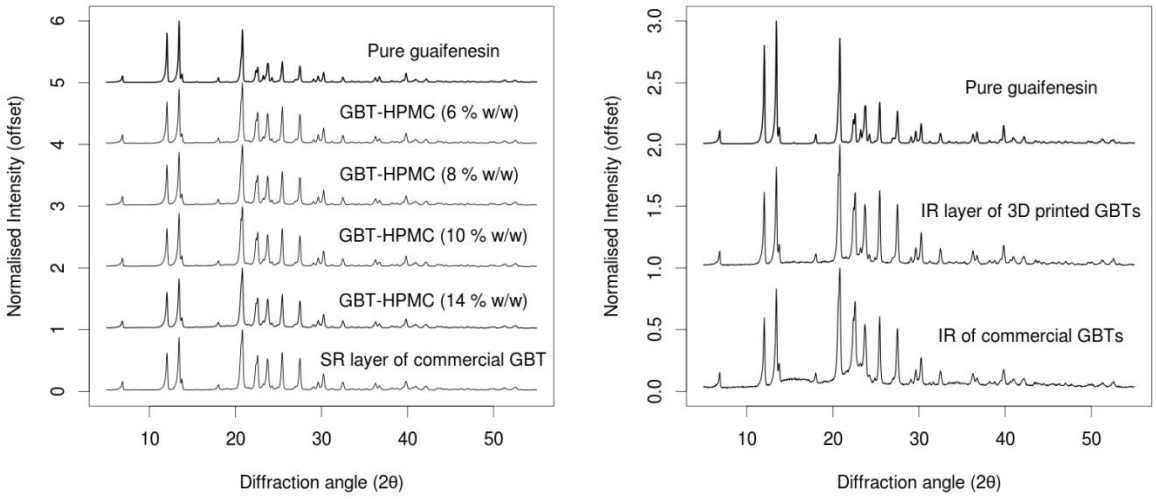

Figure 3.12: XRPD patterns of pure guaifenesin, GBT-HPMC (6 % w/w), GBT-HPMC (8 % w/w), GBT-HPMC (10 % w/w), GBT-HPMC (14 % w/w), and SR layer of the commercial GBTs (left) and pure guaifenesin, IR layer of the 3D printed GBTs and IR layer of the commercial GBTs (right).

3.6.4. DSC

DSC thermograms of the pure guaifenesin and guaifenesin IR and SR formulations of the 3D printed and commercial GBTs are shown in figure 3.13. DSC traces showed one endothermic event for the pure guaifenesin at 78.14 $^{\circ}$C and still observed in both the IR and SR guaifenesin formulations. This suggests that there is no detectable interaction (already confirmed by FTIR and XRPD results) between the active ingredient and blended excipients in IR and SR guaifenesin formulations. The results from DSC, FTIR, and XRPD suggest that is possible to use the excipients listed in tables 1 and 2 in gaufenesin formulation.

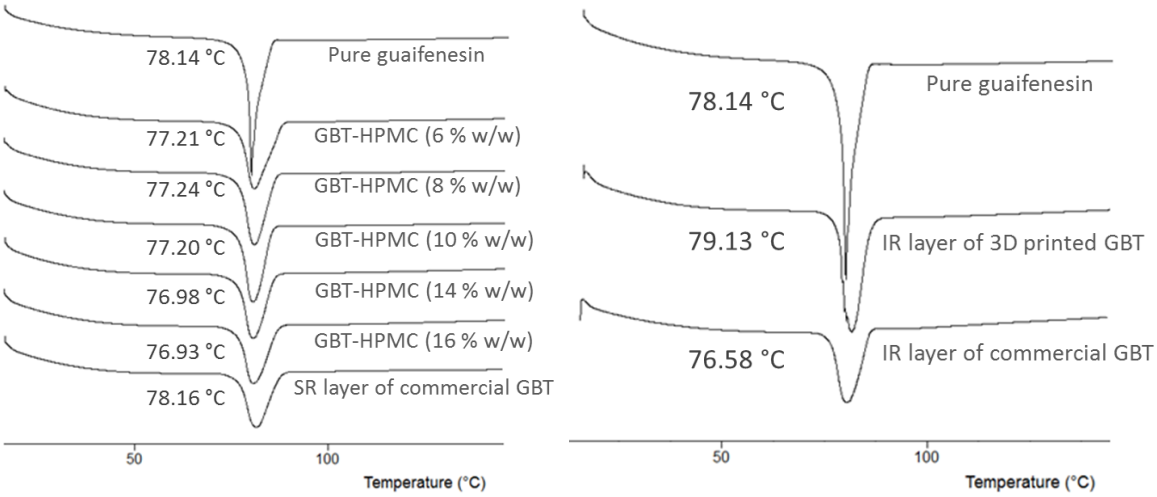

Figure 3.13: DSC scans of pure guaifenesin, GBT-HPMC (6 % w/w), GBT-HPMC (8 % w/w), GBT-HPMC (10 % w/w), GBT-HPMC (14 % w/w), GBT-HPMC (16 % w/w), and SR layer of the commercial GBTs (left) and pure guaifenesin, IR layer of the 3D printed GBTs and IR layer of the commercial GBTs (right).

3.6.5. Physical properties

The tablets were evaluated for weight variation, thickness, hardness and friability and all tablets complied with USP specifications (total weight loss is ≤ 1 % for friability, % deviation = ±5 % for weight variation) [145]. The results of these standard pharmacopeial tests for the 3D printed tablets ((GBT-HPMC (6%, w/w)), GBT-HPMC (8%, w/w), GBT-HPMC (10%, w/w) GBT-HPMC (14%, w/w)) and the commercial GBT are presented in figure 3.14 (i–iv). The weight variations of the formulations are shown in figure 3.14 (i). Although the absolute weights of the different formulations vary slightly between formulations, all tablets weights were from 650 to 730 mg, which is typical for many commercial bilayer formulations, such as Mucinex® (500 mg/100 mg, guaifenesin bilayer tablets) and Mucinex® DM (600 mg guaifenesin/30 mg dextromethorphan). The calculated weight variation for all 3D printed formulation and the commercial bilayer tablets was presented in table 3.3. The percentage of

weight deviation from the average weight was within the average specified by USP (±5% minimum 18 tablets and ±10% maximum 2 tablets.

Table 3.3: Percentage of weight variation of 3D printed formulation and commercial bilayer tablets.

	GBT-HPMC (6 % w/w)	Wieght varaition	GBT-HPMC (8 % w/w)	Wieght varaitio n	GBT-HPMC (10 % w/w)	Wieght varaitio n	GBT-HPMC (14 % w/w)	Wieght varaitio n	Comm ercial GBT	Wieght varaitio n
	712.00	0.24	705.00	0.21	700.00	1.15	720.00	1.00	720.00	-0.08
	695.00	-2.15	700.00	-0.50	704.00	1.73	700.00	-1.81	715.00	-0.78
	698.00	-1.73	698.00	-0.78	696.00	0.57	715.00	0.29	723.00	0.33
	715.00	0.66	700.00	-0.50	687.00	-0.73	710.00	-0.41	723.00	0.33
	705.00	-0.75	690.00	-1.92	700.00	1.15	730.00	2.40	725.00	0.61
	710.00	-0.04	695.00	-1.21	698.00	0.86	735.00	3.10	726.00	0.75
	720.00	1.37	699.00	-0.64	680.00	-1.74	700.00	-1.81	718.00	-0.36
	715.00	0.66	712.00	1.21	676.00	-2.32	717.00	0.58	726.00	0.75
	700.00	-1.45	705.00	0.21	681.00	-1.60	690.00	-3.21	720.00	-0.08
	719.00	1.22	710.00	0.92	701.00	1.29	699.00	-1.95	719.00	-0.22
	712.00	0.24	708.00	0.64	676.00	-2.32	690.00	-3.21	720.00	-0.08
	713.00	0.38	705.00	0.21	702.00	1.44	722.00	1.28	723.00	0.33
	718.00	1.08	710.00	0.92	683.00	-1.31	700.00	-1.81	728.00	1.03
	725.00	2.07	720.00	2.35	687.00	-0.73	715.00	0.29	720.00	-0.08
	721.00	1.51	715.00	1.63	678.00	-2.03	735.00	3.10	720.00	-0.08
	720.00	1.37	718.00	2.06	687.00	-0.73	722.00	1.28	717.00	-0.50
	714.00	0.52	700.00	-0.50	696.00	0.57	735.00	3.10	722.00	0.19
	695.00	-2.15	690.00	-1.92	700.00	1.15	716.00	0.43	716.00	-0.64
	698.00	-1.73	692.00	-1.63	705.00	1.87	717.00	0.58	716.00	-0.64
	701.00	-1.31	698.00	-0.78	704.00	1.73	690.00	-3.21	715.00	-0.78
Ave	710.30	---	703.50	---	692.05	---	712.90	---	720.60	---
Max	725.00	2.07	720.00	2.35	705.00	1.87	735.00	3.10	728.00	1.03
Min	695.00	-2.15	690.00	-1.92	676.00	-2.32	690.00	-3.21	715.00	-0.78
STD	9.26	1.34	8.62	1.26	10.07	1.49	14.66	2.11	3.75	0.53

The variation in tablet thickness is presented in figure 3.14 (ii). All formulations (commercial and printed) have similar average thicknesses.

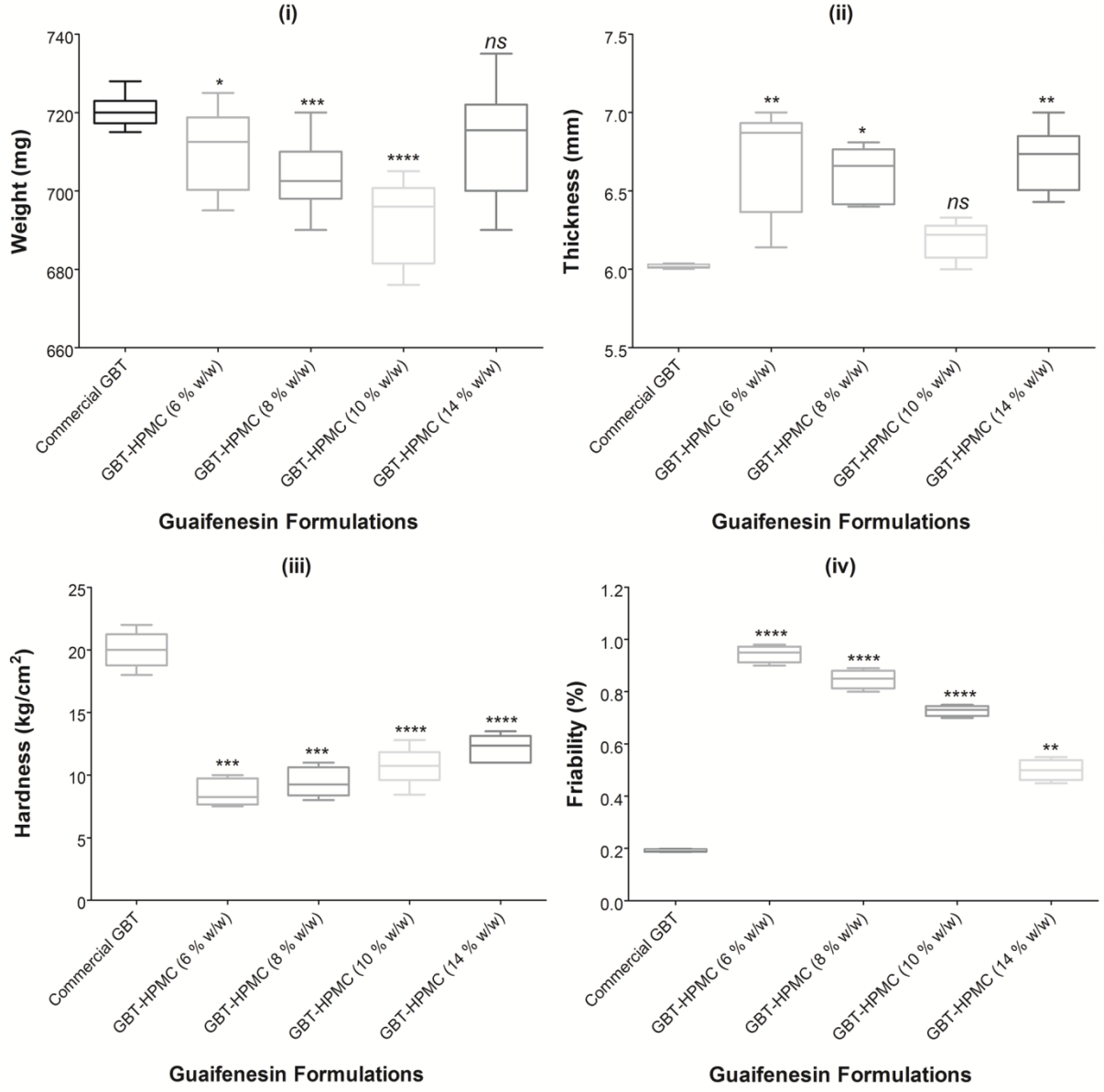

Figure 3.14: Box plot summery of weight variation (mg) (i), thickness (mm) (ii), hardness (kg cm-2) (iii) and friability (%) (iv) for GBT-HPMC (6 % w/w), GBT-HPMC (8 % w/w), GBT-HPMC (10 % w/w), GBT-HPMC (14 % w/w) and commercial GBT.

GBT-HPMC (6%, w/w) (printed) has by far the highest in-batch variation in thickness. One-way ANOVA analysis showed that the weight variation of GBT-HPMC (14%, w/w) and the thickness of GBT-HPMC (10%, w/w) were not significantly different from the commercial

GBT (ANOVA, $p > 0.05$). Weight variation of GBT-HPMC (6%, w/w) and thickness of GBT-HPMC (8%, w/w) had significant differences (ANOVA, $p < 0.05$). Weight variation of GBT-HPMC (8%, w/w) and GBT-HPMC (10%, w/w) and thickness of GBT-HPMC (6%, w/w) and GBT-HPMC (14%, w/w) had very significant differences from the commercial GBT (ANOVA, $p < 0.001$).

The simple 3D printer used has been shown to have the capability of printing tablets with a reasonable in-batch variation of drug release and weight. The lack of specialized software for precise deposition control is the main issue affecting drug dose adjustment in the 3D printed tablets. However, printing parameters such as deposition rate, tip size, push-out, suck-back, and path-speed were used successfully to alter and control tablet shape within satisfactory limits. Our 3D printing process is an experimental approach and is not expected at this stage to reproduce the very small variations seen in formulations manufactured using well-established tableting technology.

The hardness data are shown in figure 3.14 (iii). The hardness of commercial GBT is more than twice that of the printed tablets and there was a significant difference between the compressed and printed tablets (ANOVA, $p < 0.001$). With respect to the lower hardness exhibited by the 3D printed tablets, it should be noted that all the printed tablets can be handled readily without any loss of structural integrity. The parameter for which there is the greatest difference between commercial and printed tablets is the friability (ANOVA, $p \ll 0.001$) (Fig. 3.14 (iv)). This variation in friability (% in weight loss) was attributed to the low percentage of binder, low-viscosity grade HPMC 2910 (1%, w/w) in the IR layer, a binding agent which gives reasonable binding strength between active and non-active ingredients and form tablets with good mechanical properties [152]. However, the friability of GBT-HPMC (14%, w/w) was the closest to the commercial GBT. The % in weight loss can be decreased by increasing the binder percentage which will also decrease the burst release of drug from

the IR layer and decrease the overall drug release for the whole tablet and eventually shift the drug release rate to mimic the commercial GBT.

The differences in hardness and friability between compressed and printed tablets are to be expected. In a conventional tableting press, compression forces are used to control a tablet's hardness. Tablet hardness is expected to have a minimum value of 4 kg/cm^2 to be considered satisfactory [153]. In contrast, compression force is not part of 3D printing process, and therefore the tablet's hardness must be controlled by other means. These may include: adding more binder by either increasing the concentration of the binder HPMC (%, w/v) or adding dry binder (e.g., PVP). Such a binder is expected to increase the hardness and slightly affect the drug release from the printed tablets. Despite the significant difference in hardness and friability between the commercial and 3D printed bilayer tablets, the printed tablet's hardness and friability measurements were within the accepted range of 7–12 kg/cm^2 for hardness and a total weight loss of ≤1% for friability [153]. From a subjective and qualitative assessment, the printed tablets appear to be quite robust and are able to withstand a reasonable amount of rough handling, which may include dropping onto a table top from a height of around 15 cm.

3.6.6. Drug release kinetics

Finally, so as to understand the drug release mechanisms displayed by the formulations, the modes of release of guaifenesin at acidic conditions (0–2 h), buffer conditions (2–12 h) and for both conditions (0–12 h) were modelled [146, 154, 155]. For all formulations, the "best fit" model remained the same, irrespective of the dissolution conditions (Table 3.4). The commercial GBT was best fitted by the Higuchi equation (i.e., cumulative percentage drug release is proportional to the square root of time) with an r^2 value of 0.99 and an n value of 0.44. This suggests the drug is released primarily by diffusion through the hydrated HPMC gel layer for these formulations [37, 156].

Table 3.4: Fitting experimental release data, from the in vitro release of GBT-HPMC (6 % w/w), GBT-HPMC (8 % w/w), GBT-HPMC (10 % w/w), GBT-HPMC (14 % w/w) and commercial GBT to (a) Zero-order, (b) First-order, (c) Higuchi and (d) Korsmeyer-Peppas kinetic equations at different dissolution mediums; 12 hrs (acidic medium (2 hrs)-buffer medium (10 hrs)).

Formulations	GBT-HPMC (6 % w/w)			GBT-HPMC (8 % w/w)			GBT-HPMC (10 % w/w)			GBT-HPMC (14 % w/w)			Commercial GBT		
Dissolution medium	12 hrs acidic (2 hrs)-buffer medium(10 hrs)	Acidic medium (2 hrs)	Buffer mediums (10 hrs)	12 hrs acidic (2 hrs)-buffer medium(10 hrs)	Acidic medium (2 hrs)	Buffer mediums (10 hrs)	12 hrs acidic (2 hrs)-buffer medium(10 hrs)	Acidic medium (2 hrs)	Buffer mediums (10 hrs)	12 hrs acidic (2 hrs)-buffer medium(10 hrs)	Acidic medium (2 hrs)	Buffer mediums (10 hrs)	12 hrs acidic (2 hrs)-buffer medium(10 hrs)	Acidic medium (2 hrs)	Buffer mediums (10 hrs)
Zero order (r^2)	0.73	0.93	0.65	0.66	0.86	0.88	0.91	0.89	0.95	0.91	0.96	0.97	0.93	0.98	0.99
First order (r^2)	**0.97**	**0.99**	**0.86**	**0.94**	**0.99**	**0.98**	0.98	0.93	0.95	0.98	0.95	0.97	0.98	0.98	0.97
Higuchi (r^2)	0.88	0.98	0.72	0.81	0.94	0.93	0.98	0.95	0.97	0.98	0.96	0.98	**0.99**	**0.99**	**0.99**
Korsmeyer-Peppas (r^2)	0.95	0.99	0.78	0.86	0.93	0.96	**0.99**	**0.96**	**0.98**	**0.99**	**0.98**	**0.99**	0.98	0.98	0.98
n =	0.27	0.39	0.11	0.27	0.49	0.10	0.29	0.29	0.27	0.32	0.30	0.28	0.44	0.52	0.43

GBT-HPMC (10%, w/w) and GBT-HPMC (14%, w/w) were best modelled using the Korsmeyer–Peppasmodel.

$$M_t/M_\infty = Kt^n \quad (3.1)$$

Where M_t/M_∞ is the fraction of drug released at time t, K is the release rate constant and *n* the release exponent [37, 157]. They showed an *n* values of 0.29 and 0.32 fitted ($r^2 = 0.99$) which suggests Fickian diffusion, respectively. GBT-HPMC (6%, w/w) and GBT-HPMC (8%, w/w) were fitted by Fickian diffusion having the same *n* value (0.27) and fitted ($r^2 = 0.97$) and ($r^2 =$

0.94), respectively. They were best modelled using the first order model (i.e., log cumulative percentage of drug remaining vs. time) where the drug release rate depends on its concentration [37]. Overall, all formulations showed *n* values between 0.27 and 0.44 which suggests that Fickian diffusion drug release through the hydrated HPMC gel layer dominates for these formulations (Figure 3.15).

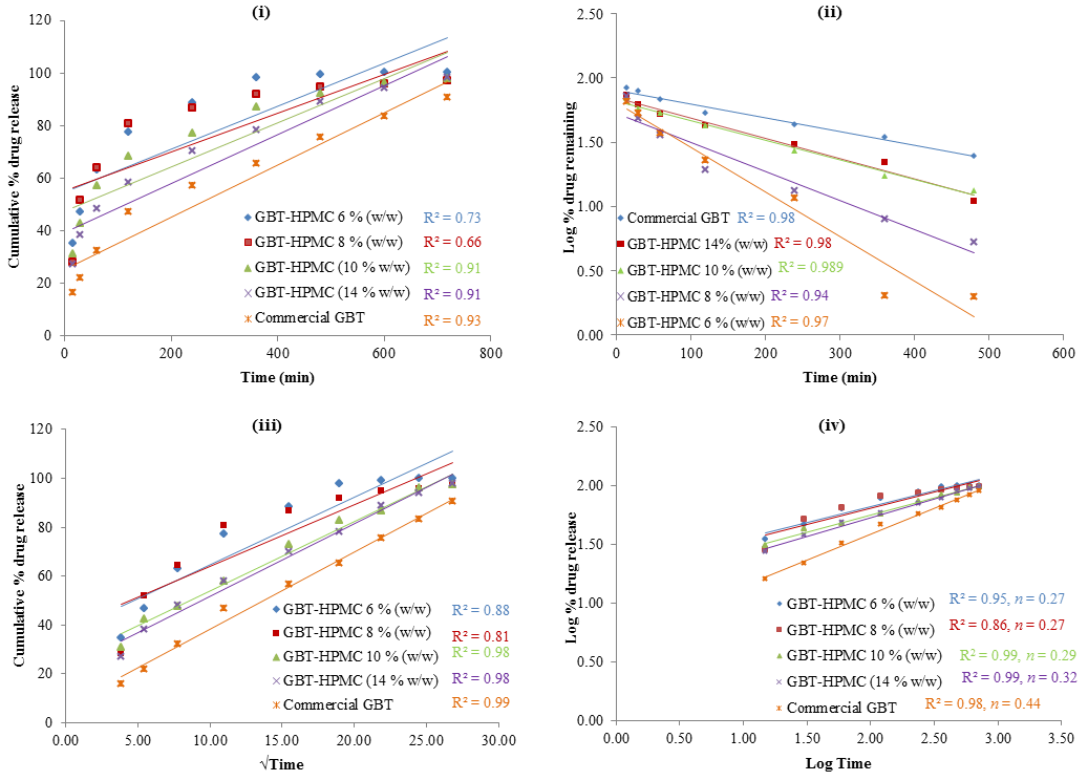

Figure 3.15: Representative release plots by fitting experimental release data, from the in vitro release of of 600 mg sustained release guaifenesin bilayer tablets; GBT-HPMC 6 % (w/w), GBT-HPMC 8 % (w/w), GBT-HPMC 10 % (w/w), GBT-HPMC 14 % (w/w) and commercial GBT to (a) Zero-order, (b) First-order, (c) Higuchi and (d) Korsmeyer-Peppas kinetic equations.

3.7. Conclusions

The production of relatively complex formulations printed into bilayer tablets using an inexpensive desktop 3D printer was demonstrated. The tablets reasonably mimic the release of a commercial GBT (manufactured using conventional tablet compression methods). The dissolution profile showed that the 3D printed GBTs are able to release guaifenesin via two different release mechanisms; immediate and sustained release. FTIR, XRPD, and DSC data were used to show that there was no detectable interaction between the drugs and the chosen excipients, and that our method of 3D printing did not lead to a detectable change in the physical form of the drugs (e.g. polymorphism, hydration etc.). The 3D printed tablets were evaluated for mechanical properties as a comparison to the commercial GBTs and were within acceptable range as defined by the international standards stated in the USP. It has believed that there is clear potential for 3D printing to allow entirely new formulation types, such as new geometries, complex multi-layer or multi-reservoir tablets, and others. The potential for using 3D printing to develop new ways to treat many chronic conditions (e.g., asthma, arthritis and diabetes) is exciting. The work in this chapter whilst preliminary was a significant step towards later work in this thesis and is a demonstration and validation of simple, low-cost 3D printing for the tailored manufacture of medicines, which has the potential to play a crucial role in future developments in personalized care and treatment. In the next chapter, more complex 3D printed geometry with well-defined drug release profiles will be presented.

Chapter 4 Desktop 3D Printing of Tablets Containing Multiple Drugs with Defined Release Profiles

4.1. Abstract

An extrusion based three-dimensional (3D) printer was employed as a medicine manufacturing technique for the production of multi-active tablets with well-defined and separate controlled release profiles for three different drugs. This 'multi-active tablet' made by a 3D additive manufacturing technique demonstrates that complex medication regimes can be combined in a single tablet and that it is possible to formulate and tailor this single tablet for the particular needs of an individual. The tablets used to illustrate this concept incorporate an osmotic pump with the drug captopril and sustained release (SR) compartments with the drugs nifedipine and glipizide. This combination of medicines could potentially be used to treat diabetics suffering from hypertension. The room temperature extrusion process used to print the formulations used excipients commonly employed in the pharmaceutical industry. Attenuated Total Reflectance Fourier Transform Infrared Spectroscopy (ATR-FTIR) and X-Ray Powder Diffraction (XRPD) were used to assess drug-excipient interaction. The printed formulations were evaluated for drug release using USP dissolution testing. It has been found that the captopril compartment could be modelled by the intended zero order drug release of an osmotic pump and noted that the nifedipine and glipizide compartments could be modelled by either first order release or Korsmeyer-Peppas release kinetics dependent upon the active/excipient ratio used.

4.2. Introduction

In chapter 3 3D printing of fairly complex GBTs with high dose loading and acceptable mechanical properties was demonstrated. Here the aim is to achieve more complex geometry containing three actives released with two distinct drug release mechanisms. Oral tablets are the most common form in which medicines are administered, but they are not easily modified for individuals due to the mass manufacturing methods used, which are primarily based upon the compression of powdered formulations [66, 158]. These large-scale manufacturing techniques are also unsuited to the production of complex multi-component dosage forms to meet the challenge of personalised therapeutic regimes for individuals [66, 106]. A medication regime using nifedipine and captopril formulated as separate tablets is currently used to treat arterial hypertension in type II diabetics and high blood pressure without significant side effects [159]. Captopril preparations, such as controlled and SR formulations, have a number of challenges, including dose dumping and burst phenomenon [86, 160], a short elimination half-life and only being effective for 6-8 hours after a single dose [86, 161]. To address these issues an osmotic pump compartment of the printed tablet was demonstrated in this chapter to deliver the drug in a controlled fashion over a long period independent on drug concentration. To achieve SR profile for the other active components (nifedipine and glipizide) a hydroxypropyl methylcellulose (HPMC 2280) matrix was employed. To date the use of HPMC 2280 as a hydrophilic barrier is the primary technology used for preparation of extended release (ER) oral dosage forms [162, 163]. This is because HPMC 2280 rapidly swells and forms a viscous gel like layer of hydrated polymer on contact with aqueous liquids. This acts as a diffusion barrier to water access and therefore reduces the release of drug either by diffusion and/or erosion [162, 164, 165].

3D printing has been proposed as a promising set of techniques for the production of tailored oral solid dosage forms [65, 66, 84, 98, 166]. However, few reports have shown printing of

multi-active tablets with well-defined and separate controlled release profiles. [45, 66, 95, 101]. Furthermore, there is little information in the literature about using the standard pharmaceutical excipients e.g., MCC and Eudragit® E100, polyvinylpyrrolidone K30 (PVP K30), lactose, and D-mannitol [101, 102, 167] in 3D printing gave another reason to explore using a smart 3D extrusion system (3D Bio-Printer RegenHU) operated at room-temperature to manufacture a complex multi-active tablets capable of delivering three drugs via two different release mechanisms, namely osmotic release through a controlled porosity shell for captopril and diffusion through gel layers for nifedipine and glipizide.

4.3. Aims and objectives

This chapter will explore the potential of 3D printing to address the specific challenge of manufacturing a complex multi-drug tablet with each drug (nifedipine, glipizide, and captopril) released with a different profile, and characterise the 3D printed tablets for physical properties. United States Pharmacopeia Convention (USP) Type I apparatus (Dissolution-Erweka Dt600 Dissolution Tester) and High Performance Liquid Chromatography (HPLC 1050) will be used to study the drugs released from the 3D multi-active tablets. Scanning Electron Microscopy (SEM) will be used to image the cellulose acetate (CA) shell before and after dissolution testing. X-Ray Powder Diffraction (XRPD) and Attenuated Total Reflectance Fourier Transform Infrared Spectroscopy (ATR-FTIR) will be used to investigate any changes in physical form of the actives within formulations after printing and drying processes.

4.4. Materials and methods

4.4.1. Materials

Nifedipine and captopril were supplied by MP Biomedicals, LLC (Bedford, UK). Glipizide, polyethylene glycol 6000 (PEG 6000), hydroxypropyl methylcellulose (HPMC 2910)

(hypromellose®), sodium chloride 99 %, and tromethamine USP grade were supplied by Sigma–Aldrich (Gillingham, UK). D-mannitol 99 % was purchased from VWR International Ltd. (Leicestershire, UK). Croscarmellose sodium (CCS) (Primellose®), microcrystalline cellulose (MCC) (Pharmacel® 102) and sodium starch glycolate (SSG) (Primojel®) were kindly supplied as a gift from DFE Pharma. Hydroxypropyl methylcelloluse (HPMC 2280) (Methocel TM) was a gift from Colorcon®. Milli-Q water (resistivity 18.2 MΩ cm) was used for all formulations and solutions. All other reagents were of either HPLC or analytical grade. The chemical structures of the actives were presented in the figure 4.1.

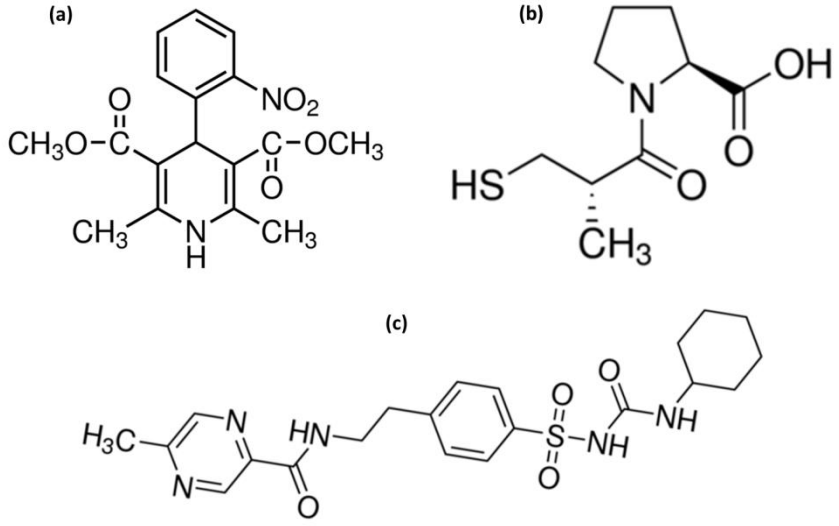

Figure 4.1: Image of chemical structures of the active ingredients in the 3 D printed multi-active tablets; (a) nifedipine, (b) captopril, (c) glipizide.

4.4.2. Methods

4.4.2.1. Design of multi-active tablets

A multi compartment strategy was chosen to ensure the active pharmaceutical ingredients were separated and could achieve the desired independent control of their release kinetics (Fig. 4.2). The complex tablet was designed to achieve different drug release profiles and also

to control each active position within the same tablet. The dimension of the multi-active tablets could also be varied according to drug/excipients loading/type and number of actives required. The dimension of the designed multi-active tablet is 10.4 mm height × 12 mm diameter. Although the size of the tablet is within the suggested range stated by FDA, However, it seems that the tablet at this size would add some difficulties in swallowing especially for patient with narrowed oesophagus. The geometry of the multi-active tablets was programmed into a 3D drawing package (BioCAD, regenHU Villaz-St-Pierre, Switzerland). The formulations described in the experimental set up were adapted from conventional materials to achieve this design. The selection of the excipients and their amounts were based on a previous research paper concerning conventional osmotic and SR tablets [168-173].

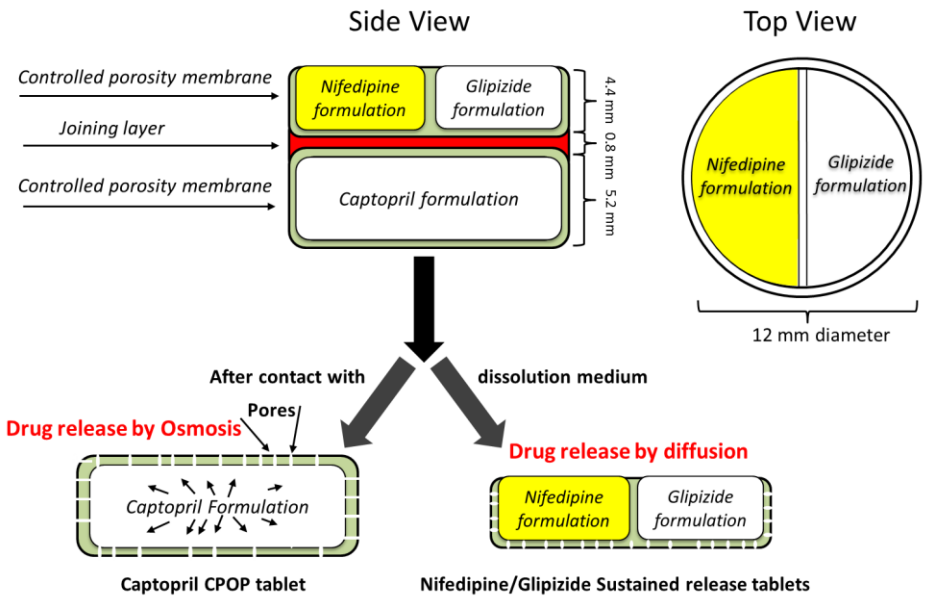

Figure 4.2: Schematic structural diagram of captopril osmotic pump and nifedipine and glipizide SR tablet.

The ideal printable ink (paste) was achieved by adjusting the ratios of the excipients to achieve good flowability of the paste through the print-head nozzles. The paste should be

smooth and homogenous to avoid nozzle blockage. Other parameters such as feed rate, extrusion pressure, line spacing, and layer thickness play a crucial role in 3D printing process. For example, the cellulose acetate shell paste was optimized by adjusting the ratios of the cellulose acetate and the D-mannitol together with the plasticizer, PEG 6000. Also, increasing the cellulose acetate concentration increased the paste viscosity, eventually making printing more difficult. Increasing the content of D-mannitol in the shell tended to produce a very fragile shell which would not hold up to the osmotic pressure experienced during dissolution testing [174]. A higher quantity of the pore forming agent would make lager pores and hence an increased drug release during the early stages of dissolution [170, 175]. Pastes for printing were optimized based on the above considerations and strategies.

4.4.2.2. Preparation of HPMC 2280 hydro-alcoholic gel

Hydro-alcoholic gel (water: ethanol 25: 75 (v/v)) was used as a binder to form a highly consistent, smooth paste. Using pure water could cause unnecessary HPMC 2280 hydration and swelling which lead to increases in size of the extruded wet tablet and problems of excessive tablet shrinking after drying. Hence, a hydro-alcoholic gel was used as it allows better penetration through the HPMC powder particles, retards surface hydration and particle swelling, and provides suitable rheological behaviour of the HPMC for printing [148-150]. The hydro-alcoholic binder also showed faster and better solvent uptake and quick evaporation rate [149]. The hydro-alcoholic gel was prepared by mixing an accurate volumes of the HPMC 2208 gel (1%, w/v) (prepared using a previously reported dispersion technique, more details found in chapter 2, page 58-59, figure 2.1 [66, 108]) and ethanol at ratio of 25:75 (v / v). The mixture was then stored in a sealed container in a cool place until required.

4.4.2.3. 3D printing process of multi-active tablets

The 3D printing process of multi-active tablets is illustrated in figure 4.3. All powders were mixed using a mortar and pestle for 15 minutes. Captopril and excipients powders were weighed and mixed together using a mortar and pestle. Sufficient quantity of the blend was weighed and mixed with a small volume of the hydro-alcoholic gel according to the formulae shown in Table 4.1 to form a paste. Three different HPMC 2280 loadings were used to investigate the effect of the hydrophilic polymer on drug release from cellulose acetate shell.

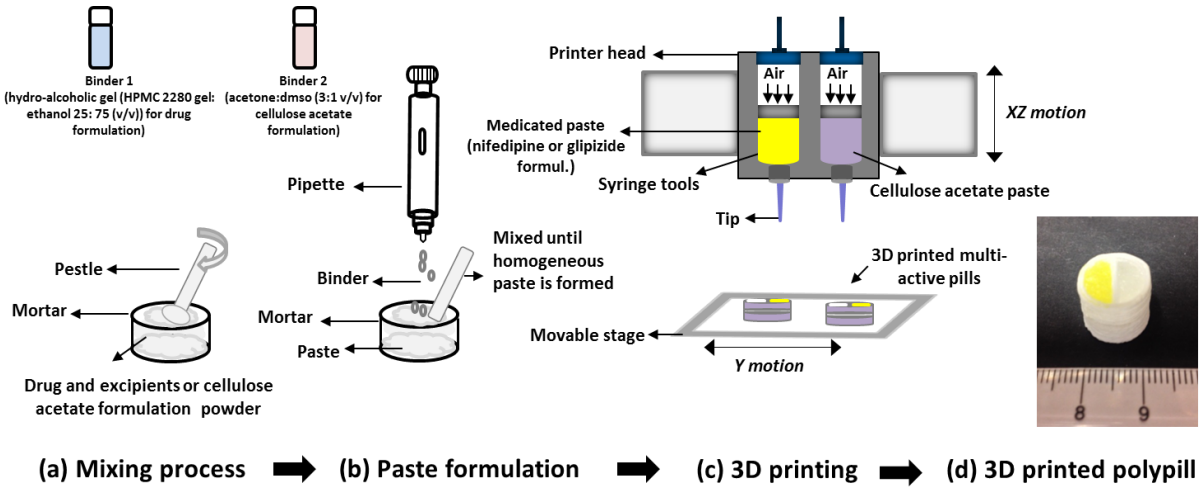

Figure 4.3: Schematic diagram of 3D printing process of multi-active tablets.

Table 4.1: The composition of various ingredients in captopril formulation at different HPMC 2280 concentration (% w/w) feed stock (dried formulae).

Ingredients	Function	Cap-HPMC (0 %, w/w)	Cap-HPMC (3.5 % w/w)	Cap-HPMC (7.5 % w/w)
Captopril	Active ingredient	18.5	18.5	18.5
HPMC* 2208	Hydrophilic matrix	0	3.5	7.5
Lactose	Osmogen	51	51	51
MCC**	Pushing agent	18.5	18.5	18.5
NaCl***	Osmogen	12	8.5	4.5

*HPMC = hydroxypropyl methylcellulose, MCC** = microcrystalline cellulose, and NaCl*** = sodium chloride. Water:ethanol (removed during drying) is used as a binder system.

The tablet shell paste was prepared by mixing 2.7 g from the blended powder mixture; cellulose acetate (CA) (to form a semi permeable membrane), D-mannitol (pore forming agent), and polyethylene glycol (PEG 6000) (plasticizer, increases shell plasticity) at the same mixing conditions as outlined above according to the formulae shown in Table 4.2. A volume (2.5 ml) of the binder (acetone and dimethyl sulfoxide (DMSO) at ratio of 3:1 v/v) was added to the powder and mixed until a smooth homogenous paste was achieved. DMSO was used to increase the boiling point of the binder system and avoid nozzle blockage due to acetone evaporation (low boiling point) during the extrusion process. The volume of DMSO per tablet was approximately 31 µl equivalent to 34.1 mg (3410 ppm) which is considered an acceptable volume/quantity in respect to DMSO human toxicity [97, 176-179]. Although DMSO received FDA approval for management of interstitial cystitis (given via intravesical) [180], however, it still not approved for use via oral rout. Therefore, these pills are not designed to be taken by a human at this stage and are illustrative of the potential of 3D printing.

Table 4.2: The percentage composition of the coating for captopril formulation in feed stock (dried formulae).

Ingredients	Function	Coating (% w/w)
Cellulose acetate (CA)	Semi-permeable membrane	55
D-Mannitol	Pore forming agent	32
Polyethylene glycol (PEG) 6000	Plasticizer	13

Acetone:DMSO (removed during drying) is used as a binder system.

Croscarmellose sodium (CCS) and sodium starch glycolate (SSG) (disintegrants), polyvinylpyrrolidone (PVP K30) (a binder) and D-mannitol (a filler) were blended and mixed with ultra-pure water to form a smooth and soft paste suitable for the joining layer according to the formulae shown in Table 4.3. This layer was designed to disintegrate quickly during the first hour in dissolution test and allow the tablet to split into two parts with different drug release mechanisms. Nifedipine and glipizide mixtures with poly ethylene glycole 6000 (PEG) at ratio of 1:5 (so as to increase solubility) were prepared using a previously reported fusion method [157]. PEG 6000 (hydrophilic carrier) was melted (60 $^{\circ}$C) in aluminium pans, and the molten carrier mass was left for 5 min at a fixed stirring rate. The active was incorporated gradually into the molten carrier mass and mixed for another 5 min at the same temperature [157]. The blend was flash-cooled on an ice bath to obtain a solid mass. The blend was transferred into glass vials and left in a freeze dryer for 24 h. The samples were milled and sifted through mesh no. 100 (150 µm) and stored in a desiccator until use.

Table 4.3: The percentage composition of various ingredients in the joining layer feed stock (dried formula).

Ingredients	Function	(% w/w)
Sodium starch glycolate (SSG)	Disintegrant	14
Croscarmellose sodium (CCS)	Disintegrant	7
Polyvinylpyrrolidone (PVP K30)	Binder	6
D-mannitol	Filler	73

Water (removed during drying) is used as a binder.

The nifedipine and glipizide PEG 6000 mixtures were separately blended with HPMC 2280 and lactose according to the formulae shown in Table 4.4. Tromethamine was added to the glipizide SR compartment as a solubility modifier to increase the micro-environmental pH of the matrix above the pKa of glipizide [171]. Each blend was mixed with a small volume of

the binder to form a soft paste and filled into two separate syringes for printing (one for nifedipine and one for glipizide).

Table 4.4: The percentage composition of various ingredients in nifedipine and glipizide formulation feed stock.

Ingredients	Nif-HPMC (3.5 % w/w)	Nif-HPMC (7.1 % w/w)	Nif-HPMC (10.7 % w/w)	Glip-HPMC (7.1 % w/w)	Glip-HPMC (10.7 % w/w)	Glip-HPMC (14.2 % w/w)
Nifedipine (active ingredient I)	10.7 (Hole I)	10.7 (Hole I)	10.7 (Hole I)	----	----	----
Glipzide (active ingredient II)	----	----	----	3.5 (Hole II)	3.5 (Hole II)	3.5 (Hole II)
HPMC 2208 (hydrophilic matrix)	3.5	7.1	10.7	7.1	10.7	14.2
PEG 6000 (solubilizer)	53.5	53.5	53.5	17.8	17.8	17.8
Tromethamine (solubilizer)	----	----	----	25	25	25
Lactose (filler)	32.3	28.7	25.1	46.6	43	39.5

Water (removed during drying) was used as a binder and solvent for HPMC 2208).

4.4.2.4. Printing parameters and ink filling

The printing settings were as follows; layer thickness 0.4 mm, tablet height 10.4 mm, tablet diameter 12 mm, initial height 0.4 mm (offset between the needle and the glass slide), extrusion pressure ranged from 3-4.5 bar, feeding rate 3 mm/s, and line spacing 0.3-0.45 mm (space between strands). Once the pastes were prepared and optimized they were rapidly loaded into the ink cartridge to minimise solvent loss. A 400 µm print tip was then attached. The air was removed by pushing the piston upwards. The multi-active tablets were extruded on a glass slide fixed on the printing area (160 × 30 × 60 mm) layer by layer starting with the captopril formulation, coating with cellulose acetate shell, printing joining layer, and SR compartments (Fig. 4.4) [181]. The whole tablets were placed in a vacuum dryer at 40 °C for 24 hours for complete drying.

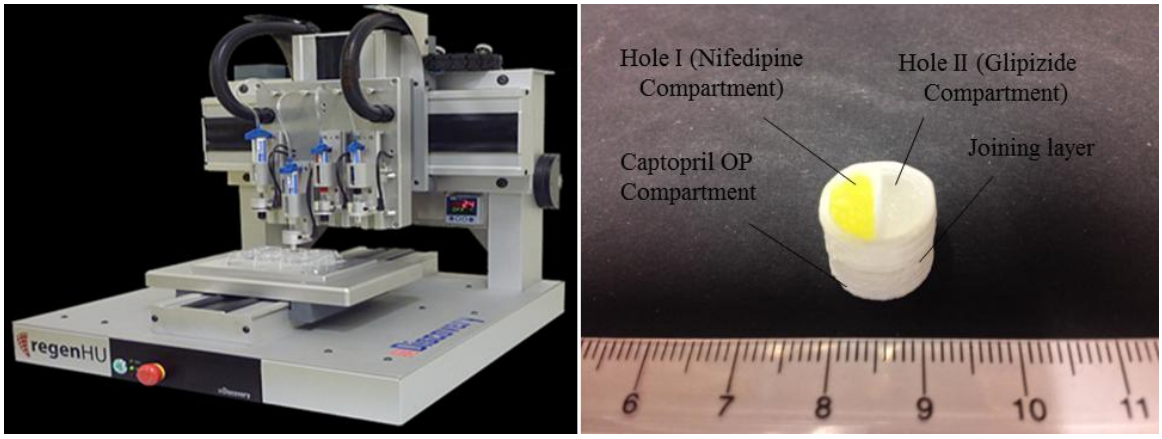

Figure 4.4: Photograph of regenHU 3D printer (left) [181], and image of multi-active tablet (right) composed of captopril osmotic pump compartment (bottom), and nifedipine (hole I) and glipizide (hole II) SR compartments (top) and joining layer (middle).

4.4.2.5. Drug concentration measurement for dissolution studies

A HP Agilent 1050 HPLC instrument was equipped with an ACE C18-AR analytical column (100 mm x 4.6 mm) with 5 µm particle size. The binary mobile phase was acetonitrile (HPLC grade with UV cut-off of 190 nm was used) and 10 mM phosphate buffer (pH 3), with a multi-step gradient. The auto-sampler was set up to make 40 µl injections, every 20 minutes. The flow rate of the mobile phase was 1 ml / min, the column temperature was 40 $^{\circ}$C and the UV detection wavelength was set to 205 nm. The mobile phase was degassed and filtered through a 0.45 µm membrane filter.

It is important to test the suitability of the developed HPLC method for the quantification of active drugs in the printed dosage forms. Three printed tablets were crushed in a mortar and passed through mesh no. 100 (150 µm). A quantity of the powder mixture equivalent to 50 mg of captopril, 30 mg nifedipine and 10 mg glipizide was transferred to a 100 mL volumetric flask. The drugs were dissolved in dissolution medium, centrifuged, and further diluted with dissolution medium and analysed by HPLC (Fig. 4.5).

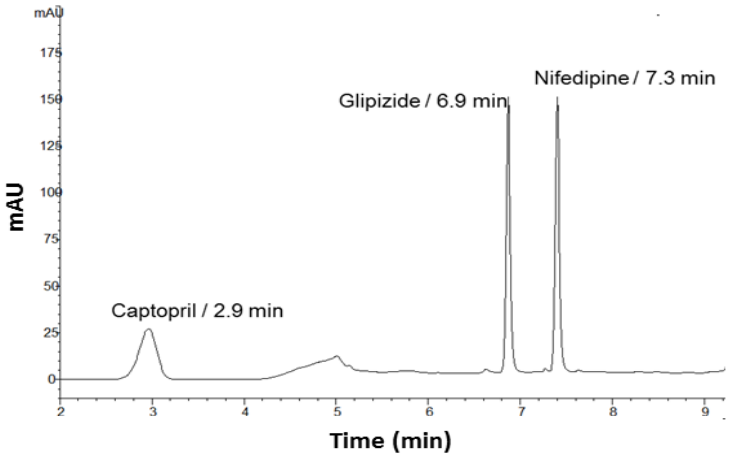

Figure 4.5: Representative chromatogram of the 3D printed tablets.

4.4.2.6. In vitro drug release

In vitro drug release studies of 3D printed osmotic tablets were performed using United States Pharmacopeia Convention (USP) Type I apparatus (rotation speed at 50 rpm, 500 ml pure water containing 0.1 % vitamin C (w/v), 0.25 % of tween 80 (v/v) and 0.25 % (w/v) tromethamine as the dissolution medium at 37°C ± 0.5°C). 5.0 ml samples were withdrawn at 2, 4, 6, 8, 10, 12, and 14 h. The samples were centrifuged for 10 min and a small volume from the supernatant was drawn and filled into HPLC amber glass vials. The samples were kept at 4 °C (to avoid nifedipine light degradation) until tested. The samples were tested using a HP Agilent 1050 HPLC with a UV detector at a wavelength of 205 nm. Drug dissolution studies were conducted in triplicate and the average of percentage cumulative of drug release as a function of time was plotted.

4.4.2.7. SEM

Variable pressure scanning electron microscopy (JEOL 6060LV, UK) was used to characterize shape and surface morphology of captopril osmotic pump compartment of the tablets. The samples were mounted onto carbon tape stubs, and sputter coated with gold (Leica EM SCD005 Sputter Coater), and SEM images were taken at different magnifications for the tablets before and after dissolution testing

4.4.2.8. XRPD

The XRPD patterns of pure captopril, nifedipine and glipizide, and their formulations were obtained at room temperature using an X'Pert PRO (PANalytical, Almelo, Netherlands) setup in reflection mode using Cu $K\alpha_1$ (λ = 1.54 A°) operating in Bragg–Brentano geometry. The generator voltage was set to 40 kV and the current to 40 mA and the samples were scanned over 2θ range of 5˚ until 30˚ in a step size of 0.026˚.

4.4.2.9. ATR-FTIR

Infra-red spectra of pure active ingredients (captopril, nifedipine, and glipizide) and their formulations were obtained using an ATR-FTIR (Agilent Cary 630 FTIR) spectrometer.

4.4.2.10. Content uniformity and weight variation

The drug content for each compound in the 3D printed multi-active tablets was determined using HPLC-UV at a wavelength of 205 nm after a suitable dilution with methanol.

To assess weight variation, 20 captopril tablet sections were individually weighed and their average calculated and compared with percentage of weight variation [144].

4.5. Results and discussion

4.5.1. In vitro drug dissolution

The captopril release data presented in figure 4.6a shows that the amount of HPMC had an effect on the captopril release rate. The release rate of captopril decreased as the amount of HPMC 2280 was increased.

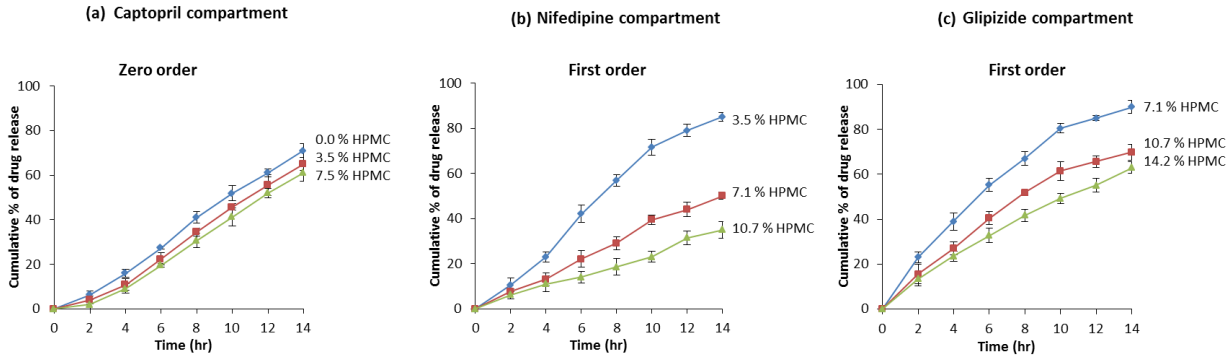

Figure 4.6: Cumulative % release from the three drug-loaded compartments of the 3D multi-active tablets.

The drug release data for glipizide and nifedipine from the printed tablets are presented in figure 4.6b and c and showed that all formulations displayed SR of the actives over a period of 14 h as required. As the amount of HPMC 2280 in the SR compartments increased from 3.5 % to 10.7 % (w/w) for nifedipine SR formulations and from 7.1 % (w/w) to 14.2 % (w/w) for glipizide SR formulations, the drugs release from the hydrophilic matrix decreased from 85 % to 35 % and from 90 % to 63 % after 14 h, respectively. Such an increase in concentration of HPMC 2280 is expected to lead to improved wettability, enhanced water uptake and greater swelling of the hydrophilic matrix and hence gel barrier formation which is consistent with the observed reduction in drug release rate from the formulation with greater amount of HPMC 2280 [66, 182].

4.5.2. SEM

SEM images of the coating membrane of the captopril containing compartment before and after dissolution are shown in figure 4.7 indicating that micro-pores were observed after dissolution. These were evenly distributed across the surface and are attributed to the dissolution of the D-mannitol pore forming agent included in the membrane formulation. Such pores would facilitate the ingress of water which is driven by the difference in osmotic pressure across the membrane. The difference in solute concentration across the membrane drives the ingress of water and triggers release of the captopril active. Form the observed micro-pores in the cellulose acetate shell after dissolution testing, it is likely that captopril was released by osmotic pump effect via these pores.

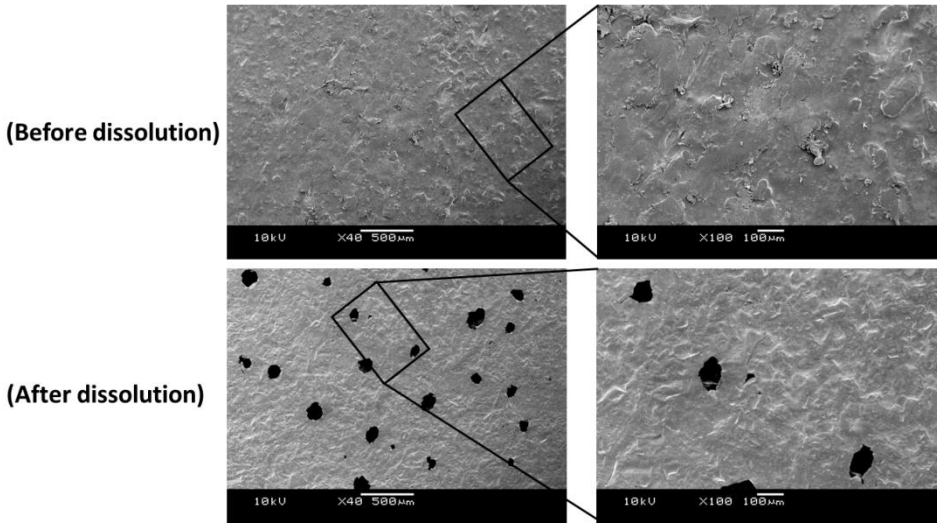

Figure 4.7: SEM micrograph of a captopril osmotic pump tablet before (top) and after (bottom) dissolution test.

4.5.3. Drug release kinetics

Mathematical models play a crucial role in determination of the drug release mechanism [37, 183]. The drug release data obtained were fitted using zero order, Higuchi, first order, and Korsmeyer-Peppas models to investigate the kinetics of captopril, nifedipine and glipizide release (Figure 4.8-10). All the captopril formulations were best modelled by zero order

release in which the release rate is constant and independent of drug concentration, as the relevant plots showed the highest linearity (r^2: 0.9967 to 0.9977).

Nifedipine and glipizide SR formulations; Nif-HPMC (3.5 %, w/w), Nif-HPMC (7.1 %, w/w), Glip-HPMC (7.1 %, w/w), and Glip-HPMC (10.7 %, w/w) were best fitted by first order kinetics (where the drug release rate depends on its concentration) with r^2 values of 0.9890, 0.9926, 0.9913 and 0.9908, respectively. Nif-HPMC (10.7 %, w/w) and Glip-HPMC (14.2 %, w/w) were best modelled by the Korsmeyer-Pappas model with r^2 values of 0.9832 and 0.9993, respectively. They showed n values (as in Eq. 4.1) ranging between 0.45 and 0.89 indicating that diffusion through the hydrated HPMC gel like layer from these formulations and erosion were the predominant mechanisms of drug release (Figure 4.9-11) [156, 182].

$$M_t/M_\infty = Kt^n \quad (4.1)$$

Where M_t/M_∞ is the fraction of drug released at time t, K is the release rate constant and n the release exponent [157].

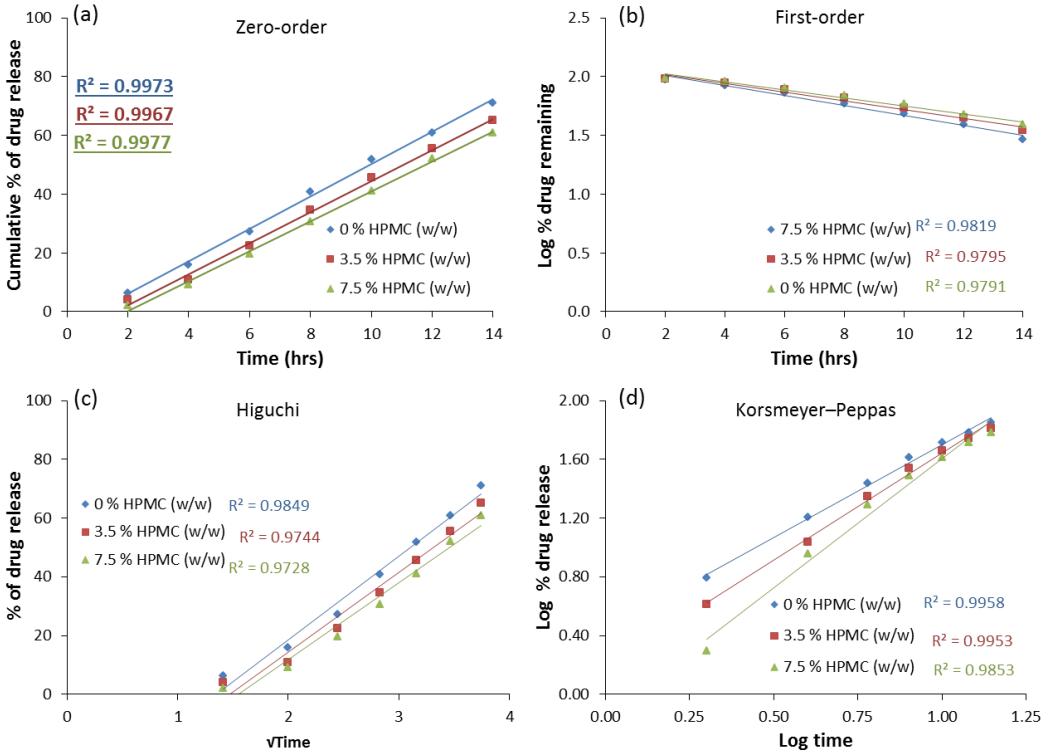

Figure 4.8: Representative release plots by fitting experimental release data, from the in vitro release of captopril osmotic pump compartments; HPMC (0 %, w/w), HPMC (3.5 %, w/w), and HPMC (7.5 %, w/w) to (a) Zero-order, (b) First-order, (c) Higuchi and (d) Korsmeyer–Peppas kinetic equations.

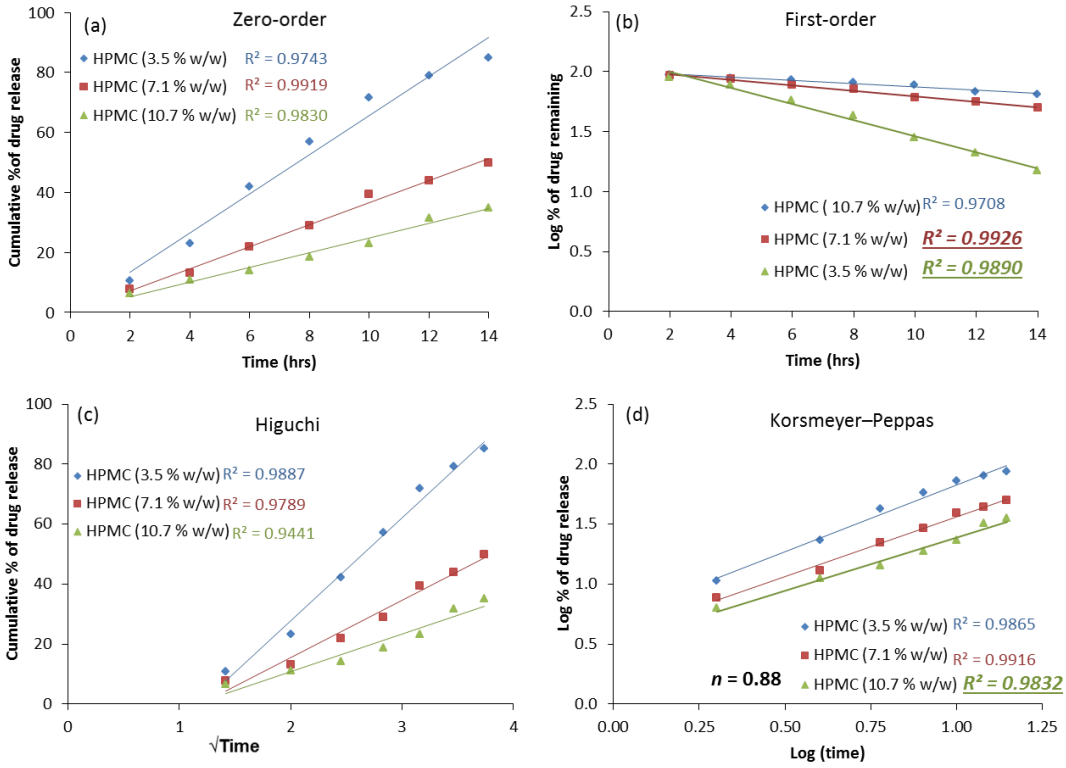

Figure 4.9: Representative release plots by fitting experimental dissolution data, from the in vitro release of nifedipine SR compartments; HPMC (3.5 %, w/w), HPMC (7.1 %, w/w), and HPMC (10.7 %, w/w) to (a) Zero-order, (b) First-order, (c) Higuchi and (d) Korsmeyer–Peppas kinetic equations.

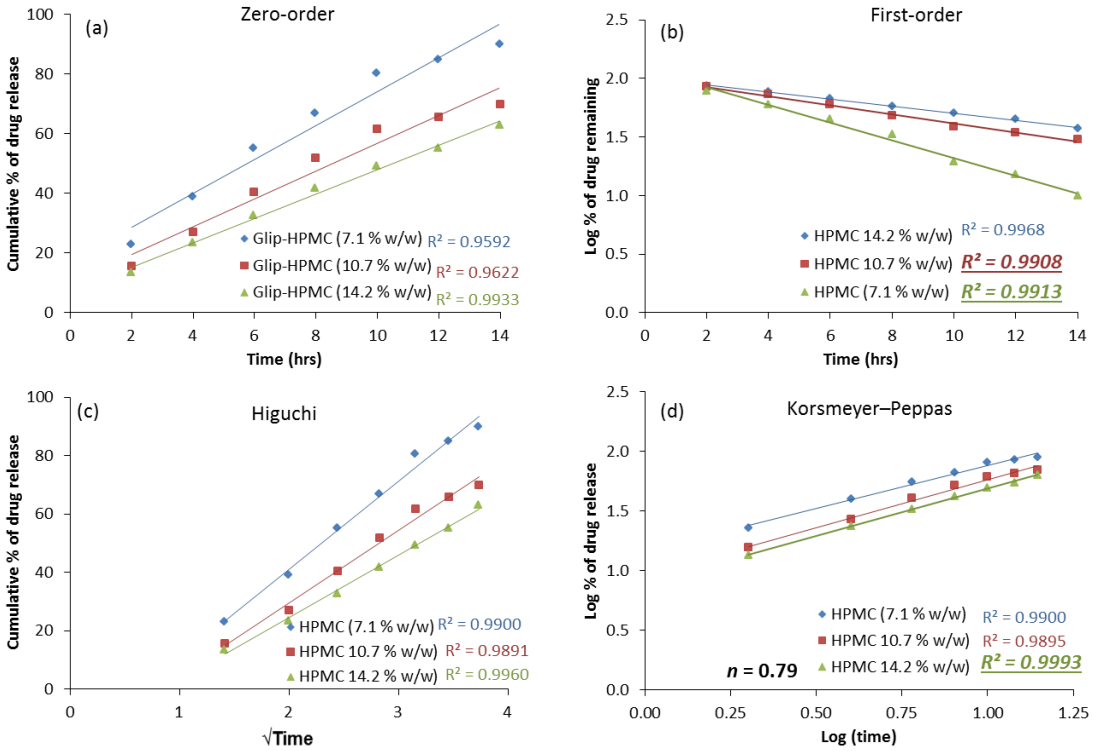

Figure 4.10: Representative release plots by fitting experimental dissolution data, from the in vitro release of glipizide SR compartments; HPMC (7.1 %, w/w), HPMC (10.7 %, w/w), and HPMC (14.2 %, w/w) to (a) Zero-order, (b) First-order, (c) Higuchi and (d) Korsmeyer–Peppas kinetic equations.

4.5.4. XRPD

XRPD data were collected on the pure as-received drugs before printing, and on the mixed formulations containing the drugs after printing, in order to investigate any changes in physical form on printing (Fig. 4.11). From visual inspection of the data, all as-received materials except HPMC exhibited multiple Bragg peaks in their XRPD patterns and are therefore crystalline. The patterns match well with those reported in the literature [184-186]. After formulation and printing, the Bragg peaks for nifedipine and captopril are still present, with extra peaks observed from the excipients. For example, the broad feature due to PEG 6000 is visible at around 23.5 degrees 2-theta for the nifedipine formulation, and the

appearance of a peak due to lactose is clearly visible at around 20 degrees for the captopril formulation. There is no obvious evidence of a change in physical form for the drug in these two formulations.

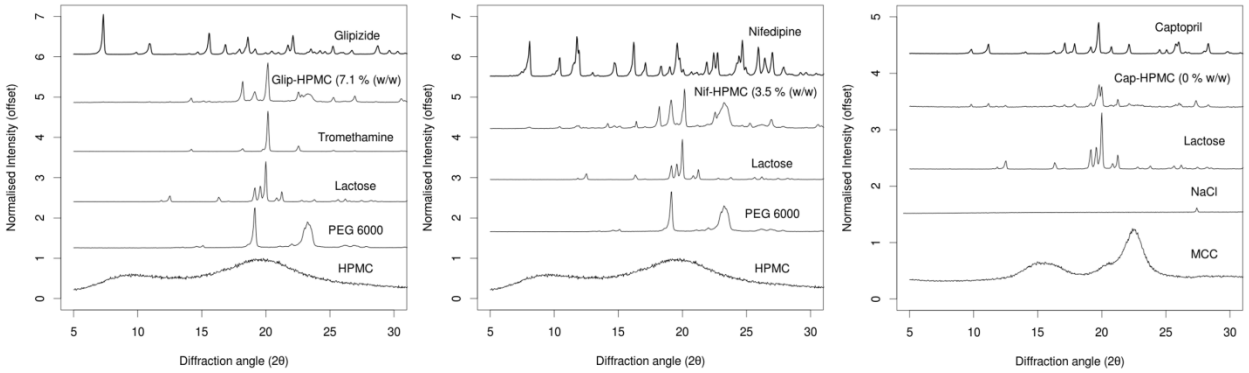

Figure 4.11: XRPD patterns of pure nifedipine, Nif-HPMC (7.1 % w/w), lactose, PEG 6000, and HPMC (left) (from the top to the bottom), pure glipizide, Glip-HPMC (10.7 % w/w), tromethamine, lactose, PEG 6000, and HPMC (middle) (from the top to the bottom), and pure captopril, Cap-HPMC (0 % w/w), lactose, NaCl, and MCC (left) (from the top to the bottom).

The situation appears to be slightly different for glipizide, for which no obvious Bragg peaks from glipizide are visible in the formulation, although they were clearly observed for the as-received pure drug. The Bragg peaks observed for this formulation appear to correspond with those expected for the excipients. It seems likely that the glipizide is present in its formulation in an amorphous or dispersed state (decomposition of glipizide can be ruled out on the basis of the ATR-FTIR and HPLC results). The increased dissolution rate of glipizide and nifedipine formulations and solubility of glipizide in multi-component formulations is a complex matter, but it may be that the dispersion of drug particles within the carrier (PEG 6000) at nearly a molecular level and the presence of the solubiliser (tromethamine) in the glipizide formulation has enabled full dissolution of the drug in the printer feed-stock, and the rapid solvent evaporation on drying has led to formation of an amorphous or dispersed form.

For nifedipine it may be that complete dissolution of the drug in the printer feed-stock did not occur and therefore crystalline material was precipitated in this case. Further work on the optimisation and understanding of printer feed-stocks would be required to resolve this difference. Given that all parts of the formulation behave appropriately in the present case, this physical form difference, while intriguing, is clearly not a key formulation parameter.

4.5.5. ATR-FTIR

The infrared results in figure 4.12 show that the actives within the separated compartments were not detectably interacting with the excipients used. The major diagnostic infrared peak positions of the actives did not change within the formulations when compared to control spectra of the drugs alone. However, the characteristics peaks (2700-2900 cm^{-1}) for both glibizide and nifedipine were slightly broadened.

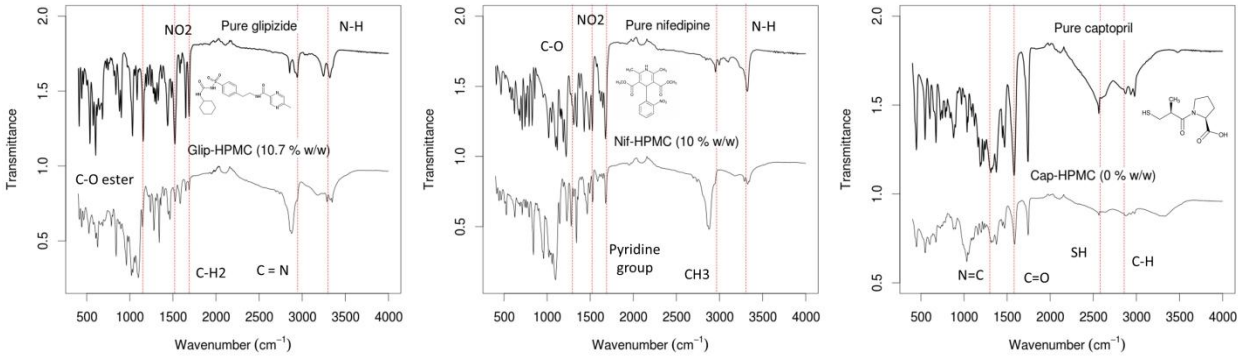

Figure 4.12: FTIR spectra of pure glipizide, and Glip-HPMC (10.7 % w/w) formulation (left), and pure nifedipine, and Nif-HPMC (7.5 % w/w) formulation (middle), and pure captopril, and Cap-HPMC (0 % w/w) formulation.

4.5.6. Content uniformity and weight variation

The average mass of the printed captopril core tablets was 240 ± 0.83 mg (n = 20). The content uniformity was 101.29 ± 0.81 %, and 99.89 ± 0.56 % for nifedipine and glipizide formulations, respectively. All formulation sections hence complied with the USP specifications in this regard.

4.6. Conclusions

3D extrusion printing of a complex multi-compartment tablet was successfully demonstrated for the first time. The complex multi-compartment tablet was able to deliver three actives via two different and defined release mechanisms; diffusion through gel layers and osmotic release through a controlled porosity shell. Based on the results, the captopril compartment showed the zero order drug release expected of an osmotic pump based mechanism and that the glipizide and nifedipine SR compartments showed either Korsmeyer-Peppas or first order release kinetics dependent upon the active/excipient ratio used. XRPD and FTIR data were used to show that there was no detectable interaction between captopril and the chosen excipients. However, the XRPD and FTIR data were showed a possible interaction between the drugs (nifedipine and glipizide) and PEG 6000 during solid dispersion formation in fusion method and that our method of 3D printing did not lead to a detectable change in the physical form of the drugs (e.g. polymorphism, hydration etc) apart from glipizide which was in an amorphous or dispersed state within its formulation compartment.

The actives were physically separated in the multi-compartment tablet to avoid incompatibility issues and to allow maximum flexibility in manipulating the environment of each drug. The present work is a significant step towards the demonstration and validation of 3D printing for the tailored manufacture of medicines, which has the potential to play a role in future developments in personalised care and treatment. In the next chapter, a more

complex 3D printed polypill with five actives and immediate and SR drug profiles will be presented

Chapter 5 Desktop 3D Printing of Five-In-One Dose Combination Polypill with Defined Immediate and Sustained Release Profiles

5.1. Abstract

A 3D extrusion printing technique was used to manufacture a multi-active solid dosage form or so called polypill. This polypill demonstrates that complex medication regimes can be combined in a single personalised tablet. This could potentially improve adherence for those patients currently taking many separate tablets and also allow ready tailoring of a particular drug combination/drug release for the needs of an individual. The polypill here represents a cardiovascular treatment regime with the incorporation of an immediate release (IR) compartment with aspirin and hydrochlorothiazide and three sustained release (SR) compartments containing pravastatin, atenolol, and ramipril. X-Ray Powder Diffraction (XRPD) and Attenuated Total Reflectance ourier transform infrared spectroscopy (ATR-FTIR) were used to assess drug-excipient interaction. The printed polypills were evaluated for drug release using USP dissolution testing. It has been found that the polypill showed the intended immediate and sustained release profiles based upon the active/excipient ratio used.

5.2. Introduction

In chapter 4 3D printing of a complex geometry containing three actives released by two distinct drug release mechanisms were demonstrated. Here, we continued the challenge, and aimed to print a polypill containing five actives physically separated by permeable cellulose acetate (CA) shell achieving more complex geometry containing three of the actives released with two distinct drug release mechanisms. The use of multiple medications to control complex illnesses such as cancer and heart failure is an increasingly used therapeutic strategy [187, 188]. Cardiovascular diseases is the most common cause of death globally and requires managing as a chronic condition in many people during large portions of their lifetime [189]. Each active pharmaceutical ingredient is traditionally administered via a separate dosage form [188]. This is inconvenient, can lead to errors in medication and presents significant patient compliance issues [188, 190]. Combining multiple actives into a single tablet with appropriate release profiles and doses (potentially optimised for individuals) is an attractive potential alternative [66, 188, 190, 191].

The term "polypill" refers to a tablet that is composed of a combination of several medicines [191]. The polypill concept has been used to treat and prevent cardiovascular disease and high blood pressure [192-195]. This polypill (in fact a capsule) manufactured by Cadila Pharmaceuticals Limited under trade name of Polycap™ is currently the only polypill formulation commercially available [193, 194, 196]. Based on previous work, we suggest that additive manufacturing or 3D printing is potentially well suited to producing a multicomponent polypill formulation [66, 194, 195]. As an approach 3D printing also offers the opportunity to produce personalised medicines and is adaptable to a distributed manufacturing model [66]. The freedom to form specific geometries in comparison to the restrictions of traditional tableting via powder compression can be used to separate

incompatible substances and to enable different release rates using shape and size as well as excipient manipulation [66, 197]. Here the designed five component polypill was based upon the currently available "polycap" commercial formulation with three sustained release compartments containing pravastatin, atenolol, and ramipril, which were physically separated by a hydrophobic cellulose acetate shell designed to act as a permeable carrier, and covered with an immediate release aspirin and hydrochlorothiazide compartment. Atenolol is a beta-blocker agent which is used to treat hypertension and also prevent and/or treat heart attack [198]. Hydrochlorothiazide is a thiazide diuretic used to prevent absorption of too much salt and to treat oedema or fluid retention in individuals with congestive heart failure, kidney disorder, and liver cirrhosis [199]. Ramipril is an angiotensin converting enzyme (ACE) used for treatment of hypertension and congestive heart failure which improves heart function after a heart attack [200]. Aspirin is an antiplatelet used to reduce the risk of blood clotting and reduce heart attacks or strokes [201]. Pravastatin is a 3-hydroxy-3-methylglutaryl–coenzyme A (HMG-CoA) reductase inhibitor used to reduce blood cholesterol and triglycerides in hyperlipidaemic patients and lower rates of strokes and heart attacks [202].

There has been a significant recent growth in interest of 3D printing as a tool in pharmaceutics and personalised medicine [78, 84, 98, 106, 203]. However, to date no reports have shown printing five actives in a single tablet with a multiple release mechanisms. Furthermore, issues such as low drug loading [87], stability during and after printing process [65, 84], poor mechanical properties, ink bleeding, migration, and capillary effect due to deposition of binder on powder bed (formulation/binder saturation) [101, 102], possible toxicity due to incorporation of photo-initiators, photo-curable polymers or degradants from UV curing could cause obstacles in pharmaceutical industries [45]. To address the above mentioned problems an extrusion based 3D system operated at room-temperature was

employed to print a polypill capable of delivering the five drugs via two predictable release mechanisms.

5.3. Aims and objectives

This chapter will investigate the 3D printing process of a polypill contains five compartmentalised actives (hydrochlorothiazide, aspirin, pravastatin, atenolol, and ramipril) with two controlled release profiles, and to characterise the 3D printed polypill for physical properties. A 3D Bio-Printer RegenHU will be used to print the polypill. United States Pharmacopeia Convention (USP) Type I apparatus (Dissolution-Erweka Dt600 Dissolution Tester) and High Performance Liquid Chromatography (HPLC 1050) will be used to study the drugs release from the 3D polypill. XRPD will be used to identify the physical form of the actives and match their patterns with the calculated patterns found in Cambridge Structural Database (CSD). Additionally, XRPD and ATR-FTIR will be used to investigate any changes in physical form of the actives within formulations after printing and drying processes.

5.4. Material and methods

5.4.1. Materials

Ramipril and pravastatin sodium were supplied by Kemprotec Limited (Cumbria, UK). Atenolol, aspirin, and hydrochlorothiazide, polyvinylpyrrolidine (PVP) and lactose were supplied by Sigma–Aldrich (Gillingham, UK). D-mannitol 99% was purchased from VWR International Ltd. (Leicestershire, UK). Sodium starch glycolate (Primojel®) was kindly supplied as a gift from DFE Pharma. Hydroxypropyl methylcellulose (HPMC 2280) (Methocel TM) was a gift from Colorcon®. Milli-Q water (resistivity 18.2 MΩ cm) was used for all formulations and solutions. All other reagents were of either HPLC or analytical grade. The chemical structures of the actives are presented in the figure 5.1.

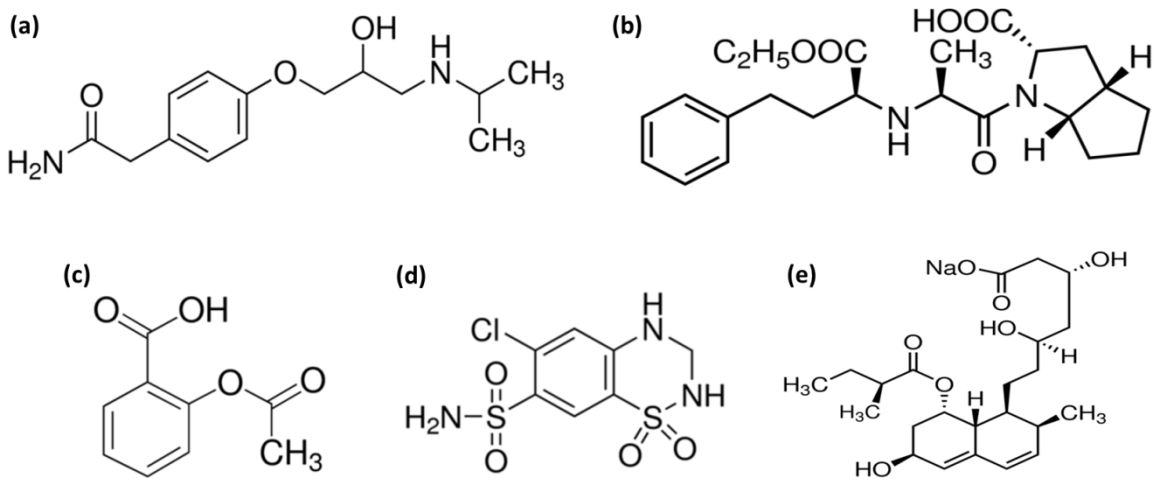

Figure 5.1**:** image of chemical structures of the active ingredients in the 3 D printed polypill; (a) Atenolol, (b) ramirpil, (c) aspirin, (d) hydrochlorothiazide, (e) pravastatin.

5.4.2. Methods

5.4.2.1. Design of polypill

A segmented tablet strategy was chosen to ensure that the actives were separated and could achieve the desired independent control of their release (Fig. 5.2). This concept provides flexibility in production of a 3D printed polypill with controlled drug release based on modifying the drug loading and excipient composition in the separate parts of the formulation. The dimensions of the polypill were selected according to the drug loading in respect of selected excipients (5.85 mm (height) × 6 mm (radius)). The geometry of the polypill was designed using a 3D drawing package (BioCAD, regenHU Villaz-St-Pierre, Switzerland). The combined drugs and their loadings in the polypill described in the experimental set up were adapted from clinical studies based on assessment of the effect of combination therapy on healthy middle aged individuals with one or more risk factors [194].

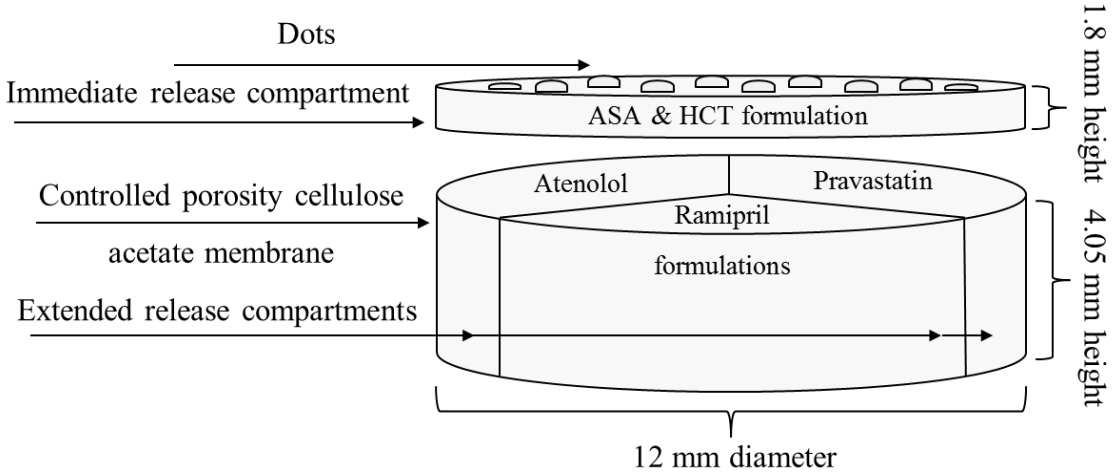

Figure 5.2: Schematic structural diagram of the polypill design, showing the aspirin and hydrochlorothiazide immediate release compartment and atenolol, pravastatin, and ramipril sustained release compartments.

5.4.2.2. Extrusion based 3D printing process of polypill

The 3D printing process of polypill is shown in figure 5.3. All powders were mixed using a mortar and pestle for 15 min. The printable paste used to form the barrier for the SR actives was prepared by mixing 3.15 g from the blended powder mixture; cellulose acetate (hydrophobic membrane/shell), D-mannitol (a filler), and polyethylene glycol (PEG 6000) (plasticizer) with 1.7 ml of the binder (acetone and dimethyl sulfoxide (DMSO)) until a smooth homogenous paste was achieved according to the formulae in Table 5.1.

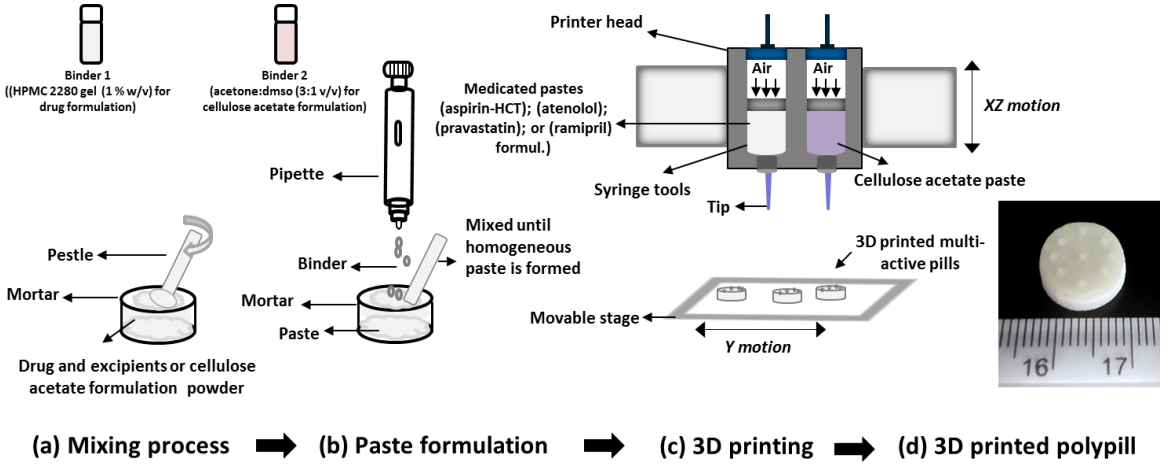

Figure 5.3: Schematic diagram of 3D printing process polypill.

Table 5.1: The weight percentage composition of various ingredients in cellulose acetate shell for SR formulation in feed stock (dried formulae).

Ingredients	Function	Coating (% w/w)
Cellulose acetate	Hydrophobic shell	22.64
D-mannitol	Filler	62.26
PEG (6000)	Plasticizer	15.10

Acetone:DMSO (removed during drying) is used as a binder.

DMSO was used to increase the boiling point of the binder system and avoid nozzle blockage due to acetone evaporation (low boiling point) during the extrusion process. Acetone/DMSO at a ratio of 3:1 v/v was used as a binder. The volume of DMSO per tablet was approximately 28 µl, equivalent to 30.8 mg (3080 ppm) which is considered an acceptable volume/quantity in respect to DMSO human toxicity and was within the limit of the class 3 solvents (5000 ppm/day) which stated in ICH Harmonised Tripartite Guidance [97, 176-178, 204]. However, these tablets are not going to be tested on a human at this stage and are illustrative of the potential of 3D printing. Powders of atenolol, pravastatin, and ramipril were separately

blended using a mortar and pestle for 15 min with the required excipients, to ensure a homogeneous powder blend. Ultra-pure water was added to the powder and mixed as per the method above according to the formulae shown in Table 5.2.

Table 5.2: The weight percentage composition of various ingredients in atenolol, pravastatin, and ramipril formulation feed stock for the sustained release compartments of the polypill.

Ingredients	Function	ATEN-HPMC* (15 % w/w)	PRA-HPMC** (15 % w/w)	RAM-HPMC*** (15 % w/w)
Atenolol	Active ingredient I	30.00	----	----
Pravastatin	Active ingredient II	----	20.00	----
Ramipril	Active ingredient III	----	----	15.00
HPMC 2208	Hydrophilic matrix	15.00	15.00	15.00
Lactose	Filler	55.00	65.00	70.00

*ATEN = atenolol, **PRA = pravastatin, and ***RAM = ramipril, HPMC = hydroxypropyl methylcellulose. Water (removed during drying) is used as a binder and solvent for HPMC 2208.

The IR layer was composed of aspirin and hydrochlorothiazide (active ingredients), sodium starch glycolate (disintegrant), and polyvinylpyrrolidone (PVP K30) (binder). The powder was blended and mixed with ultra-pure water to form a smooth and soft paste according to the formulae shown in Table 5.3.

Table 5.3: The weight percentage composition of various ingredients in aspirin and hydrochlorothiazide IR formulation feed stock for the IR compartment of the polypill.

Ingredients	Function	ASA_HCT-IR* compartment
Aspirin	Active ingredient	28.62
Hydrochlorothiazide	Active ingredient	5.86
Sodium starch glycolate (SSG)	Disintegrant	55.18
Polyvinylpyrollidine K30 (PVP)	Binder	10.34

*ASA = acetylsalicylic acid (aspirin), HCT = hydrochlorothiazide, and IR = immediate release. Water (removed during drying) is used as a binder

All the pastes were loaded into separate ink cartridges for extrusion through a 400 μm print tip. The hydrophobic cellulose acetate shell was first extruded (no drying step needed), followed by extrusion of the SR pastes containing the actives, pravastatin, atenolol, and ramipril inside the segmented compartments of cellulose acetate to form SR compartments. The IR paste containing aspirin, hydrochlorothiazide, SSG, and PVP K30 was then extruded on the top to cover the SR compartments to form IR compartment. A series of raised dots were also printed onto the top of the tablet to facilitate identification of the formulation both visually and by touch, the composition of these was the same as the upper "IR" layer (Fig. 5.4).

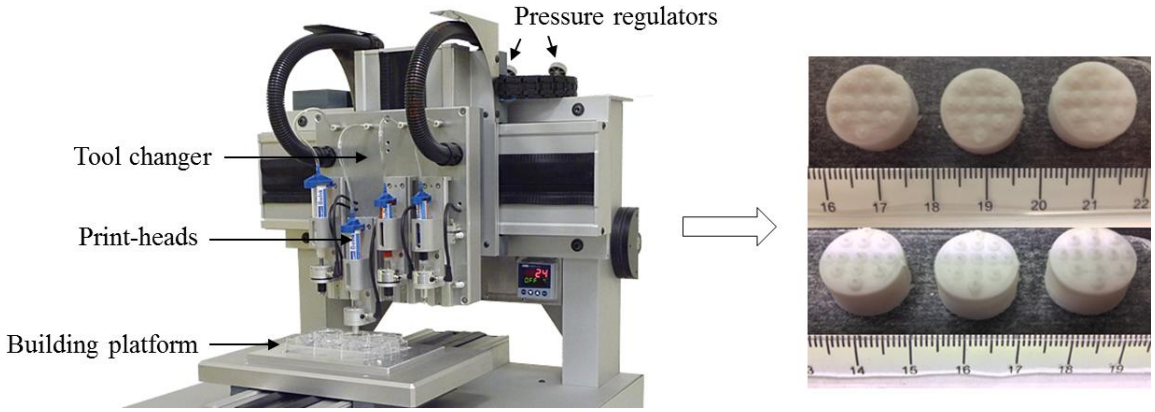

Figure 5.4: Photograph of regenHU 3D printer (left) [181], and image of multi-active tablet (right) (5.85mm(height) × 6mm (radius) composed of SR compartments, and IR dotted compartment.

The total printing time was 25 min followed by being placed in a vacuum dryer at 40 °C for 24 h for complete drying. The main challenging in this chapter is the fact that five different pastes were extruded into the same tablet (CA shell, atenolol, pravastatin, ramipril and aspirin formulations) using the same printer.

5.4.2.3. Dissolution studies

A HP Agilent 1050 HPLC equipped with an ACE C18-AR analytical column (100 mm× 4.6 mm) with 5 µm particle size was used to analyse dissolution release media for drug content. The auto-sampler was set up to make 40 µl injections, every 25 min. The flow rate of the mobile phase was 1 ml/min, the column temperature was 40 °C and the UV detection wavelength was 215nm. The mobile phase (acetonitrile HPLC grade and water containing 0.1% v/v of trifluoroacetic acid) was degassed and filtered through a 0.45 µm membrane filter. A mixture of actives (75 mg of aspirin, 12.5 mg of hydrochlorothiazide, 25 mg of atenolol, 20 mg of pravastatin, and 5 mg of ramipril) was dissolved in the dissolution medium and separated using the above HPLC method (Fig. 5.5). *In vitro* drug release studies of the 3D printed polypill were performed using USP Type I apparatus (rotation speed at 50 rpm,

900 ml phosphate buffer, pH 6.8 containing 0.5% of Tween 80 (v/v) as the dissolution media at 37 °C ± 0.5 °C). 5.0 ml samples were withdrawn at 5, 15, 30, 60, 120, 240, 360, 480, 600, 720 min. The samples were centrifuged and a small volume from the supernatant was drawn and filled into HPLC amber glass vials. The samples were kept at 4 °C (to decrease drug degradation) until tested. Drug dissolution studies were conducted in triplicate and the average of percentage of cumulative drug release as a function of time was determined.

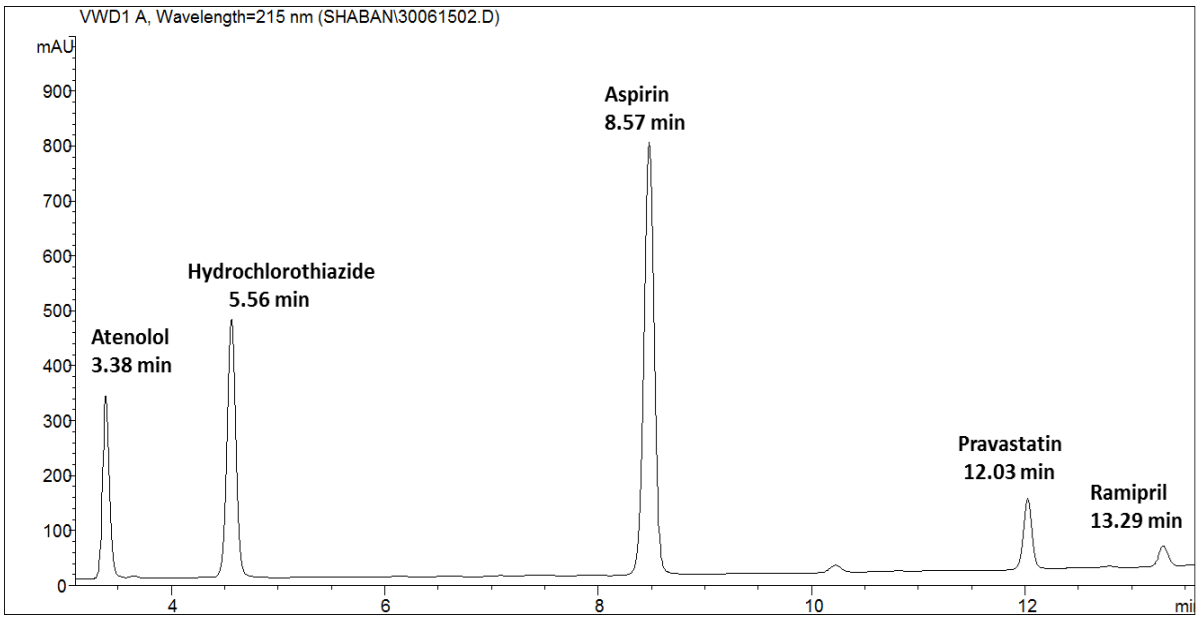

Figure 5.5: Representative Chromatogram of the 3D printed polypill.

5.4.2.4. XRPD

The XRPD patterns of pure atenolol, pravastatin, ramipril, hydrochlorothiazide, and aspirin and their formulations (immediate and sustained release formulations) were obtained at room temperature using an X'Pert PRO (PANalytical, Almelo, Netherlands) setup in reflection mode using Cu $K\alpha_1$ (lambda =1.54 Å) operating in Bragg– Brentano geometry. The generator voltage was set to 40 kV and the current to 40 mA and the samples were scanned over 2θ range of 5° until 30° in a step size of 0.026°.

5.4.2.5. ATR-FTIR

In order to investigate possible interactions between the actives and the selected excipients in their formulations, infrared spectra of pure active ingredients and their formulations were obtained using an ATR-FTIR (Agilent Cary 630 FTIR) spectrometer.

5.5. Results and discussion

5.5.1. In vitro drug dissolution

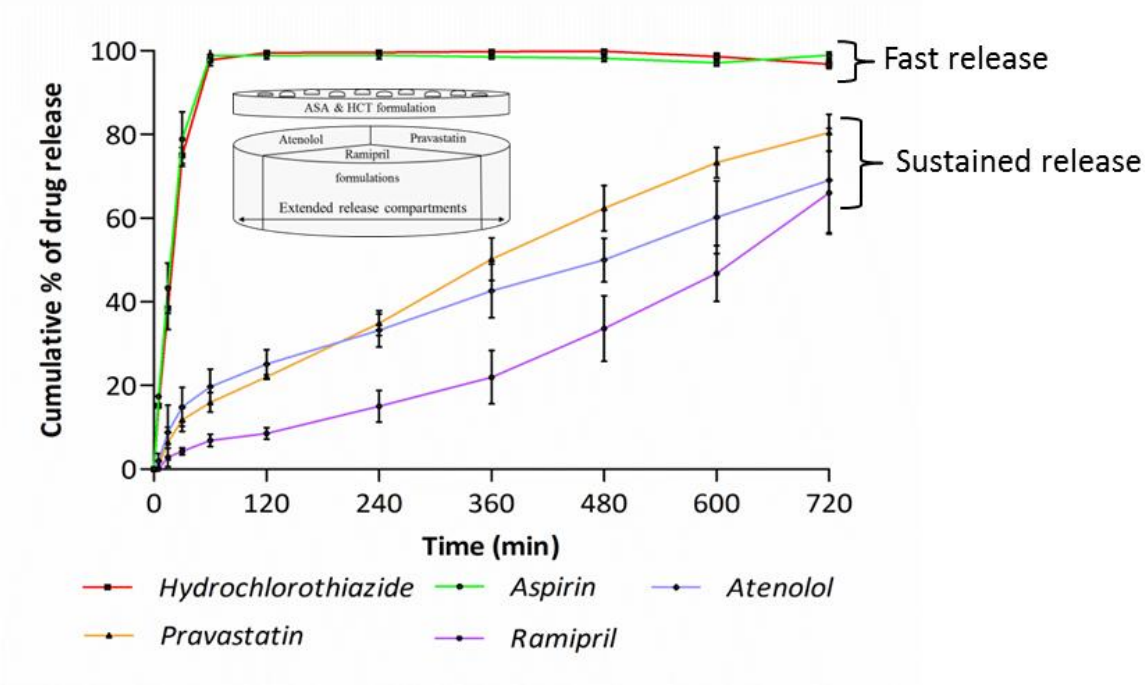

Figure 5.6: In vitro cumulative drug release profile of each drug from the five drug-loaded compartments of the polypill.

Dissolution data from the polypill (Fig. 5.6) show that more than 75% of the aspirin and hydrochlorothiazide were released within the first 30 min. This drug release is attributed to the inclusion of the disintegrant, sodium starch glycolate, which rapidly absorbs water and swells leading to rapid disintegration of this portion of the polypill and fast drug release. The same figure also shows that atenolol, pravastatin, and ramipril displayed sustained release over a period of 720 min as required; with 69%, 81%, and 66% released respectively. This release is consistent with the effects of rapid hydration of the HPMC 2280 leading to a gel

like layer formation and swelling to form a hydrophilic matrix that slows drug release and also to the presence of the permeable cellulose acetate shell, which is expected to retard drug release [95, 205, 206]. These data clearly illustrate the potential to achieve different drug release profiles from the same tablet for different drugs. As the three drugs that require sustained release are in separate compartments this also clearly shows the opportunity that 3D printing provides to vary loading and the fine detail of each drug release.

5.5.2. XRPD

XRPD data were collected on the pure as-received drugs before printing, and on the mixed formulations (immediate and sustained release formulations) containing the drugs after printing, in order to investigate any changes in physical form on printing (Fig. 5.7 and 5.8).

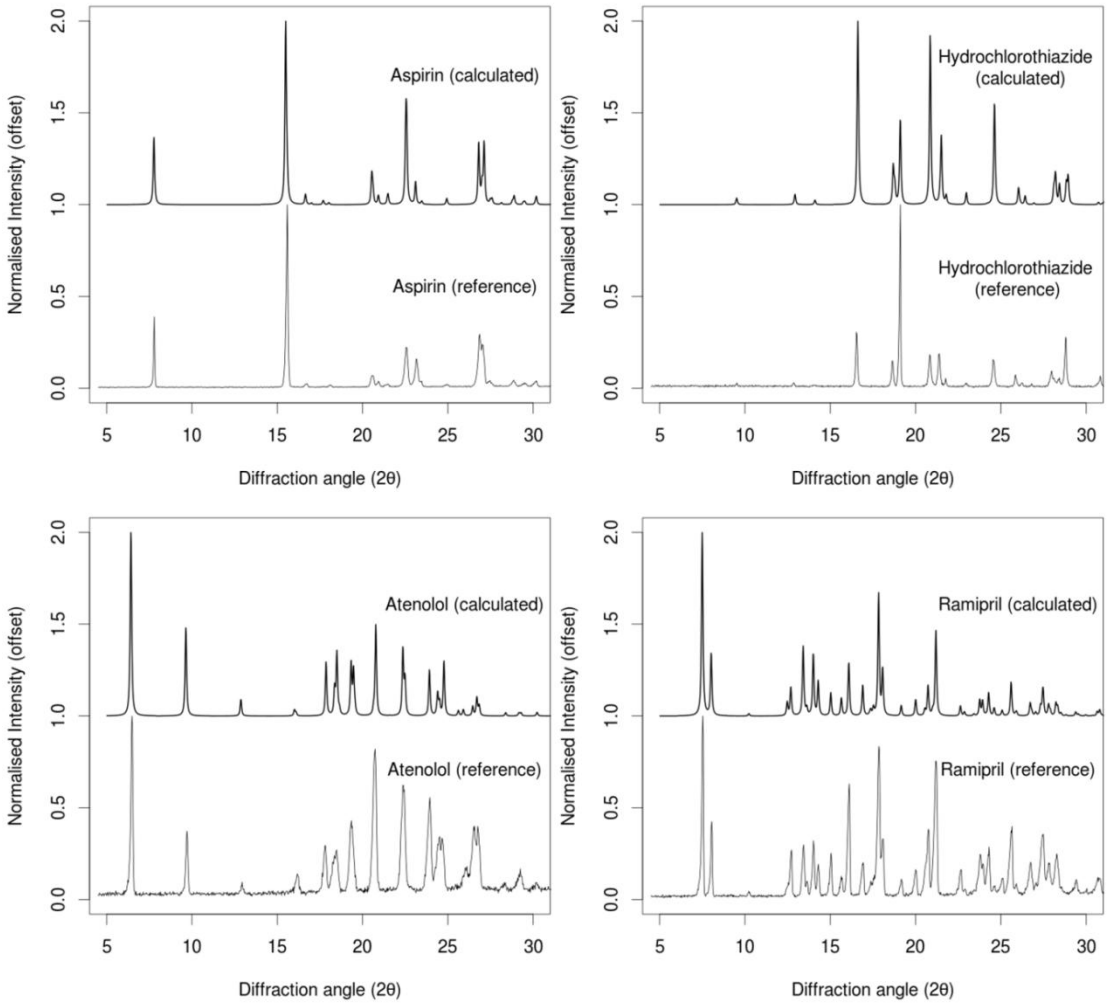

Figure 5.7: XRPD patterns of the calculated and reference (measured) aspirin (top-left), hydrochlorothiazide (top-right), atenolol (bottom-left), and ramipril (bottom-right).

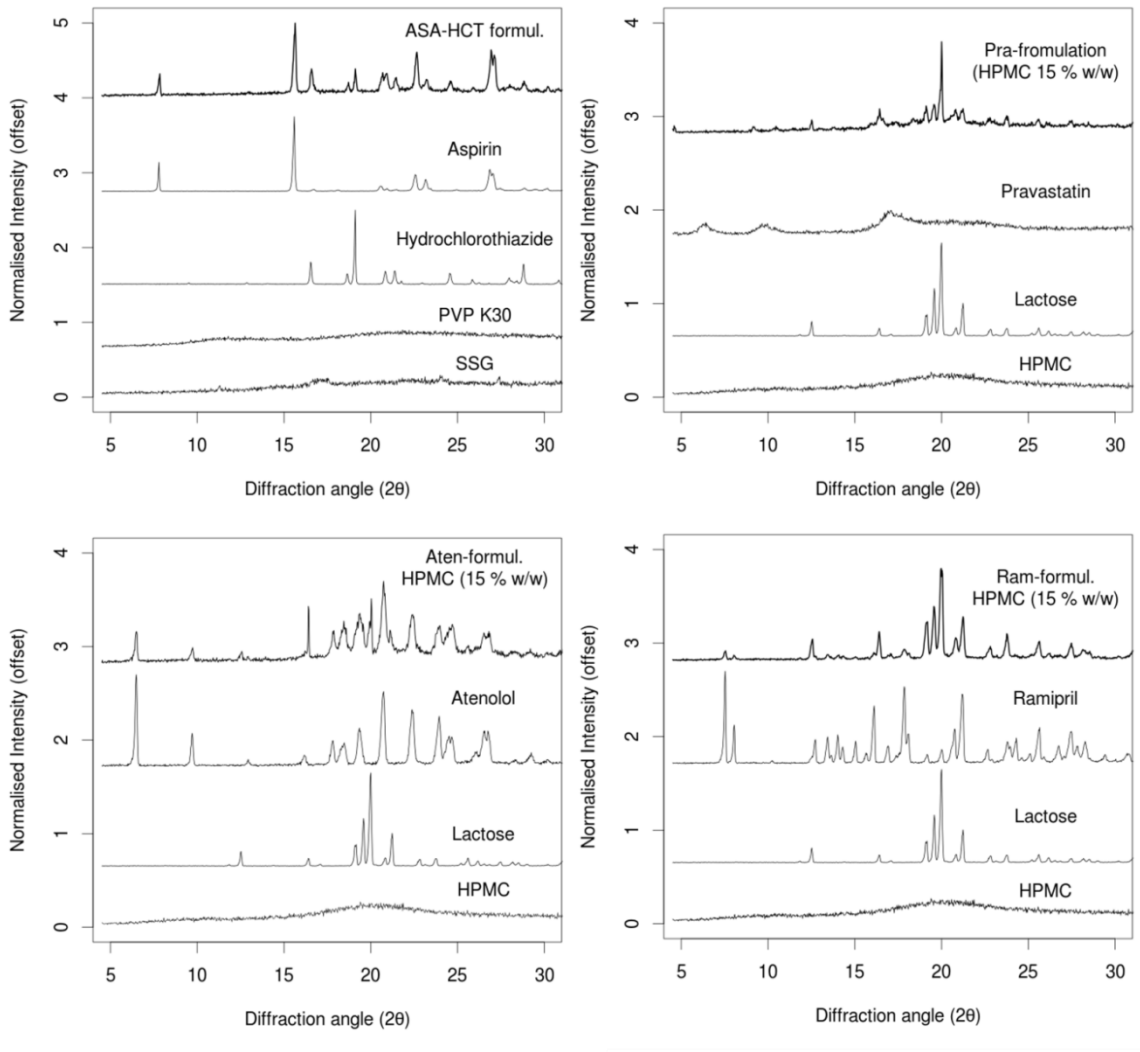

Figure 5.8: XRPD patterns of ASA-HCT-formul., pure aspirin, pure hydrochlorothiazide, (polyvinylpyrrolidine) PVP k30, and sodium starch glycolate (top-left), Pra-formul. (HPMC 15% w/w), pure pravastatin, lactose, and HPMC (top-right), Aten-formul. (HPMC 15% w/w), pure atenolol, lactose, and HPMC (bottom-left), and Ram-formul. (HPMC 15% w/w), pure ramipril, lactose, and HPMC (bottom-right).

All as-received materials exhibited multiple sharp Bragg peaks in their XRPD patterns related to their crystalline nature, except pravastatin which exhibits no sharp Bragg peaks indicating that it exists in an amorphous state. The patterns for the crystalline materials match those reported in the Cambridge Structural Database (CSD) [207-210]. After formulation and

printing, the Bragg peaks for ramipril, aspirin, hydrochlorothiazide, and atenolol are still present, with peaks also observed as expected from the excipients. For example, the appearance of a sharp peaks due to lactose are clearly visible at 20, 19, and 18° 2-theta for the pravastatin, ramipril, and atenolol formulations, and the broad feature due to HPMC 2280 is visible at around 20° 2-theta for the atenolol formulation. There is therefore no evidence of a change in physical form for the drugs in these three formulations. The situation is comparable for pravastatin, for which no obvious Bragg peaks from pravastatin are visible in both as-received and in the final formulation.

5.5.3. ATR-FTIR

The infrared results in figure 5.9 show that the actives within the separated compartments were not detectably interacting with the excipients used. The major diagnostic infrared peaks of the actives did not change within the formulations as compared to control spectra of the drugs alone, indicating that there were no detectable interactions between the drugs and the selected excipients.

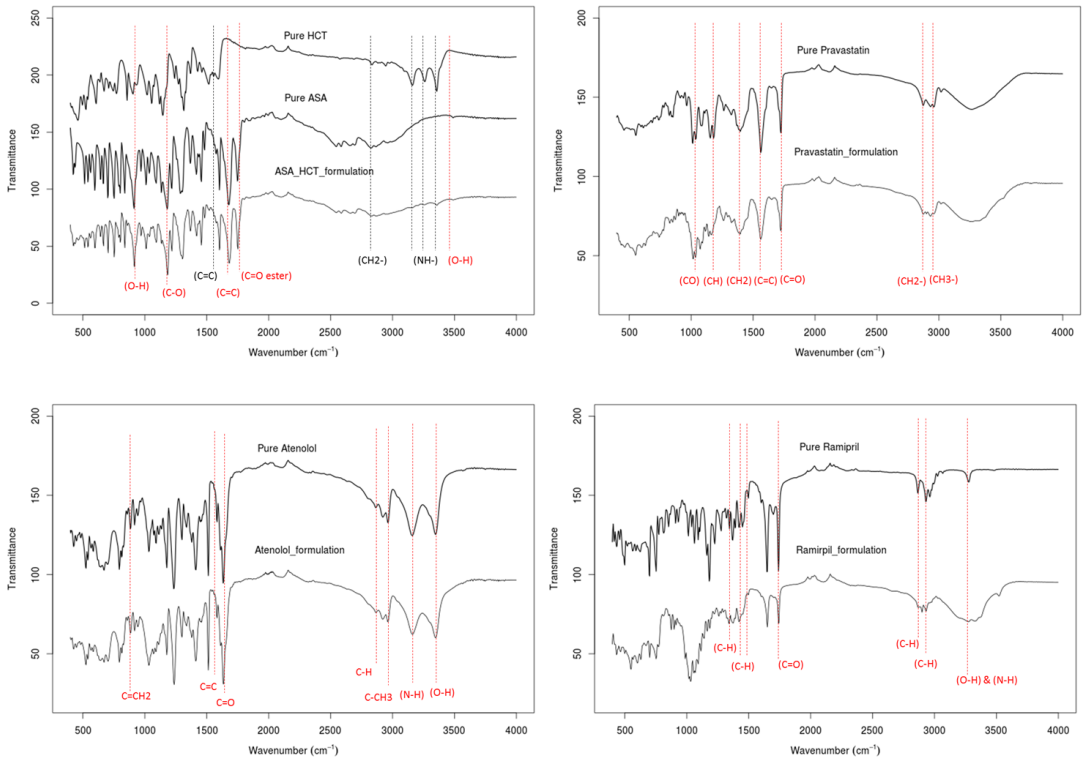

Figure 5.9: FTIR spectra of pure actives; aspirin (top left), hydrochlorothiazide (top left), pravastatin (top right), atenolol (bottom left), and ramirpil (bottom right) and its formulations (from the top to the bottom).

5.6. Release Kinetics

Mathematical models for the drug release can be used to help determine the nature of a drug release mechanism [37]. The drug release data obtained were fitted using *zero order*, *Higuchi*, *first order*, and *Korsmeyer-Peppas* models (Fig. 5.10-11). Aspirin and hydrochlorothiazide formulations were best fitted by *first order* kinetics (where the drug release rate depends on its concentration) with R^2 values of = 0.9781 and 0.9897, respectively (Figure 5.10). Atenolol, pravastatin, and ramipril formulations; *ATEN-HPMC (15 % w/w), PRA-HPMC (15 % w/w), and RAM-HPMC (15 % w/w)* were best modelled by the *Korsmeyer-Pappas* model with R^2 values of 0.9928, 0.9878, and 0.9575, respectively (Fig. 5.11). These showed *n* values (as in Equation 1) ranging between 0.45 and 0.89 indicating

that diffusion through the hydrated HPMC gel layer from these formulations and erosion were the predominant mechanisms of drug release [156, 182].

$$M_t/M_\infty = Kt^n \quad (5.1)$$

Where M_t/M_∞ is the fraction of drug released at time t, K is the release rate constant and n the release exponent [37, 157].

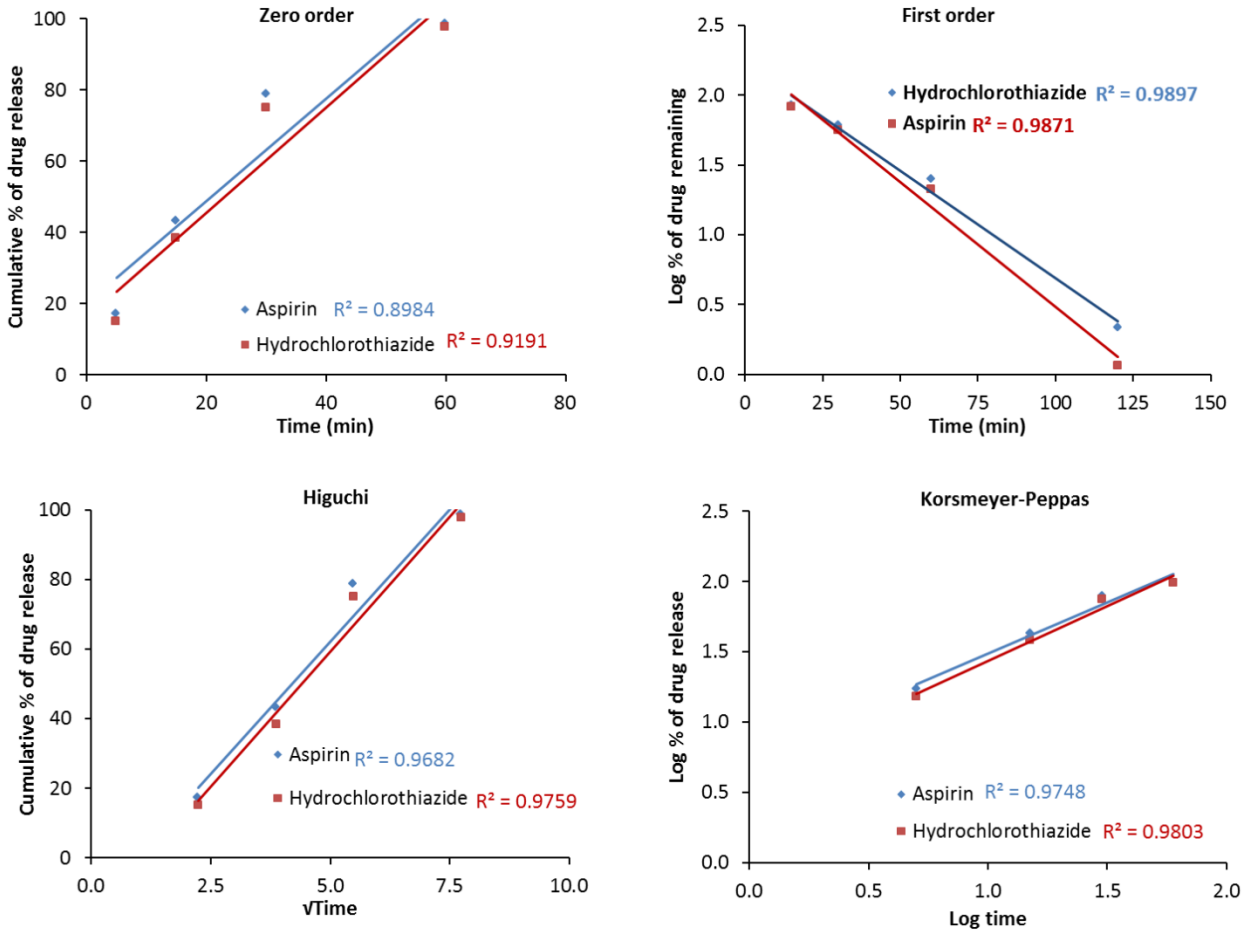

Figure 5.10: Representative release plots by fitting experimental release data, from the in vitro release of ASA_HCT-IR compartment to (a) *Zero-order*, (b) *First-order*, (c) *Higuchi* and (d) *Korsmeyer–Peppas* kinetic equations. The first four data points (5, 15, 30, and 60 min) only were used due to the drug release being complete.

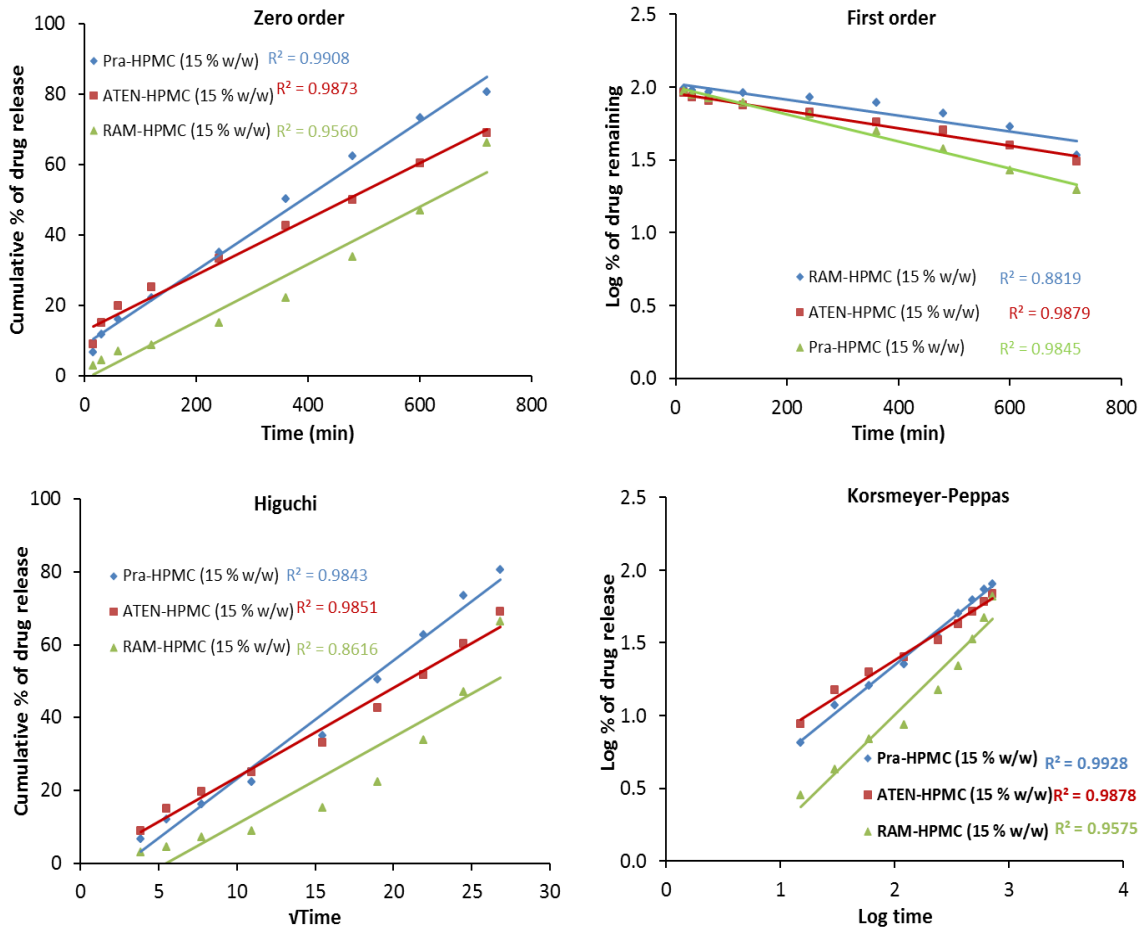

Figure 5.11: Representative release plots by fitting experimental release data, from the in vitro release of pravastatin sustained release compartment; PRA-HPMC (15 %, w/w), ATEN-HPMC (15 %, w/w), and RAM-HPMC (15 %, w/w) to (a) *Zero-order*, (b) *First-order*, (c) *Higuchi* and (d) *Korsmeyer–Peppas* kinetic equations.

5.7. Pharmaceutical considerations

A relationship has been shown between heart disease and renal failure and various modifiable risk factors, such as hypertension, dyslipidaemia, and platelet capacity [174, 211-213]. Therefore, patients over 55 years old with one or more risk factors, including hypertension, obesity, and diabetes can benefit from a combined medications such as that demonstrated here that includes an antiplatelet, cholesterol and blood pressure lowering agents [214-216]. To use a combined medication approach successfully a number of challenges need to be considered, including: making the novel dosage form acceptable to health professionals and

patients; formulation issues; additional cost; achieving regulatory approval; ensuring this becomes a first-line therapy (should be more effective and have no more side effects than drugs taken individually) [190]. The polypill demonstrated here addresses some of these issues, it is of an acceptable size and appearance for a patient, offers the prospect of increasing patient adherence since only one tablet needs to be taken [66], and also should reduce risk of mistakes by patients who forget to take a certain medicine within a combination of different tablets [190] Issues such as cost and regulatory approval are beyond the scope of the current work. Furthermore, application of 3D printing in pharmaceutics could offer a flexible tool to tailor the combined drug doses according to the patient's needs. For example, control of tablet size and shape for children and elderly patient with difficulty handling tablets or swallowing, and printing 'special' tablets for patients with allergies to certain excipients. A simple visual/tactile identifier can readily be added to 3D printed tablets to aid sight compromised patient as well.

5.8. Conclusions

3D extrusion printing of a novel complex geometry five-in-one polypill was successfully demonstrated. The dissolution release profile is also showed that the polypill is able to deliver five actives via two different and well defined release mechanisms: immediate and sustained release. The drugs were physically separated in the polypill to avoid incompatibility issues and allow maximum flexibility in manipulating the environment of each drug. XRPD and FTIR data were used to show that there was no detectable interaction between the drugs and the chosen excipients, and that our method of 3D printing did not lead to a detectable change in the physical form of the drugs (e.g. polymorphism, hydration). Such a combination of actives as used here has been shown to be important in prevention and treatment of cardiovascular diseases. The drugs combined as a polypill provide the prospect of improved adherence to such combination therapies due to the convenience of a single tablet and the

potential to optimise and personalise dosages and release for each drug independently in such multi-drug dosage forms.

Chapter 6 General Conclusion and Future Work

The aim of the thesis was to investigate whether extrusion based 3D printing can be used at room temperature as a novel tool to produce a realistic and complex drug formulation product with acceptable physico-chemical properties. At the start of this PhD project, there was a very few limited amount of literature studying feasibility of 3D printing of tailored oral solid dosage forms [65, 84, 87, 102]. During the PhD some other studies were conducted to emphasise the importance of this technology for the future of drug manufacturing process [45, 65, 84, 98, 99, 217]. Most of these studies were investigated the capability of the technology to print a single active with one drug release profile, i.e., either sustained or rapid release (RR) mechanism. However, one study was done to investigate multi-mechanism oral dosage forms containing single active ingredient [101]. To date, no report has showed 3D printing of multi-actives in a single tablet with a distinct multiple release mechanisms. Furthermore, issues such as low drug loading [87], stability during and after printing process [65, 84], poor mechanical properties, ink bleeding, migration, and capillary effect due to deposition of binder on powder bed (formulation/binder saturation) [101, 102], possible toxicity due to incorporation of photo-initiators, photo-curable polymers or degradants from UV curing could cause obstacles in pharmaceutical industries [45]. Therefore, to address the above mentioned issues, an extrusion based 3D printing technique operated at room-temperature was used to print pharmaceutical tablets. The drug loadings in all 3D printed formulations in this work were designed to mimic the therapeutic doses of the currently available conventionally manufactured commercial formulations.

The work presented in chapter 3 investigated the use of a standard pharmaceutical ingredients and a single step extrusion based 3D printing process with a low cost (less than $1000) desktop Fab@Home 3D printer to produce a 3D printed guaifenesin bi-layer tablets (GBTs) capable of mimicking the release of standard commercial GBTs. The characterisations showed that the 3D printed GBTs could mimic the release of a commercial GBT (manufactured using conventional tablet compression methods). However, there was a significant difference in the physical properties (hardness and friability) between the 3D printed and the commercial GBTs. With respect to the lower hardness and high friability exhibited by the 3D printed GBTs, it should be noted that all the printed tablets can be handled readily without any loss of structural integrity. Other characterisations, such as XRPD, FTIR, and DSC were confirmed that there is no detectable interaction between the active ingredient (guaifenesin) and the used excipients.

A continuing study on the ability of 3D printer to produce more complex 3D printed tablets with higher resolution (300-400 µm instead of 700-800 µm) and looked more professional than the tablets printed in chapter 3 using the Fa@Home 3D printer was shown in chapter 4. An extrusion based 3D Bio-Printer RegenHU operated at room-temperature was used to manufacture complex multi-active tablets capable of delivering three drugs via two different release mechanisms, namely osmotic release through a controlled porosity cellulose acetate shell for captopril and diffusion through HPMC 2208 gel layers for nifedipine and glipizide. The 3D printed tablets were successfully characterised for drug release using USP type I apparatus (Dissolution-Erweka Dt600 Dissolution Tester) and HPLC 1050. XRPD and FTIR results were confirmed that there was no detectable interaction between the active ingredients (captopril, glipizide and nifedipine) and the relevant excipients.

Finally in chapter 5, the 3D printer used in chapter 3 was used again to print a very complex polypill containing five actives (aspirin, hydrochlorothiazide, atenolol, pravastatin, and ramipril) with acceptable size. To our knowledge, 3D printing of polypill has not been attempted before. The 3D printed polypill here represents a cardiovascular treatment regime which has been adapted from clinical studies based on assessment of the effect of combination therapy on healthy middle aged individuals with one or more risk factors [194]. Atenolol, ramipril, and pravastatin SR compartments were physically separated by a hydrophobic cellulose acetate shell designed to act as a permeable carrier, and covered with an RR aspirin and hydrochlorothiazide compartment. It has been found that atenolol, ramipril, and pravastatin compartments showed drugs released over 12 hrs while aspirin and hydrochlorothiazide compartment showed release over 60 minutes. XRPD and FTIR results were confirmed that there was no detectable interaction between the active ingredients (aspirin, hydrochlorothiazide, atenolol, pravastatin, and ramipril) and the relevant excipients.

The Bio-Printer RegenHU allows print this complex polypill within acceptable period of time 25 min (based on the current tools number (2)) makes it a lot more efficient than the standard Fab@Home 3D printer. The Bio-Printer RegenHU has quicker printing speed, higher resolution, better printing mechanism, and more friendly software than the Fab@Home 3D printer used earlier in chapter 3 (Table 6.1).

Table 6.1: Outlining the key properties of different types of the 3D printers used in the this thesis

Key properties	**Bio-Printer RegenHU**	**Fab@Home**
Printer dimension X*Y*Z	55 cm* 55 cm* 59 cm	47 cm* 46 cm* 41 cm
Printer price	125,000,00 (£)	1700,00 (£)
Manufacturing materials	Stainless steel	Acrylic sheet parts
Contact dispensing (needle)	Yes	Yes
Number of printing tools	Up to 4	Up to 2
Printing mechanism	Pressure based printing (the printer fitted with air compressor)	Motor lead screw ended with metal nut to fit the piston
Printing resolution	Up to 50 µm	Up to 160 µm
Printing speed (mm/sec.)	Up to 25 mm/sec.	Up to 5.8 mm/sec.
UV curing capability	Yes	No
Contactless (jetting)	Yes	No
Hot-melting extrusion	Yes	No
Protective hood	Yes	No
Need high calibration	automated	Manually
Controlled temperature of printing tools	Yes (Medium heater and cooler	No
Printing on a heat controlled platform	Yes	No

Even though, this work showed that extrusion based 3D printing technique is a promising drug formulation method, there are still lot of rooms for development in this area. First of all, 3D printing can be used to print implantable formulation using bio-relevant excipients such as printing implantable scaffolds with fully customizable drug release profiles which can fit the disease symptoms or therapeutic needs. For instance, hormonal treatment needs pulsating doses at regular intervals. Furthermore, different drug concentration in the blood at different time during day is very important for some diseases. For example, patients with rheumatoid

arthritis require high dose at early morning to alleviate the pain and improve joint movement. Secondly, 3D printing could be used to formulate paediatric and geriatric oral dosage forms. This can be done by masking the bitter taste of some medications such as paracetamol or printing different tablets shapes and sizes to help patients with dysphagia (swallowing problems). Thirdly, drugs with narrow therapeutic index (small difference in dose or drug concentration in the blood may lead to serious health problems) could be printed in a tailored dose for individuals according to the patient's biological results, disease stage, and patient's medical history.

Other room in 3D printing drug development in which 3D printer may play an important role by bringing the final product closer to the patient (distribution manufacturing). Distribution manufacturing is defined as raw materials and methods of fabrications are decentralised and the final product is manufactured very close to the final customer. It offers quick point of care manufacturing process and fast drug supply, produce accurate tailored dose for individuals (good bye for one size fit all approaches) with less side effects, improve patient compliance and recovery time, cheap products, low investment, insure supply highly stable drugs (in-process stability monitoring and short time between 3D printing and patient consumption), and multiple suppliers (quick, efficient, high quality service. The following schematic diagram shows how 3D printer could change the drug manufacturing process into better way than the traditional distribution process (Figure 6.1).

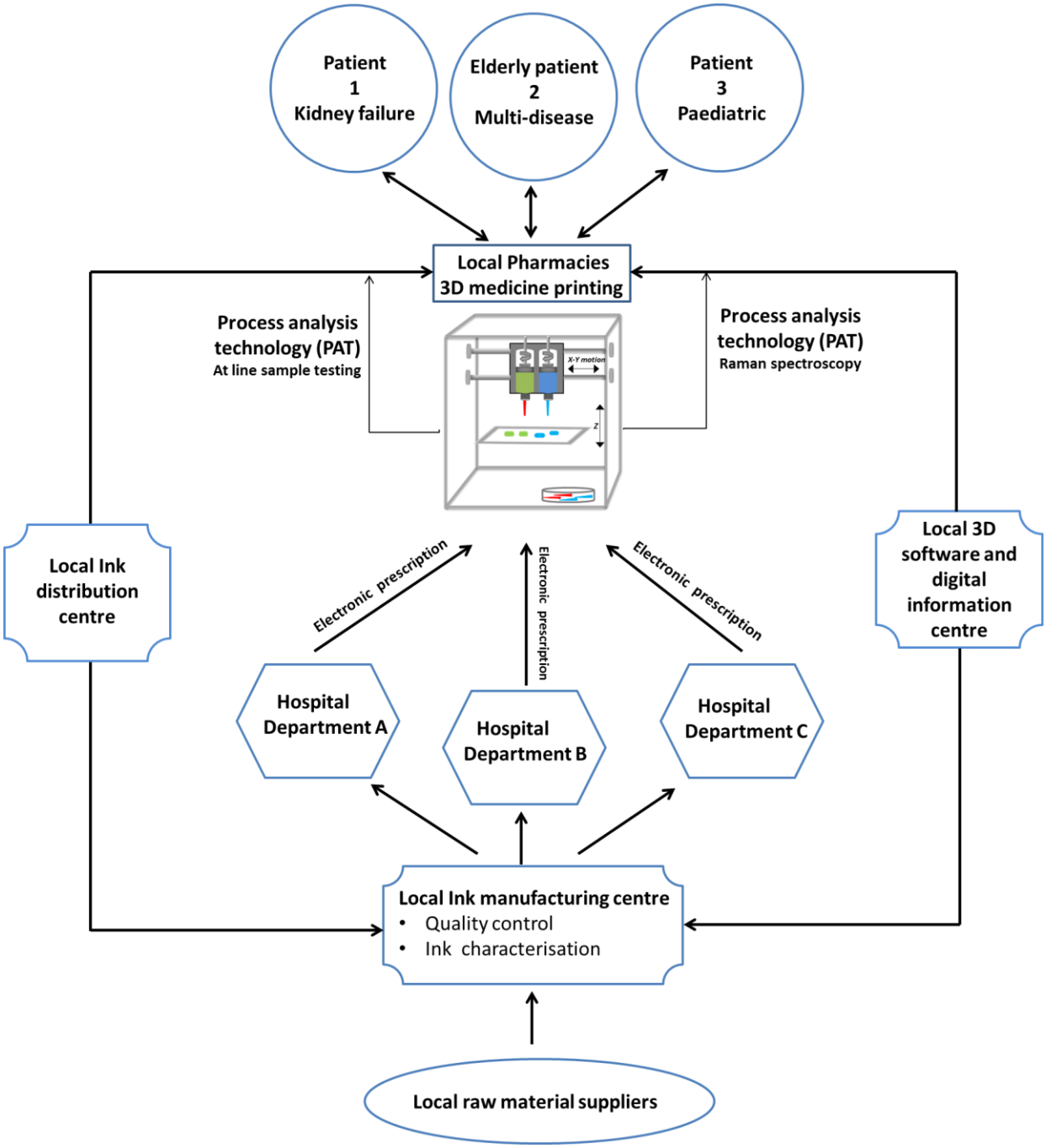

Figure 6.1: Schematic diagram represents how application of 3D printer in manufacturing distribution could change the drug manufacturing process.

Moreover, 3D printer could be used in continuous process for manufacturing drug formulation and this may offer some advantageous over batch process; integrated processing with few steps, small equipment and facilities, on-line process monitoring (consistent quality

and quality assurance in real time) and lower capital cost. The following schematic diagram shows how 3D printer could be used in continuous drug production process (Figure 6.2).

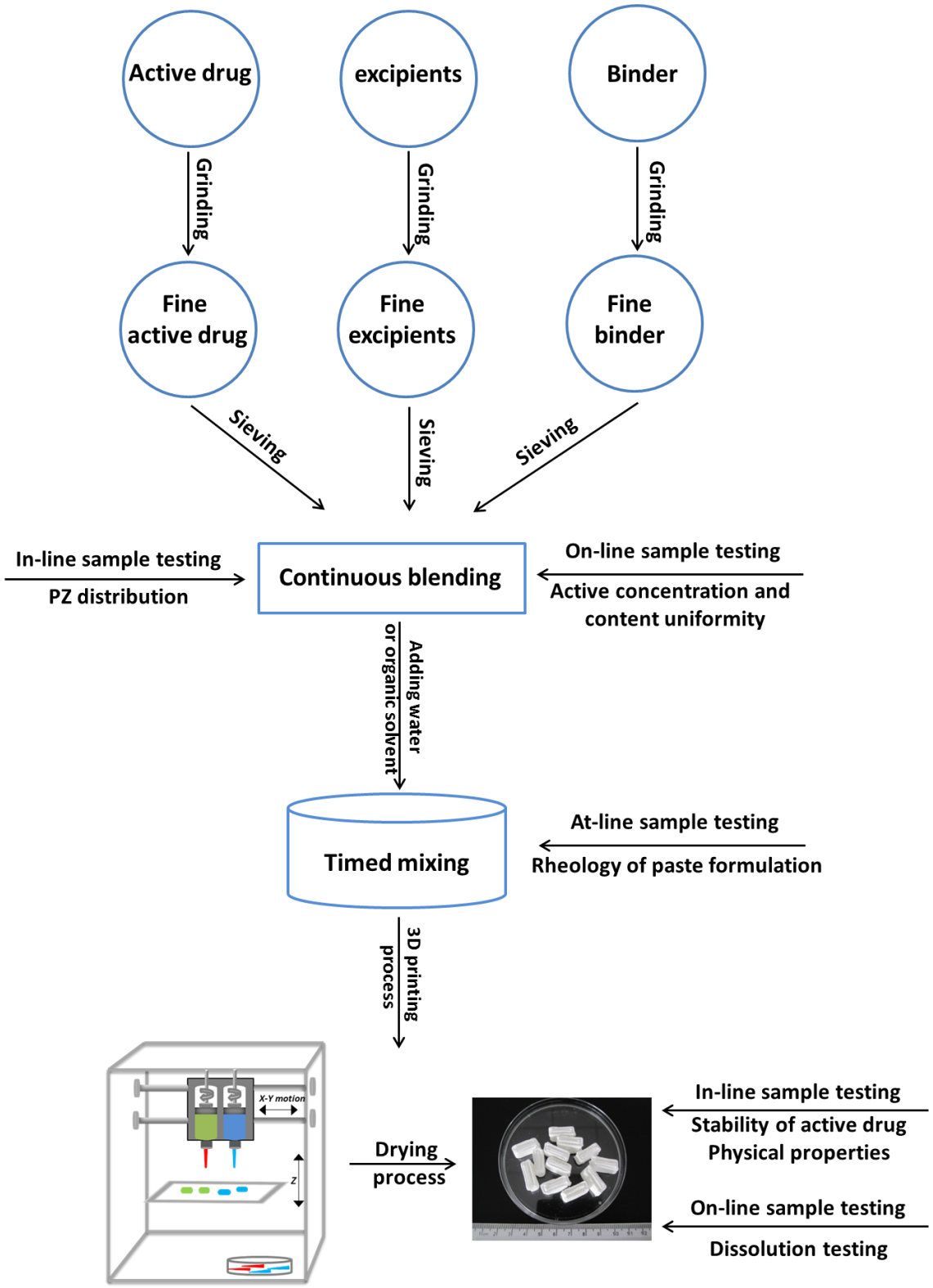

Figure 6.2: Schematic diagram continuous process of 3D printer of oral solid dosage forms.

To conclude, the work in this thesis has detailed the use of extrusion based 3D printing technique to print oral solid dosage forms. It has also shown that this technique can be used to print highly tailored multi-actives dosage forms with a controlled drug release profiles. The flexibility of 3D printing to produce tailored drugs gained the interest of pharmaceutical industries. On the 31st of July 2015, the first Food and Drug Administration (FDA) approved 3D printed tablet (Spritam® (levetiracetam)) was manufactured by a pharmaceutical company called Aprecia®. Finally, the 3D printing technology is continuously developed to overcome and replace the existing problems in the current drug formulation methods. From the fact that pharmaceutical companies working on developing this technology, the production of highly tailored drugs is not far away.

Biography

[1] E.M. Rudnic, J.B. Schwartz, Oral solid dosage forms, in: J.P. Remington, D.B. Troy, P. Beringer (Eds.) Remington: The science and practice of pharmacy, Lippincott Williams & Wilkins, 2006, pp. 889-937.

[2] P.R. Ravi, S. Ganga, R.N. Saha, Design and study of lamivudine oral controlled release tablets, *Journal of the American Association of Pharmaceutical Scientists*, 8 (2007) 167-175.

[3] S.V. Sastry, J.R. Nyshadham, J.A. Fix, Recent technological advances in oral drug delivery – a review, *Pharmaceutical Science and Technology Today*, 3 (2000) 138-145.

[4] M. Jivraj, L.G. Martini, C.M. Thomson, An overview of the different excipients useful for the direct compression of tablets, Pharmaceutical Science and Technology Today 3(2000) 58-63.

[5] S.G. Gattani, S.S. Khabiya, J.R. Amrutkar, S.S. Kushare, Formulation and evaluation of bilayer tablets of metoclopramide hydrochloride and diclofenac sodium, *Journal of Pharmaceutical Science and Technology*, 66 (2012) 151-160.

[6] S. Shanmugam, Granulation techniques and technologies: recent progresses, *Bioimpacts*, 5 (2015) 55-63.

[7] R.C. Rowe, P.J. Sheskey, W.G. Cook, M.E. Fenton, Handbook of pharmaceutical excipients, Pharmaceutical Press, London, 2012.

[8] L.S. Taylor, G. Zografi, Sugar–polymer hydrogen bond interactions in lyophilized amorphous mixtures, *Journal of Pharmaceutical Sciences*, 87 (1998) 1615-1621.

[9] R. Surana, L. Randall, A. Pyne, N.M. Vemuri, R. Suryanarayanan, Determination of glass transition temperature and in situ study of the plasticizing effect of water by inverse gas chromatography, Pharm Res, 20 (2003) 1647-1654.

Biography

[10] S. Yoshioka, V.J. Stella, Stability of drugs and dosage forms, Kluwer Academic/Plenum Publishers, New York, United State, 2000.

[11] R. Price, P.M. Young, S. Edge, J.N. Staniforth, The influence of relative humidity on particulate interactions in carrier-based dry powder inhaler formulations, *International Journal of Pharmaceutics*, 246 (2002) 47-59.

[12] J. Parmar, M. Rane, Tablet formulation design and manufacture: oral immediate release application, *Pharma Times* 41 (2009) 21-29.

[13] G. Morin, L. Briens, The effect of lubricants on powder flowability for pharmaceutical application, *American Association of Pharmaceutical Scientists*, 14 (2013) 1158-1168.

[14] A.A. Saker, F.K. Alanazi, Oral solid dosage forms in: L. Felton (Eds.) Essential of pharmaceutics, Pharmaceutical Press, London, 2013, pp. 581-610.

[15] P. Davies, Oral solid dosage forms, in: M. Gibson (Eds.) Pharmaceutical preformulation and formulation: a practical guid from candidate drug selection to commercial dosage form, Informa Healthcare USA, Inc., New York, 2009, pp. 367-431.

[16] E. Snejdrova, M. Dittrich, Pharmaceutical applications of plasticized polymers in: M. Luqman (Eds.) Recent advances in plasticizers, InTech Europe, Rijeka, 2012, pp. 70-90.

[17] G. Crotts, A. Sheth, J. Twist, I. Ghebre-Sellassie, Development of an enteric coating formulation and process for tablets primarily composed of a highly water-soluble, organic acid, *European Journal of Pharmaceutics and Biopharmaceutics*, 51 (2001) 71-76.

[18] N.A. Farooqui, A.A. Smith, H. Sharma, R. Manavalan, Formulation and evaluation of secnidazole film coated tablets, *Journal of Pharmaceutical Science and Technology*, 3 (2011) 2011.

[19] T.P. Reddy, V.D. Rao, K.R. Kumar, Bi-layer technology-an emerging trend: a review, *International Journal of Research and Development in Pharmacy and Life Sciences* 2(2013) 404-411.

Biography

[20] K. Singh, M.K. Walia, G. Agarwal, S. Harikumar, Osmotic pump drug delivery system: a novel approarch, *Journal of Drug Delivery and Therapeutics*, 3 (2013) 156-162.

[21] Y. Perrie, T. Rades, Fast track pharmaceutics: drug delivery and targeting, Pharmaceutical press, 2012.

[22] A. Hoffman, Pharmacodynamic aspects of sustained release preparations, *Advanced Drug Delivery Reviews*, 33 (1998) 185-199.

[23] D. Patel, A. Patel, T. Solanki, Formulation and evaluation of bilayer tablet by using melt granulation technique for treatment of diabetes mellitus, *Journal of Pharmacy And Bioallied Sciences*, 4 (2012) S37.

[24] R.D. Deshpande, D. Gowda, N. Mahammed, D.N. Maramwar, Bi-layer tablets-an emerging trend: a review, *International Journal of Pharmaceutical Sciences and Research*, 2 (2011) 2534.

[25] H.A. Panchal, A.K. Tiwari, A novel approach of bilayer tablet technology: a review, *International Research Journal of Pharmacy*, 3 (2012) 44-49.

[26] S. Abdul, S.S. Poddar, A flexible technology for modified release of drugs: multi layered tablets, *Journal of Controlled Release*, 97 (2004) 393-405.

[27] P. k Shende, C. Shrawne, R. Gaud, Multi-layer tablet: current scenario and recent advances, International Journal of Solids and Structure, 4 (2012) 418.

[28] U. Conte, L. Maggi, M.L. Torre, P. Giunchedi, A. La Manna, Press-coated tablets for time-programmed release of drugs, *Biomaterials*, 14 (1993) 1017-1023.

[29] S.S. Bharate, S.B. Bharate, A.N. Bajaj, Incompatibilities of pharmaceutical excipients with active pharmaceutical ingredients: a comprehensive review, *Journal of Excipients and Food Chemicals*, 1 (2010) 3-26.

[30] A. Banerjee, P. Verma, S. Gore, Controlled porosity solubility modulated osmotic pump tablets of gliclazide, *American Association of Pharmaceutical Scientists*, 16 (2015) 554-568.

Biography

[31] E. Chevalier, D. Chulia, C. Pouget, M. Viana, Fabrication of porous substrates: a review of processes using pore forming agents in the biomaterial field, *Journal of Pharmaceutical Science*, 97 (2008) 1135-1154.

[32] C.K. Sahoo, N.K. Sahoo, S.R.M. Rao, M. Sudhakar, K. Satyanarayana, A review on controlled porosity osmotic pump tablets and its evaluation, *Bulletin of Faculty of Pharmacy, Cairo University*, 53 (2015) 195-205.

[33] R.A. Keraliya, C. Patel, P. Patel, V. Keraliya, T.G. Soni, R.C. Patel, M.M. Patel, Osmotic drug delivery system as a part of modified release dosage form, *International Scholarly Research Notices* 2012 (2012) 528079.

[34] Z.H. Zhang, Y. Wang, W.F. Wu, X. Zhao, X.C. Sun, H.Q. Wang, Development of glipizide push-pull osmotic pump controlled release tablets by using expert system and artificial neural network, *Acta pharmaceutica Sinica*, 47 (2012) 1687-1695.

[35] K.E. Uhrich, S.M. Cannizzaro, R.S. Langer, K.M. Shakesheff, Polymeric systems for controlled drug release, *Chemical Reviews*, 99 (1999) 3181-3198.

[36] M. Zaman, J. Qureshi, H. Ejaz, R.M. Sarfraz, H.u. Khan, F.R. Sajid, M.S.u. Rehman, Oral controlled release drug delivery system and characterization of oral tablets; a review, *Pakistan Journal of Psychological Research*, 2 (2016) 10.

[37] S. Dash, P.N. Murthy, L. Nath, P. Chowdhury, Kinetic modeling on drug release from controlled drug delivery systems, Acta poloniae pharmaceutica, 67 (2010) 217-223.

[38] P. Colombo, Swelling-controlled release in hydrogel matrices for oral route, *Advanced Drug Delivery Reviews*, 11 (1993) 37-57.

[39] M. Hamidi, A. Azadi, P. Rafiei, Hydrogel nanoparticles in drug delivery, *Advanced Drug Delivery Reviews*, 60 (2008) 1638-1649.

[40] C.G. Varelas, D.G. Dixon, C.A. Steiner, Zero-order release from biphasic polymer hydrogels, *Journal of Controlled Release*, 34 (1995) 185-192.

Biography

[41] J. Siepmann, A. Göpferich, Mathematical modeling of bioerodible, polymeric drug delivery systems, *Advanced Drug Delivery Reviews*, 48 (2001) 229-247.

[42] R.K. Verma, D.M. Krishna, S. Garg, Formulation aspects in the development of osmotically controlled oral drug delivery systems, *Journal of Controlled Release*, 79 (2002) 7-27.

[43] G. Santus, R.W. Baker, Osmotic drug delivery: a review of the patent literature, *Journal of Controlled Release*, 35 (1995) 1-21.

[44] D.L. Cohen, E. Malone, H. Lipson, L.J. Bonassar, Direct freeform fabrication of seeded hydrogels in arbitrary geometries, *Tissue Engineering*, 12 (2006) 1325-1335.

[45] Y. Sun, S. Soh, Printing tablets with fully customizable release profiles for personalized medicine, *Advanced Materials*, 27 (2015) 7847-7853.

[46] T. Ghosh, A. Ghosh, Drug delivery through osmotic systems—an overview, *Journal of Applied Pharmaceutical Science*, 1 (2011) 38-49.

[47] B.P. Gupta, N. Thakur, N.P. Jain, J. Banweer, S. Jain, Osmotically controlled drug delivery system with associated drugs, *Journal of Pharmacy and Pharmaceutical Sciences*, 13 (2010) 571-588.

[48] A.A. Robitzki, R. Kurz, Biosensing and drug delivery at the microscale : novel devices for controlled and responsive drug delivery, Handb Exp Pharmacol, 197 (2010) 87-112.

[49] S.N. Makhija, P.R. Vavia, Controlled porosity osmotic pump-based controlled release systems of pseudoephedrine: I. Cellulose acetate as a semipermeable membrane, *Journal of Controlled Release* 89 (2003) 5-18.

[50] S. Bajaj, D. Singla, N. Sakhuja, Stability testing of pharmaceutical products, *Journal of Applied Pharmaceutical Science*, 2 (2012) 129-138.

Biography

[51] J. Bauer, S. Spanton, R. Henry, J. Quick, W. Dziki, W. Porter, J. Morris, Ritonavir: an extraordinary example of conformational polymorphism, *Pharmacetical Research*, 18 (2001) 859-866.

[52] A.H. Gerhardt, Moisture effects on solid dosage forms formulation, processing, and stability, *Journal GXP Compliance*, 13 (2009) 58-67.

[53] R. Price, P. Young, S. Edge, J. Staniforth, The influence of relative humidity on particulate interactions in carrier-based dry powder inhaler formulations, *Int. J. Pharm.*, 246 (2002) 47-59.

[54] J. Carstensen, Effect of moisture on the stability of solid dosage forms, *Drug Development and Industrial Pharmacy*, 14 (1988) 1927-1969.

[55] R.K. Palsmeier, D.M. Radzik, C.E. Lunte, Investigation of the degradation mechanism of 5-aminosalicylic acid in aqueous solution, Pharm Res, 9 (1992) 933-938.

[56] D. Jain, R. Raturi, V. Jain, P. Bansal, R. Singh, Recent technologies in pulsatile drug delivery systems, *Biomatter*, 1 (2011) 57-65.

[57] M.V. Holmes, T. Shah, C. Vickery, L. Smeeth, A.D. Hingorani, J.P. Casas, Fulfilling the promise of personalized medicine? Systematic review and field synopsis of pharmacogenetic studies, *PLoS One*, 4 (2009) e7960.

[58] N. Scoutaris, Home based formulation of personalised medicines by means of inkjet printing technique, in: Pharmacy, Nottingham, U.K, 2011.

[59] N. Malandrino, R.J. Smith, Personalized medicine in diabetes, *Clinical Chemistry*, 57 (2011) 231-240.

[60] S.T. Weiss, H.L. McLeod, D.A. Flockhart, M.E. Dolan, N.L. Benowitz, J.A. Johnson, M.J. Ratain, K.M. Giacomini, Creating and evaluating genetic tests predictive of drug response, *Nature Reviews Drug Discovery*, 7 (2008) 568-574.

Biography

[61] C.R. Yates, E.Y. Krynetski, T. Loennechen, M.Y. Fessing, H.L. Tai, C.H. Pui, M.V. Relling, W.E. Evans, Molecular diagnosis of thiopurine S-methyltransferase deficiency: genetic basis for azathioprine and mercaptopurine intolerance, *Annals Internal Medicine*, 126 (1997) 608-614.

[62] M.V. Relling, M.L. Hancock, G.K. Rivera, J.T. Sandlund, R.C. Ribeiro, E.Y. Krynetski, C.H. Pui, W.E. Evans, Mercaptopurine therapy intolerance and heterozygosity at the thiopurine S-methyltransferase gene locus, *Journal of the National Cancer Institute* 91 (1999) 2001-2008.

[63] E. Schaeffeler, C. Fischer, D. Brockmeier, D. Wernet, K. Moerike, M. Eichelbaum, U.M. Zanger, M. Schwab, Comprehensive analysis of thiopurine S-methyltransferase phenotype-genotype correlation in a large population of German-Caucasians and identification of novel TPMT variants, *Pharmacogenetics*, 14 (2004) 407-417.

[64] H. Win, P. H., Oral controlled release formulation design and drug delivery: theory to practice, in: X. Chen, H. Wen, K. Park (Eds.) Challenges and new technologies of oral controlled release, John Wiley & Sons, New Jersy, 2010, pp. 296-271.

[65] A. Goyanes, A.B.M. Buanz, G.B. Hatton, S. Gaisford, A.W. Basit, 3D printing of modified-release aminosalicylate (4-ASA and 5-ASA) tablets, *European Journal of Pharmaceutics and Biopharmaceutics*, 89 (2015) 157-162.

[66] S.A. Khaled, J.C. Burley, M.R. Alexander, C.J. Roberts, Desktop 3D printing of controlled release pharmaceutical bilayer tablets, *International Journal of Pharmaceutics*, 461 (2014) 105-111.

[67] J. Trachtenberg, J.K. Placone, B.T. Smith, C.M. Piard, M. Santoro, D.W. Scott, J.P. Fisher, A.G. Mikos, Extrusion-based 3D printing of poly (propylene fumarate) in a full-factorial design, *ACS Biomaterials Science & Engineering*, (2016).

Biography

[68] E.J. Mott, M. Busso, X. Luo, C. Dolder, M.O. Wang, J.P. Fisher, D. Dean, Digital micromirror device (DMD)-based 3D printing of poly (propylene fumarate) scaffolds, *Materials Science and Engineering C: Materials for Biological Applications*, 61 (2016) 301-311.

[69] S.R. Shin, R. Farzad, A. Tamayol, V. Manoharan, P. Mostafalu, Y.S. Zhang, M. Akbari, S.M. Jung, D. Kim, M. Comotto, A bioactive carbon nanotube based ink for printing 2D and 3D flexible electronics, *Advanced Materials*, (2016).

[70] P. Walters, D. Huson, C. Parraman, M. Stanić, 3D printing in colour: technical evaluation and creative applications, (2011).

[71] J. Holländer, N. Genina, H. Jukarainen, M. Khajeheian, A. Rosling, E. Mäkilä, N. Sandler, Three-dimensional printed PCL-based implantable prototypes of medical devices for controlled drug delivery, *Journal of Pharmacy and Pharmaceutical Sciences*.

[72] I.S. Kinstlinger, A. Bastian, S.J. Paulsen, D.H. Hwang, A.H. Ta, D.R. Yalacki, T. Schmidt, J.S. Miller, Open-source selective laser sintering (OpenSLS) of nylon and biocompatible polycaprolactone, *PloS one*, 11 (2016) 1-25.

[73] B. Utela, D. Storti, R. Anderson, M. Ganter, A review of process development steps for new material systems in three dimensional printing (3DP), *Journal of Mathematical Physics*, 10 (2008) 96-104.

[74] C. Voura, M. Gruber, N. Schroedl, D. Strohmeier, B. Eitzinger, W. Bauer, G. Brenn, J. Khinast, A. Zimmer, Printable medicines: a microdosing device for producing personalised medicines, *Pharmaceutical Technology Europe*, 23 (2011) 32-36.

[75] C. Barnatt, 25 Things you need to know about the future. , Constable & Robinson Limited, London, 2012.

[76] F.P.W. Melchels, J. Feijen, D.W. Grijpma, A review on stereolithography and its applications in biomedical engineering, *Biomaterials*, 31 (2010) 6121-6130.

Biography

[77] E. Malone, H. Lipson, Fab@ Home: the personal desktop fabricator kit, *Rapid Prototype Journal*, 13 (2007) 245-255.

[78] N. Scoutaris, A.L. Hook, P.R. Gellert, C.J. Roberts, M.R. Alexander, D.J. Scurr, ToF-SIMS analysis of chemical heterogenities in inkjet micro-array printed drug/polymer formulations, *Journal of Materials Science: Materials in Medicine*, 23 (2012) 385-391.

[79] B. Partee, S.J. Hollister, S. Das, Selective laser sintering process optimization for layered manufacturing of CAPA® 6501 polycaprolactone bone tissue engineering scaffolds, *Journal of Manufacturing Science and Engineering*, 128 (2006) 531-540.

[80] G. Ryder, B. Ion, G. Green, D. Harrison, B. Wood, Rapid design and manufacture tools in architecture, *Automation in Construction*, 11 (2002) 279-290.

[81] J. Wang, A. Goyanes, S. Gaisford, A.W. Basit, Stereolithographic (SLA) 3D Printing of Oral Modified-Release Dosage Forms, *International Journal of Pharmaceutics*, (2016).

[82] I. Zein, D.W. Hutmacher, K.C. Tan, S.H. Teoh, Fused deposition modeling of novel scaffold architectures for tissue engineering applications, *Biomaterials*, 23 (2002) 1169-1185.

[83] A. Sidambe, Biocompatibility of advanced manufactured titanium implants—a review, *Materials*, 7 (2014) 8168.

[84] J. Skowyra, K. Pietrzak, M.A. Alhnan, Fabrication of extended-release patient-tailored prednisolone tablets via fused deposition modelling (FDM) 3D printing, *European Journal of Pharmaceutical Sciences*, 68 (2015) 11-17.

[85] N. Guo, M.C. Leu, Effect of different graphite materials on the electrical conductivity and flexural strength of bipolar plates fabricated using selective laser sintering, *International Journal of Hydrogen Energy*, 37 (2012) 3558-3566.

[86] I. Jiménez-Martínez, T. Quirino-Barreda, L. Villafuerte-Robles, Sustained delivery of captopril from floating matrix tablets, *International Journal of Pharmaceutics*, 362 (2008) 37-43.

Biography

[87] N. Sandler, A. Määttänen, P. Ihalainen, L. Kronberg, A. Meierjohann, T. Viitala, J. Peltonen, Inkjet printing of drug substances and use of porous substrates-towards individualized dosing, *Journal of Pharmaceutical Sciences*, 100 (2011) 3386-3395.

[88] H.P. Le, Progress and trends in ink-jet printing technology, *Journal of Interdisciplinary Science Topics*, 42 (1998) 49-62.

[89] D. Radulescu, N. Schwade, D. Wawro, Uniform paclitaxel-loaded biodegradable microspheres manufactured by ink-jet technology, in: Proc Winter Symp and 11th Int Symp On Adv Drug Del Sys., Salt Lake City, 2003.

[90] D. Radulescu, H. Trost, D. Taylor, B. Antohe, D. Silva, N. Schwade, P. Tarcha, S. Dhar, G. Evans, 3d printing of biological materials for drug delivery and tissue engineering applications, *Digital Fabrication*, 2005 (2005) 96-99.

[91] S.C. Kim, D.W. Kim, Y.H. Shim, J.S. Bang, H.S. Oh, S.W. Kim, M.H. Seo, In vivo evaluation of polymeric micellar paclitaxel formulation: toxicity and efficacy, *Journal of Controlled Release*, 72 (2001) 191-202.

[92] E. Rowinsky, E. Eisenhauer, V. Chaudhry, S. Arbuck, R. Donehower, Clinical toxicities encountered with paclitaxel (Taxol), *Seminars in oncology*, 20 (1993) 1-15.

[93] A. Skardal, J. Zhang, L. McCoard, X. Xu, S. Oottamasathien, G.D. Prestwich, Photocrosslinkable hyaluronan-gelatin hydrogels for two-step bioprinting, *Tissue Engineering Part A*, 16 (2010) 2675-2685.

[94] S.A. Khaled, J.C. Burley, M.R. Alexander, J. Yang, C.J. Roberts, 3D printing of five-in-one dose combination polypill with defined immediate and sustained release profiles, *Journal of Controlled Release*, 217 (2015) 308-314.

[95] S.A. Khaled, J.C. Burley, M.R. Alexander, J. Yang, C.J. Roberts, 3D printing of tablets containing multiple drugs with defined release profiles, *International Journal of Pharmaceutics*, 494 (2015) 643-650.

Biography

[96] X. Cui, T. Boland, D.D. D'Lima, M.K. Lotz, Thermal inkjet printing in tissue engineering and regenerative medicine, *Recent Patents on Drug Delivery & Formulation*, 6 (2012) 149.

[97] H. Changqin, L. Ying, Quality control in pharmaceuticals: residual solvents testing and analysis, in: I. Akyar (Eds.) Wide spectra of quality control, InTech, 2013, pp. 184-210.

[98] C.L. Ventola, Medical applications for 3D printing: current and projected uses, *Pharmacology and Therapeutics*, 39 (2014) 704-711.

[99] A. Goyanes, P. Robles Martinez, A. Buanz, A.W. Basit, S. Gaisford, Effect of geometry on drug release from 3D printed tablets, *International Journal of Pharmaceutics*, (2015).

[100] P. Rattanakit, S.E. Moulton, K.S. Santiago, S. Liawruangrath, G.G. Wallace, Extrusion printed polymer structures: a facile and versatile approach to tailored drug delivery platforms, *International Journal of Pharmaceutics*, 422 (2012) 254-263.

[101] C.W. Rowe, W.E. Katstra, R.D. Palazzolo, B. Giritlioglu, P. Teung, M.J. Cima, Multimechanism oral dosage forms fabricated by three dimensional printing™, *Journal of Controlled Release*, 66 (2000) 11-17.

[102] W. Katstra, R. Palazzolo, C. Rowe, B. Giritlioglu, P. Teung, M. Cima, Oral dosage forms fabricated by three dimensional printing™, *Journal of Controlled Release*, 66 (2000) 1-9.

[103] D.L. Cohen, J.I. Lipton, L.J. Bonassar, H. Lipson, Additive manufacturing for in situ repair of osteochondral defects, *Biofabrication*, 2 (2010) 035004.

[104] P.Y. Noritomi, A.L.L.o. Filho, H. Lipson, P.Y.C. Cheung, H. Kang, J.V.L.d. Silva, J.T. Butcher, N. Colangelo, P.I. Neto, E. Malone, Construction and adaptation of an open source rapid prototyping machine for biomedical research purposes?a multinational collaborative development, in: (Eds.) Innovative developments in design and manufacturing, CRC Press, 2009.

Biography

[105] J.P. Mazzoccoli, D.L. Feke, H. Baskaran, P.N. Pintauro, Mechanical and Cell Viability Properties of Crosslinked Low and High Molecular Weight Poly(ethylene glycol) Diacrylate Blends, Journal of biomedical materials research. Part A, 93 (2010) 558-566.

[106] N. Scoutaris, M.R. Alexander, P.R. Gellert, C.J. Roberts, Inkjet printing as a novel medicine formulation technique, *Journal of Controlled Release*, 156 (2011) 179-185.

[107] B. Kommanaboyina, C.T. Rhodes, Trends in stability testing, with emphasis on stability during distribution and storage, *Drug Development and Industrial Pharmacy*, 25 (1999) 857-868.

[108] F.I. Abd-Allah, H.M. Dawaba, A. Ahmed, Preparation, characterization, and stability studies of piroxicam-loaded microemulsions in topical formulations, *Drug Discoveries and Therapeutics*, 4 (2010) 267-275.

[109] E. Malone, H. Lipson, Freeform fabrication of ionomeric polymer-metal composite actuators, *Rapid Prototype Journal*, 12 (2006) 244-253.

[110] M. Chung, E. Malone, M.T. Tolley, A.J. Chepaitis, H. Lipson, Object augmentation for the visually impaired using RP, in: Proceedings of the 19th solid freeform fabrication symposium, Austin TX, 2008.

[111] E. Malone, H. Lipson, Multi-material freeform fabrication of active systems, in: ASME 2008 9th biennial conference on engineering systems design and analysis, American Society of Mechanical Engineers, 2008, pp. 345-353.

[112] E. Freire, Differential scanning calorimetry, *Methods in Molecular Biology*, 40 (1995) 191-218.

[113] P. Gill, T.T. Moghadam, B. Ranjbar, Differential Scanning Calorimetry Techniques: Applications in Biology and Nanoscience, *Journal of Biomolecular Techniques*, 21 (2010) 167-193.

Biography

[114] T. Detoisien, M. Arnoux, P. Taulelle, D. Colson, J.P. Klein, S. Veesler, Thermal analysis: A further step in characterizing solid forms obtained by screening crystallization of an API, *International Journal of Pharmaceutical Research*, 403 (2011) 29-36.

[115] L.C. Thomas, An introduction to the techniques of differential scanning calorimetry (DSC) and modulated DSC, (2005) 9-25.

[116] J.L. Keddie, R.A.L. Jones, R.A. Cory, Size-dependent depression of the glass transition temperature in polymer films, *Europhysics Letters* 27 (1994) 59-64.

[117] S.D. Clas, C.R. Dalton, B.C. Hancock, Differential scanning calorimetry: applications in drug development, *Pharmaceutical Science Technology Today*, 2 (1999) 311-320.

[118] J.L. Ford, P. Timmins, Pharmaceutical thermal analysis: Techniques and applications, John Wiley & Sons, New York, 1989.

[119] A. Singh, L. Nath, Evaluation of compatibility of tablet excipients and novel synthesized polymer with lamivudine, Journal of Thermal Analysis and Calorimetry, 108 (2012) 263-267.

[120] H.A. Schneider, J. Rieger, E. Penzel, The glass transition temperature of random copolymers: 2. extension of the Gordon-Taylor equation for asymmetric Tg vs composition curves, *Polymer*, 38 (1997) 1323-1337.

[121] B.C. Hancock, G. Zografi, Characteristics and significance of the amorphous state in pharmaceutical systems, *Journal of Pharmaceutical Sciences*, 86 (1997) 1-12.

[122] M.T. Kalichevsky, E.M. Jaroszkiewicz, J.M.V. Blanshard, A study of the glass transition of amylopectin—sugar mixtures, *Polymer*, 34 (1993) 346-358.

[123] J.M. Thomas, P.L. Gai, Electron microscopy and the materials chemistry of solid catalysts, Advances in Catalysis, 48 (2004) 171-227.

[124] M.A. Saghiri, K. Asgar, M. Lotfi, K. Karamifar, A.M. Saghiri, P. Neelakantan, J.L. Gutmann, A. Sheibaninia, Back-scattered and secondary electron images of scanning electron

microscopy in dentistry: a new method for surface analysis, *Acta Odontologica Scandinavica*, 70 (2012) 603-609.

[125] L.E. Verhoeven, The advantages of the scanning electron microscope in the investigative studies of hair, *Journal of Criminal Law and Criminology*, (1972) 125-128.

[126] A.D. Emanuele, C. Gilpin, Applications of the environmental scanning electron microscope to the analysis of pharmaceutical formulations, *Scanning*, 18 (1996) 522-527.

[127] G. Vergote, C. Vervaet, I. Van Driessche, S. Hoste, S. De Smedt, J. Demeester, R. Jain, S. Ruddy, J.P. Remon, An oral controlled release matrix pellet formulation containing nanocrystalline ketoprofen, *International Journal of Pharmaceutics*, 219 (2001) 81-87.

[128] A.V. Ewing, G.D. Biggart, C.R. Hale, G.S. Clarke, S.G. Kazarian, Comparison of pharmaceutical formulations: ATR-FTIR spectroscopic imaging to study drug-carrier interactions, *International Journal of Pharmaceutics*, 495 (2015) 112-121.

[129] B. Duc Hanh, R.H.H. Neubert, S. Wartewig, Investigation of drug release from suspension using FTIR-ATR technique: part I. Determination of effective diffusion coefficient of drugs, *International Journal of Pharmaceutics*, 204 (2000) 145-150.

[130] K. Punčochová, A.V. Ewing, M. Gajdošová, N. Sarvašová, S.G. Kazarian, J. Beránek, F. Štěpánek, Identifying the mechanisms of drug release from amorphous solid dispersions using MRI and ATR-FTIR spectroscopic imaging, *International Journal of Pharmaceutics*, 483 (2015) 256-267.

[131] S.G. Kazarian, K.A. Chan, ATR-FTIR spectroscopic imaging: recent advances and applications to biological systems, *Analyst*, 138 (2013) 1940-1951.

[132] R.B. McClurg, J.P. Smit, X-ray powder diffraction pattern indexing for pharmaceutical applications, *Pharmaceutical Technology Europe*, (2013).

Biography

[133] M. Skotnicki, J.A. Aguilar, M. Pyda, P. Hodgkinson, Bisoprolol and bisoprolol-valsartan compatibility studied by differential scanning calorimetry, nuclear magnetic resonance and X-ray powder diffractometry, Pharm Res, 32 (2015) 414-429.

[134] C. Suryanarayana, M.G. Norton, X-ray diffraction: a practical approach, Springer Science & Business Media, New York, 2013.

[135] T. Kupiec, Quality-control analytical methods: High-performance liquid chromatography, *International Journal of Pharmaceutical Compounding*, 8 (2004) 223-227.

[136] M. Serdar, Z. Knežević, Determination of artificial sweeteners in beverages and special nutritional products using high performance liquid chromatography, *Archives of Industrial Hygiene and Toxicology*, 62 (2011) 169-172.

[137] R. Asija, S. Bhatt, S.L. Sharma, P.C. Dhaker, Formulation and evaluation of tramadol, and diclofenac sofium multimodel tablet dosage form: an overview, *Journal of Drug Discovery and Theraputics*, 2 (2014) 30-37.

[138] I.-D. Rosca, J.-M. Vergnaud, Evaluation of the characteristics of oral dosage forms with release controlled by erosion, *Computers in Biology and Medicine* 38 (2008) 668-675.

[139] A.L. Hook, C.Y. Chang, J. Yang, S. Atkinson, R. Langer, D.G. Anderson, M.C. Davies, P. Williams, M.R. Alexander, Discovery of novel materials with broad resistance to bacterial attachment using combinatorial polymer microarrays, *Advanced Materials*, 25 (2013) 2542-2547.

[140] A.D. Celiz, H.C. Harrington, A.L. Hook, High throughput assessment and chemometric analysis of the interaction of epithelial and fibroblast cells with a polymer library, *Applied Surface Science* 313 (2014) 926-935.

[141] A.L. Hook, C.Y. Chang, J. Yang, J. Luckett, A. Cockayne, S. Atkinson, Y. Mei, R. Bayston, D.J. Irvine, R. Langer, D.G. Anderson, P. Williams, M.C. Davies, M.R. Alexander,

Biography

Combinatorial discovery of polymers resistant to bacterial attachment, *Nature Biotechnology* 30 (2012) 868-875.

[142] A.K. Patel, A.D. Celiz, D. Rajamohan, D.G. Anderson, R. Langer, M.C. Davies, M.R. Alexander, C. Denning, A defined synthetic substrate for serum-free culture of human stem cell derived cardiomyocytes with improved functional maturity identified using combinatorial materials microarrays, *Biomaterials*, 61 (2015) 257-265.

[143] S. Bennett, N. Hoffman, M. Monga, Ephedrine- and guaifenesin-induced nephrolithiasis, *Journal of Alternative and Complementary Medicine*, 10 (2004) 967-969.

[144] R. Bushra, M.H. Shoaib, N. Aslam, D. Hashmat, M. Rehman, Formulation development and optimization of ibuprofen tablets by direct compression method, *Pakistan Journal of Pharmaceutical Sciences*, 21 (2008) 113-120.

[145] U.S. Pharmacopoeia XXIV. US Pharmacopeia Convention, Inc., Rockville, MD, 2000.

[146] H. Folttmann, A. Quadir, Polyvinylpyrrolidone (PVP) - One of the most widely used excipients in pharmaceuticals: An overview, *Journal of Drug Delivery Science and Technology*, 8 (2008) 22-27.

[147] R.A. Keraliya, T.G. Soni, V. Thakkar, T. Gandhi, R. Patel, Formulation and physical characterization of microcrystals for dissolution rate enhancement of tolbutamide, *International Journal of Research in Pharmaceutical Sciences*, 1 (2010) 69-77.

[148] S. Missaghi, K.A. Fegely, A.R. Rajabi-Siahboomi, Investigation of the effects of hydroalcoholic solutions on textural and rheological properties of various controlled release grades of hypromellose, *American Association of Pharmaceutical Scientists*, 10 (2009) 77-80.

[149] N.H. Shah, A.S. Railkar, W. Phuapradit, F.-W. Zeng, A. Chen, M.H. Infeld, A. Malick, Effect of processing techniques in controlling the release rate and mechanical strength of

hydroxypropyl methylcellulose based hydrogel matrices, *European Journal of Pharmaceutics and Biopharmaceutics*, 42 (1996) 183-187.

[150] B.T. Tiwari, J. DiNunzio, A.R. Siahboomi, Drug-polymer matrices for extended release in: C.G. Wilson, P.J. Crowley (Eds.) Controlled release in oral drug delivery Springer US, New York, 2011, pp. 150.

[151] A.A. Bredikhin, A.T. Gubaidullin, Z.A. Bredikhina, D.B. Krivolapov, A.V. Pashagin, I.A. Litvinov, Absolute configuration and crystal packing for three chiral drugs prone to spontaneous resolution: Guaifenesin, methocarbamol and mephenesin, *Journal of Molecular Structure*, 920 (2009) 377-382.

[152] P. Nagadivya, R. Ramakrishna, G. Sridhar, R. Bhanushashank, Effect of various binding agents on tablet hardness and release rate profiles of diclofenac sodium tablets, *International Journal of Research in Pharmaceutical Sciences*, 3 (2012) 12–16.

[153] L. Lachman, H.A. Lieberman, J.L. Kanig, The theory and practice of industrial pharmacy, Third ed., Lea & Febiger, Philadelphia, United States, 1986.

[154] C. Patra, A. Kumar, H. Pandit, S. Singh, M. Devi, Design and evaluation of sustained release bilayer tablets of propranolol hydrochloride, *Acta Pharmaceutica*, 57 (2007) 479-489.

[155] D.P. Pattanayak, S.C. Dinda, U.L. Narayan, Formulation and development of sustained release bilayer tablet for biphasic drug release: a novel approach in management of diabetes, *Journal of Pharmacy Research*, 4 (2011) 2025-2031.

[156] E.I. Nep, B.R. Conway, Polysaccharide gum matrix tablets for oral controlled delivery of cimetidine, *Journal of Pharmaceutical Sciences and Research* 2(2010) 708–716.

[157] M. Grassi, G. Grassi, Mathematical modelling and controlled drug delivery: matrix systems, *Current Drug Delivery* 2(2005) 97-116.

Biography

[158] N. Ramadhani, M. Shabir, C. McConville, Preparation and characterisation of Kolliphor® P 188 and P 237 solid dispersion oral tablets containing the poorly water soluble drug disulfiram, *International Journal of Pharmaceutics*, 475 (2014) 514-522.

[159] R.A. Souvirón, M.M. Martínez, [Captopril+ hydrochlorothiazide versus captopril+ nifedipine in the treatment of arterial hypertension in diabetes mellitus type II], *Revista Española de Cardiología*, 45 (1991) 432-437.

[160] A.O. Nur, J.S. Zhang, Recent progress in sustained/controlled oral delivery of captopril: an overview, *International Journal of Pharmaceutics*, 194 (2000) 139-146.

[161] A.P. Gadad, A.D. Reddy, P.M. Dandagi, V.S. Masthiholimath, Design and characterization of hollow/porous floating beads of captopril for pulsatile drug delivery, *Asian Journal of Pharmacy and Pharmacology*, 6 (2012) 137.

[162] H.D. Williams, R. Ward, I.J. Hardy, C.D. Melia, The extended release properties of HPMC matrices in the presence of dietary sugars, *Journal Controlled Release*, 138 (2009) 251-259.

[163] M.U. Ghori, G. Ginting, A.M. Smith, B.R. Conway, Simultaneous quantification of drug release and erosion from hypromellose hydrophilic matrices, *International Journal of Pharmaceutics*, 465 (2014) 405-412.

[164] C.L. Li, L.G. Martini, J.L. Ford, M. Roberts, The use of hypromellose in oral drug delivery, *Journal of Pharmacy and Pharmacology*, 57 (2005) 533-546.

[165] J. Siepmann, N.A. Peppas, Modeling of drug release from delivery systems based on hydroxypropyl methylcellulose (HPMC), *Advanced Drug Delivery Reviews*, 48 (2001) 139-157.

[166] I.D. Ursan, L. Chiu, A. Pierce, Three-dimensional drug printing: a structured review, *Journal of the American Pharmaceutical Association*, 53 (2013) 136-144.

Biography

[167] D.-G. Yu, C. Branford-White, Y.-C. Yang, L.-M. Zhu, E.W. Welbeck, X.-L. Yang, A novel fast disintegrating tablet fabricated by three-dimensional printing, *Drug Development and Industrial Pharmacy*, 35 (2009) 1530-1536.

[168] L. Xu, S. Li, H. Sunada, Preparation and evaluation in vitro and in vivo of captopril elementary osmotic pump tablets, *Asian Journal of Pharmaceutical Sciences* 1(2006) 236-245.

[169] S. Wan, Y. Sun, X. Qi, F. Tan, Improved bioavailability of poorly water-soluble drug curcumin in cellulose acetate solid dispersion, *American Association of Pharmaceutical Scientists*, 13 (2012) 159-166.

[170] H. Patel, M. Patel, Formulation and evaluation of controlled porosity osmotic drug delivery system of metoprolol succinate, *International Journal of Pharmaceutical Research*, 3 (2012) 1761-1767.

[171] R.K. Verma, S. Garg, Development and evaluation of osmotically controlled oral drug delivery system of glipizide, *European Journal of Pharmaceutics and Biopharmaceutics*, 57 (2004) 513-525.

[172] M.N. Siddiqui, G. Garg, P.K. Sharma, Fast dissolving tablets: preparation, characterization and evaluation: an overview, *International Journal of Pharmaceutical Sciences Review and Research*, 4 (2010) 87-96.

[173] P. Lokesh, S. Abdul Althaf, P. Sailaja, Design, development and formulation of orodispersible tablets of a model drug using response surface methodology, *Pharmaceutica Analytica Acta*, 3 (2012).

[174] JAMA network webcasts, executive summary of the third report of the national cholesterol education program (NCEP) expert panel on detection, evaluation, and treatment of high blood cholesterol in adults (adult treatment panel III), *Journal of the American Medical Association* 285 (2001) 2486-2497.

Biography

[175] J.-E. Kim, S.-R. Kim, S.-H. Lee, C.-H. Lee, D.-D. Kim, The effect of pore formers on the controlled release of cefadroxil from a polyurethane matrix, *International Journal of Pharmaceutics*, 201 (2000) 29-36.

[176] R.D. Brobyn, The human toxicology of dimethyl sulfoxide, *Annals of the New York Academy of Sciences*, 243 (1975) 497-506.

[177] S.W. Jacob, C. Jack, Dimethyl sulfoxide (DMSO) in trauma and disease, CRC Press, Florida, 2015.

[178] K. Wong, E. Reinertson, Clinical considerations of dimethyl sulfoxide, *Lowa State University's College of Veterinary Medicine*, 46 (1984) 89-95.

[179] International conference on harmonization of technical requirements for the registration of pharmaceuticals for human use, Q3C (R4) impurities: guideline for residual solvents, (2009).

[180] J. Parkin, C. Shea, G.R. Sant, Intravesical dimethyl sulfoxide (DMSO) for interstitial cystitis--a practical approach, Urology, 49 (1997) 105-107.

[181] RegenHU. (2015). 3D Discovery® instrument, 3D Bio-Printer [Photograph] Retrieved April 04 2015, from http://www.regenhu.com/products/3d-bio-printing.html

[182] S.R. Pygall, S. Kujawinski, P. Timmins, C.D. Melia, Mechanisms of drug release in citrate buffered HPMC matrices, *International Journal of Pharmaceutics*, 370 (2009) 110-120.

[183] J. Siepmann, N.A. Peppas, Modeling of drug release from delivery systems based on hydroxypropyl methylcellulose (HPMC), *Adv. Drug Deliv. Rev.*, 64, Supplement (2012) 163-174.

[184] D. Grooff, M. De Villiers, W. Liebenberg, Thermal methods for evaluating polymorphic transitions in nifedipine, *Thermochimica acta*, 454 (2007) 33-42.

Biography

[185] H. Kadin, Captopril in: K. Florey (Eds.) Analytical profiles of drug substances Academic Press, INC, New York, 1982, pp. 79-138.

[186] S.K. Singh, M. Gulati, I. Kaur, Characterization of solid state forms of glipizide, *Powder Technology*, 264 (2014) 365-376.

[187] J. Gao, C. Chen, J.-X. Chen, L.-M. Wen, G.-L. Yang, F.-P. Duan, Z.-Y. Huang, D.-F. Li, D.-R. Yu, H.-J. Yang, S.-J. Li, Synergism and rules of the new combination drug yiqijiedu formulae (YQJD) on ischemic stroke based on amino acids (AAs) metabolism, *Scientific Report*, 4 (2014) 1-11.

[188] S. Bangalore, A. Shahane, S. Parkar, F.H. Messerli, Compliance and fixed-dose combination therapy, *Current Hypertension. Report*, 9 (2007) 184-189.

[189] D.M. Lloyd-Jones, E.P. Leip, M.G. Larson, R.B. d'Agostino, A. Beiser, P.W. Wilson, P.A. Wolf, D. Levy, Prediction of lifetime risk for cardiovascular disease by risk factor burden at 50 years of age, *Circulation*, 113 (2006) 791-798.

[190] P. Sleight, H. Pouleur, F. Zannad, Benefits, challenges, and registerability of the polypill, *European Heart Journal*, 27 (2006) 1651-1656.

[191] M. Lafeber, D.E. Grobbee, M.L. Bots, S. Thom, R. Webster, A. Rodgers, F.L. Visseren, W. Spiering, The evening versus morning polypill utilization study: the TEMPUS rationale and design, *European Journal of Preventive Cardiology*, 4 (2013) 425-433.

[192] J.D. Spence, Polypill: for Pollyanna*, *International Journal of Stroke*, 3 (2008) 92-97.

[193] K.M. Carey, M.R. Comee, J.L. Donovan, A.O. Kanaan, A polypill for all? Critical review of the polypill literature for primary prevention of cardiovascular disease and stroke, *Annals of Pharmacotherapy* 46 (2012) 688-695.

[194] S. Yusuf, P. Pais, R. Afzal, D. Xavier, K. Teo, J. Eikelboom, A. Sigamani, V. Mohan, R. Gupta, N. Thomas, Effects of a polypill (Polycap) on risk factors in middle-aged

individuals without cardiovascular disease (TIPS): a phase II, double-blind, randomised trial, *Lancet*, 373 (2009) 1341-1351.

[195] J. Hippisley-Cox, C. Coupland, Effect of combinations of drugs on all cause mortality in patients with ischaemic heart disease: nested case-control analysis, *British Medical Journal*, 330 (2005) 1059-1063.

[196] C.P. Limited. (2015). Polycap Retrieved 26/06/2015, from http://www.polycap.org/index.html

[197] E. Lonn, J. Bosch, K. Teo, P. Pais, D. Xavier, S. Yusuf, The polypill in the prevention of cardiovascular diseases: key concepts, current status, challenges, and future directions, *Circulation*, 122 (2010) 2078-2088.

[198] J. Jia, C. Dong, W. Zhang, Y. Cui, J. Liu, Evaluation of pharmacokinetic and pharmacodynamic relationship for oral sustained-release atenolol pellets in rats, *Journal of Pharmaceutical and Biomedical Analysis*, 55 (2011) 342-348.

[199] A.V. Noor, G. Niharika, P. Deepak, S. Nazan, S.A. Mohammed, Formulation design, characterisation and in vitro evaluation of bilayered tablets containing telmisartan and hydrochlorthizide, *International Journal of Biological*, 4 (2013) 1-9.

[200] S. Shafiq, F. Shakeel, S. Talegaonkar, F.J. Ahmad, R.K. Khar, M. Ali, Development and bioavailability assessment of ramipril nanoemulsion formulation, *European Journal of Pharmaceutics and Biopharmaceutics*, 66 (2007) 227-243.

[201] A.T. Cohen, S. Imfeld, J. Markham, S. Granziera, The use of aspirin for primary and secondary prevention in venous thromboembolism and other cardiovascular disorders, *Thrombosis Research*, 135 (2015) 217-225.

[202] S.C. Halbert, B. French, R.Y. Gordon, J.T. Farrar, K. Schmitz, P.B. Morris, P.D. Thompson, D.J. Rader, D.J. Becker, Tolerability of red yeast rice (2,400 mg twice daily)

versus pravastatin (20 mg twice daily) in patients with previous statin intolerance, *American Journal of Cardiology*, 105 (2010) 198-204.

[203] N. Scoutaris, M. Snowden, D. Douroumis, Taste masked thin films printed by jet dispensing, *International Journal of Pharmaceutics*, 494 (2015) 619-622.

[204] International Conference on Harmonization of Technical Requirements for the Registration of Pharmaceuticals for Human Use, Q3C (R4) Impurities: Guideline for Residual Solvents, (2009).

[205] P. Ige, B. Swami, T. Patil, J. Pradhan, P. Patil, P. Nerkar, S.J. Surana, Design and development of sustained release swelling matrix tablets of glipizide for type II diabetes mellitus, *Farmacia*, 61 (2013) 883-901.

[206] J.L. Ford, Design and evaluation of hydroxypropyl methylcellulose matrix tablets for oral controlled release: a historical perspective, in: R.P. Samuel, T. Peter, D.M. Colin (Eds.) Hydrophilic matrix tablets for oral controlled release, Springer, New York, 2014, pp. 17-51.

[207] C.C. Wilson, Interesting proton behaviour in molecular structures. Variable temperature neutron diffraction and ab initio study of acetylsalicylic acid: characterising librational motions and comparing protons in different hydrogen bonding potentials, *New Journal Of Chemistry*, 26 (2002) 1733-1739.

[208] R. Esteves de Castro, J. Canotilho, R.M. Barbosa, M.R. Silva, A.M. Beja, J. Paixao, J.S. Redinha, Conformational isomorphism of organic crystals: racemic and homochiral Atenolol, *Crystal Growth Design*, 7 (2007) 496-500.

[209] N. Nagel, H. Schweitzer, H. Urbach, W. Heyse, B. Müller, H. Berchtold, Ramipril, *Acta Crystallographica Section B*, 57 (2001) 463-465.

[210] L. Dupont, O. Dideberg, Structure cristalline de l'hydrochlorothiazide, C7H8ClN3O4S2, *Acta Crystallographica Section B*, 28 (1972) 2340-2347.

Biography

[211] S. Lewington, R. Clarke, N. Qizilbash, R. Peto, R. Collins, Age-specific relevance of usual blood pressure to vascular mortality: a meta-analysis of individual data for one million adults in 61 prospective studies, *Lancet*, 360 (2002) 1903-1913.

[212] T. Pedersen, Randomised trial of cholesterol lowering in 4444 patients with coronary heart disease: the Scandinavian Simvastatin Survival Study (4S), *Atherosclerosis Supplements,* 5 (2004) 81-87.

[213] Antithrombotic trialists' collaboration, collaborative meta-analysis of randomised trials of antiplatelet therapy for prevention of death, myocardial infarction, and stroke in high risk patients, *British Medical Journal*, 324 (2002) 71-86.

[214] N.J. Wald, M.R. Law, A strategy to reduce cardiovascular disease by more than 80%, *British Medical Journal*, 326 (2003) 1419.

[215] M. Law, N. Wald, J. Morris, R. Jordan, Value of low dose combination treatment with blood pressure lowering drugs: analysis of 354 randomised trials, *British Medical Journal*, 326 (2003) 1427.

[216] M.R. Law, N.J. Wald, A. Rudnicka, Quantifying effect of statins on low density lipoprotein cholesterol, ischaemic heart disease, and stroke: systematic review and meta-analysis, *British Medical Journal*, 326 (2003) 1423.

[217] W. Liu, Y. Li, J. Liu, X. Niu, Y. Wang, D. Li, Application and Performance of 3D Printing in Nanobiomaterials, *Journal of Nanomater.*, 2013 (2013) 1-7.